DISSERTATION

INTRALUMINAL IMPEDANCE: ELECTROMAGNETIC MODELING, SIGNAL ANALYSIS, AND COMPUTER-ASSISTED DIAGNOSIS OF GASTROESOPHAGEAL REFLUX

Submitted by

Awad Al-Zaben

Electrical and Computer Engineering

In partial fulfillment of the requirements

for the Degree of Doctor of Philosophy

Colorado State University

Fort Collins, Colorado

Fall 2003

COLORADO STATE UNIVERSITY

August 21, 2003

WE HEREBY RECOMMEND THAT THE DISSERTATION PREPARED UNDER OUR SUPERVISION BY AWAD AL-ZABEN ENTITLED INTRALUMINAL IMPEDANCE: ELECTROMAGNETIC MODELING, SIGNAL ANALYSIS, AND COMPUTER-ASSISTED DIAGNOSIS OF GASTROESOPHAGEAL REFLUX BE ACCEPTED AS FULFILLING IN PART REQUIREMENTS FOR THE DEGREE OF DOCTOR OF PHILOSOPHY.

Committee on Graduate Work

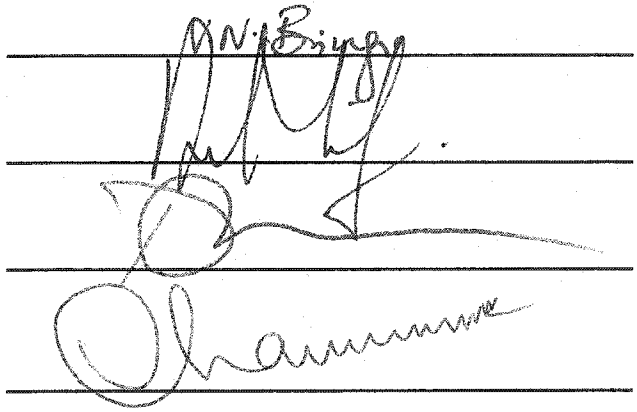

Adviser

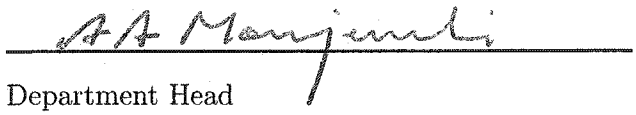

Department Head

ABSTRACT OF DISSERTATION INTRALUMINAL IMPEDANCE: ELECTROMAGNETIC MODELING, SIGNAL ANALYSIS, AND COMPUTER-ASSISTED DIAGNOSIS OF GASTROESOPHAGEAL REFLUX

Multichannel intraluminal impedance modeling and analysis research consists of two parts as in any remote sensing problem namely: a) The forward problem that models the process, and b) The inverse problem of signal analysis and extraction.

The low frequency electric field in the human body resulting from the injection of a constant current is described by Laplace's equation. In multichannel intraluminal impedance the problem is further complicated by the varying impedance of bolus and multiple layers in the esophagus. Numerical technique used to model the forward problem in order to establish the feasibility of this procedure for monitoring the esophagus. Various conditions of the esophagus are considered. Both normal and diseased situations are modeled.

Biomedical problems are typically fairly complex and the biomedical measurements such as the multiple intraluminal impedance varies widely due to the change of various factors including internal factors such as acid reflux, bolus swallow and

external factors such as respiration and patient movement. An analytical technique to study the impedance signals, detect gastroesophageal reflux episodes as well as their classification is developed and presented in this dissertation.

Awad Smairan Al-Zaben
Electrical & Computer Engineering
Colorado State University
Fort Collins, Colorado 80523
Fall 2003

Acknowledgments

I would like to express my sincere appreciation to Dr. V. Chandrasekar who served as my adviser and was available for technical and scientific assistance. My thanks also extends to Dr. V. Bringi, Dr. Derek Lile, and Dr. Donna Wheeler who provided advice and critical review during the development of this dissertation.

Mr. Tom Stuebe of Sandhill Scientific, Inc., is acknowledged for his technical feedback and numerous discussions which enhanced the development of this research. Mr. Vincent Waites of Sandhill Scientific, Inc., is also acknowledge for his assistance in software implementation.

Dr. Steven Shay of Cleveland clinic is acknowledged for his help and guidance in understanding the medical interpretations of the signals used in this research.

I also express my appreciation to the Yarmouk university faculty members. The solid background they provided me on the fundamentals, made my life enjoyable, and my graduate study easier.

This research was supported in various forms by Sandhill Scientific, Inc.

Dedication

To the memory of my mother, my beloved wife, and my daughter Jude.

Contents

Abstract iii

Acknowledgments v

Dedication vi

Chapter 1 Multiple Interluminal Impedance 1

1.1 Introduction 1

1.2 Background on gastreoesophageal reflux 2

1.3 Impedance measurements of motility and reflux 4

1.4 MII system construction 6

1.5 MII signals 7

1.6 Summary 9

Chapter 2 Electromagnetic of MII 11

2.1 Introduction 11

2.2 Simple model of the esophagus 13

2.3 Finite element method of MII 18

2.3.1 Weak form 21

2.4 Summary 25

Chapter 3 Computation of Impedance in the Esophagus 27

3.1 Introduction 27

3.2 Analytical solution 28

3.3 Numerical solution 31

3.3.1 Line sources 34

3.4 Electrodes location 35

3.4.1 Catheter diameter 38

3.5 Modeling of electrical properties of the esophagus 41

3.5.1 Esophagus thickness 48

3.5.2 Catheter position 48

3.5.3 Catheter diameter 53

3.5.4 Length of electrode 56

3.6 Summary 59

Chapter 4 MII Signals and Analysis of Esophageal Episodes 60

4.1 Introduction 60

4.2 Characteristics of reflux episodes 61

4.3 Reflux patterns 69

4.3.1 Liquid reflux 69

4.3.2 Mixed reflux 69

4.3.3 Gas reflux 70

4.4 Other patterns 70

4.5 Summary 79

Chapter 5 Algorithm for Reflux Episode Detection 81

5.1 Introduction 81

5.2 Expert system 83

5.2.1 Wavelet analysis of MII 83

5.2.2 Normal (and semi-normal) impedance signals 90

5.2.3 Low baseline 92

5.2.4 pH based observations 93

5.3 Neural networks 94

5.3.1 False positive neural network 94

5.4 Other analysis 98

5.5 Data analysis and discussion 99

5.6 Summary 102

Chapter 6 Discussion and Summary 104

References 110

List of Figures

1.1 Catheter configuration and placement inside esophagus. 5

1.2 Typical impedance signals along with one pH channel: dotted line shows a region where a reflux episode occurs. The common abscissa of the graphs is time and the various ordinates are the various impedance values. Note the propagation direction of the inverse pulse shape starting from ch_6. 8

1.3 Typical impedance signals along with pressure signals along the esophagus. Swallow episode is shown at this time of the study. 9

2.1 Simple cylindrical model of two electrodes inside the esophagus. . . 14

3.1 Potential obtained from a pair of electrodes as a function of distance from the center. The two curves show the potentials for two Z values coinciding with the electrode locations. Boundary of the esophagus is assumed at $\rho_1 = 0.5\ cm$. 29

3.2 Impedance as a function of the bolus thickness, obtained from equation (2.15). 30

3.3 Examples of the cases of the bolus around the catheter (cylindrical coordinate), electrodes thickness = 0.008cm. Electrodes are of steel material carrying current of 4 μA, esophagus thickness 0.1 cm with conductivity of 5×10^{-6} S/cm, the outside layer conductivity 1×10^{-3} S/cm, and the bolus conductivity 5×10^{-3} S/cm. 33

3.4 Mesh generated for finite element computation (FEM, 2003). 34

3.5 Conductivity map obtained from the application of the point form of Ohm's law ($\sigma = \frac{J}{E}$) for the case of bolus conductivity 5×10^{-3} and outside layer conductivity 1×10^{-3}. 35

3.6 Impedance as a function of inter electrode spacing 36

3.7 Impedance as a function of catheter radius. 39

3.8 The basic model used in the study of the impact of the various parameters on the impedance. 42

3.9 Mesh used in the FE. 43

3.10 Example of the potential map obtained from activation of all the channels. Note that the figure is a cut at the center. 44

3.11 Reflux patterns: (a) results of finite element analysis; (b) real data obtained from normal esophageal condition. 46

3.12 Resistance as a function of the esophagus wall thickness: catheter diameter=2.13 mm, electrode length=4 mm, electrode thickness=0.008 mm, and mucosa membrane thickness=0.008 mm. 49

3.13 Model used in the simulation of the centered and non-centered catheter inside the esophagus. 50

3.14 Resistance as a function of catheter diameter. 54

3.15 Resistance as a function of electrode length. 57

4.1 Typical impedance traces during a reflux episode obtained from patient due. 61

4.2 Typical impedance signals along with one pH channel: dotted line shows a region where a reflux episode occurs. The common abscissa of the graphs is time and the various ordinates are the various impedance values. Note the propagation direction of the inverse pulse shape starting from ch_6. 62

4.3 Reflux episode. Note the propagation direction of the impedance drop is not clearly visible, possible swallow interpretation of this episode. 63

4.4 Histogram of baseline impedance of a typical (randomly selected) patient. 64

4.5 Histogram of the baseline impedance of different patients. 65

4.6 Histogram of normalized gastric content impedance to the baseline impedance. 67

4.7 Minimum impedance reached during reflux episodes. Note the large values corresponds to minimum impedance reached during some mixed episodes. 68

4.8 Different forms of liquid type reflux episode. 71

4.9 Different forms of mixed-type reflux episode. 73

4.10 Different forms of gas type reflux episode. 75

4.11 Other patterns. 77

5.1 Expert system used to detect reflux episodes. NN stands for neural network, LB stands for low baseline, and FP stands for false positive. 82

5.2 Spline wavelet. 86

5.3 Low-pass and high-pass filter responses. 88

5.4 Signal of one channel (ch_6), the resulting smooth version, and the corresponding sum of the energy in the negative details and that of the positive details (normalized). Dotted lines shows the location of the maxima and the corresponding location on the signal. 89

5.5 Adaptively changing gastric content thresholds. Two thresholds are shown in the Figure, one corresponds to acid reflux episodes and one corresponds to non-acid reflux episodes. 92

5.6 Neural network structure. 95

5.7 ROC curve of the features used as network inputs. 96

5.8 Supporting routines used to enhance the FP removal. 98

Chapter 1

Multiple Interluminal Impedance

1.1 Introduction

The esophagus is a hollow cylindrical organ that extends from the pharynx to the stomach and provides the pathway by which ingested food and drink reach the stomach. The wall of the esophagus consists of three major layers: the mucosa, the submucosa, and the muscularis propria. The undesirable passage of air from the pharynx into the esophagus is prevented by the upper sphincter, and the lower sphincter prevents gastroesophageal reflux. The way in which a bolus (a soft mass of chewed food) is moved downward through the various regions of the digestive tract is referred to as motility, which is highly regulated by neural and hormonal mechanisms. Many studies show that reflux of acid, pepsin, or bile and the duration of contact of these substances with the esophagus, in addition to the speed with which the esophagus returns these contents to the stomach, are very important in determining the resulting complications that could occur in the esophagus (Rahbek, 1973). Current techniques used to evaluate the gastrointestinal tract (GIT)

include extracorporeal image procedures and manometry. Multichannel intraluminal impedance measurement (MII) (Silny, 1991; Silny et al., 1993; Srinivasan et al., 2001; Trachterna et al., 1999) is a new and emerging technique that shows great promise in the study of GIT. MII has shown great promise in accurate estimation of the bolus speed and size, in addition to the detection of any activity inside the esophagus such as swallow or gastroesophageal reflux (GER) (Silny, 1991; Al-zaben et al., 2001; Al-zaben and Chandrasekar, 2003; Skopnik et al., 1996). When MII is combined with pH measurements, the acidity of the reflux, its duration, and the distance the acid reaches in the esophagus can be detected. When it is combined with pressure measurements, swallow patterns can be studied.

1.2 Background on gastreoesophageal reflux

Gastroesophageal reflux (GER) is a normal physiological phenomenon experienced by most people, particularly after a meal. Gastroesophageal reflux disease (GERD) is defined as mucosal damage produced by the abnormal reflux of gastric contents into the esophagus (Katz, 2001). GERD may be due to a number of conditions, including:

- Lower esophageal sphincter (LES) malfunction:

  LES, working like a one-way switch, is essential for maintaining a pressure barrier against contents from the stomach. When the LES weakens, it cannot

close completely after food empties into the stomach, resulting in backward flow of gastric contents into the esophagus.

- Stomach abnormalities: Abnormal contractions resulting from abnormal nerve or muscle function in the stomach. This causes delays in stomach emptying, increasing the risk for stomach contents backflow.
- Esophagus abnormalities.
- Hiatal hernia: Hiatal hernia may impair LES muscle function.
- Genetic factors: An inherited risk exists in many cases of GERD.
- Asthma: Coughing and sneezing accompanying asthmatic attacks cause changes in pressure in the chest that can trigger reflux. Certain asthma drugs that dilate the airways may relax the LES and contribute to GERD. On the other hand, GERD has been associated with a number of other upper respiratory problems, and may be a cause of asthma rather than a result.

Typical symptoms of acid reflux are heartburn, regurgitation, and difficulty in swallowing. However, abnormal reflux can also cause symptoms such as coughing, chest pain, and wheezing, and damage to the lungs (pneumonia, asthma, idiopathic pulmonary fibrosis), vocal cords (laryngitis, cancer), ears (otitis media), and teeth (enamel decay).

The damage in the esophagus resulting from gastric contents exposure depends on many factors, including (Pope, 1994):

- Duration of contact between gastric fluid and the mucosa, which depends on the number of reflux episodes per time unit and the efficiency of the reflux clearance (including neutralization and esophageal peristalsis).
- Characteristics of the refluxed fluid. Acid and pepsin together are more damaging than either one is alone).
- Intrinsic resistance of the esophageal epithelium to damage.

Treatment of GERD may be achieved using drugs or surgery. Surgery is considered when a person requires large doses of medications, the medications are insufficient, or the patient cannot tolerate long medical treatment. Typical surgery involves wrapping the top part of the stomach around the junction of the esophagus and stomach.

1.3 Impedance measurements of motility and reflux

Bio-impedance measurement (Baker, 1989) is used in a number of areas, such as estimation of body composition, thoracic electrical bio-impedance, and electrical impedance tomography (Breckon and Pidcock, 1987; Gutman, 1989). The use of the bio-impedance in the measurement of motility and reflux monitoring is based on the fact that the electrical conductivity of the bolus material and the gastric contents are much larger than that of the esophagus wall as well as air (Silny, 1991; Al-zaben et al., 2001). Therefore, measuring the impedance inside the gastrointestinal tract (GIT) will reflect the GIT status.

MII measurement can be made using a catheter with a number of current-carrying electrodes placed into the GIT as shown in Figure (1.1), where the catheter is placed in the GIT through the nasal cavity. The differential voltage between pairs of electrodes (for a fixed current) will represent the average electrical impedance of the volume of materials around the electrodes. The measured impedance depends on many factors, including: thickness and contents of the bolus, geometry and arrangement of the electrodes, patient status (type of disease, stomach content, etc.) and the catheter position. The impact of each of these variables on the measured impedance will be discussed in the next chapters.

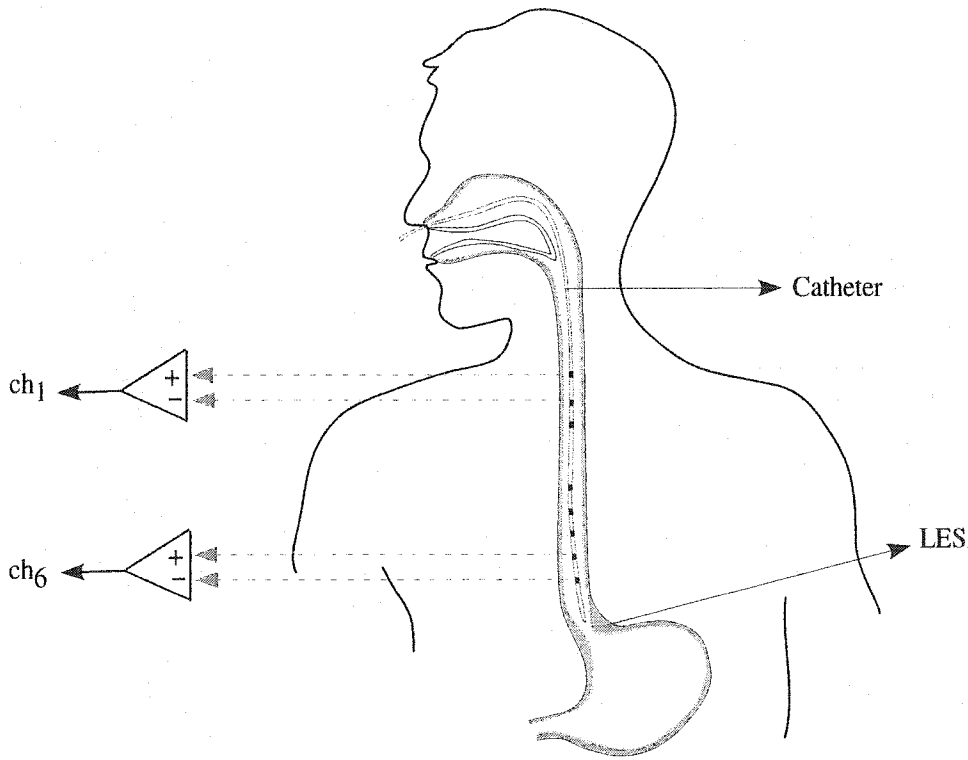

Figure 1.1: Catheter configuration and placement inside esophagus.

1.4 MII system construction

MII system design must take into consideration the following factors:

- Patient safety: All biomedical instrumentation must be safe for both patient and medical staff. MII safety can be achieved by isolation and limitation of the current and power in the probes.
- Patient comfort: Because the MII probe is placed inside the GIT, the MII probe must not impair any organ function.
- Ability to reflect a wide range of changes inside the esophagus as impedance variations.
- Ambulatory: Because measurement takes 24 hours, patient daily activity must be maintained.

The MII system consists of an insulated catheter on which current-carrying metallic ring electrodes are mounted. The differential potential between each pair of electrodes is referred to as channel. The system can be designed with a number of channels such that it covers the esophagus length. In addition to the impedance measurements channels, there is at least one pH measurement electrode. This electrode can be placed anywhere on the esophagus, and the best acidity detection can be achieved when the electrode is placed close to the lower esophageal sphincter (LES). The choice of the catheter diameter and electrodes location and the corresponding impact of these parameters on the MII performance will be discussed later.

1.5 MII signals

Gastroesophageal reflux episodes are seen in MII as an impedance change from a baseline impedance to a differenet level in the presence of gastric contents. Therefore, the impedance of the gastric contents is a very important value that distinguishes reflux episodes from other episodes. However, the impedance of gastric contents is not constant, and it changes over the study period. The baseline impedance is also not constant, and can vary during the study period. It is also patient dependent. Figure (4.2) shows sample impedance traces observed over various observation points along the esophagus. There are six observation points, from the upper part of the esophagus to a point just above the lower esophageal sphincter. In addition, there is one pH observation point. These points are denoted as $ch_1, ch_2, \cdots ch_6$ for further discussion. The impedance graphs shown on Figure (4.2) correspond to a reflux episode. The common abscissa of the graphs is time and the various ordinates are the various impedance values. The leading edge of the decreased impedance (or the inverse pulse shape) can be seen to have a movement from ch_6 (distal) to ch_1 (proximal), indicative of movement in that direction. The combination of drop in impedance values and the direction of movement of the "inverse pulse" indicates that it is a reflux. On the contrary, if it were a swallow, the "inverse pulse" would have moved from ch_1 to ch_6. The above provides a simple description of swallow and reflux as observed by MII measurements.

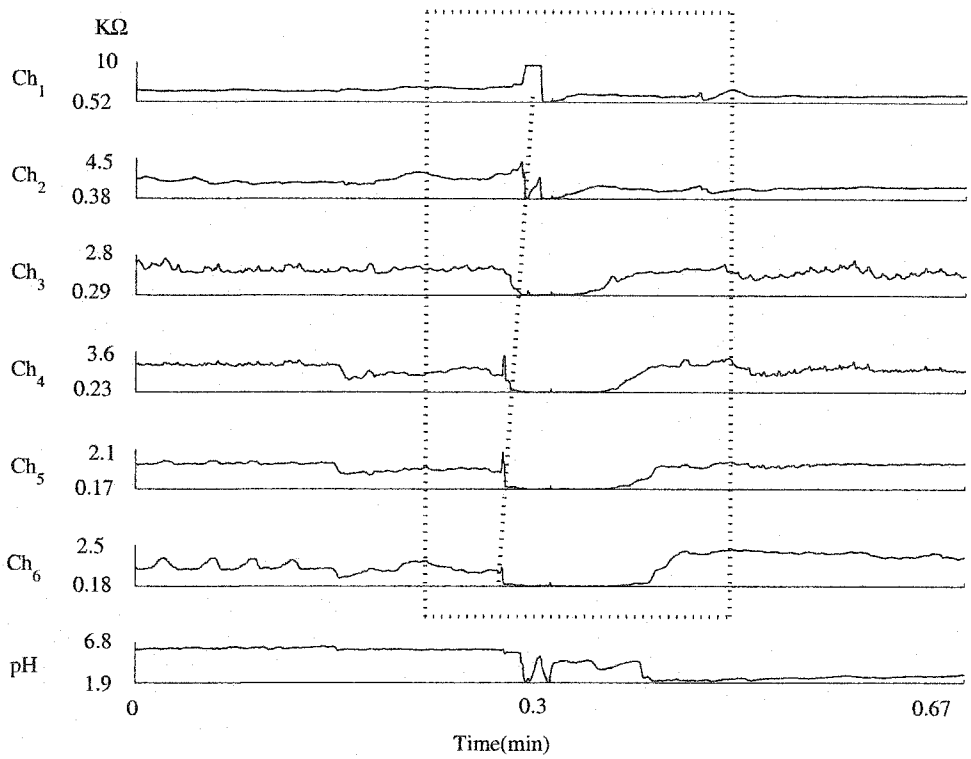

Figure 1.2: Typical impedance signals along with one pH channel: dotted line shows a region where a reflux episode occurs. The common abscissa of the graphs is time and the various ordinates are the various impedance values. Note the propagation direction of the inverse pulse shape starting from ch_6.

Another area of MII measurements can be seen in Figure (1.3), where the impedance channels go along with pressure measurements (Shay et al., 2002). This type of measurement gives a very good indications of the swallow patterns, the peristaltic contractions, and the motility of the esophagus.

The MII study is usually performed over 24 hours, needing many hours of physician time to read and mark the occurrence of episodes. In the next chapters, an algorithm to detect the events occurring in the GIT from the impedance traces.

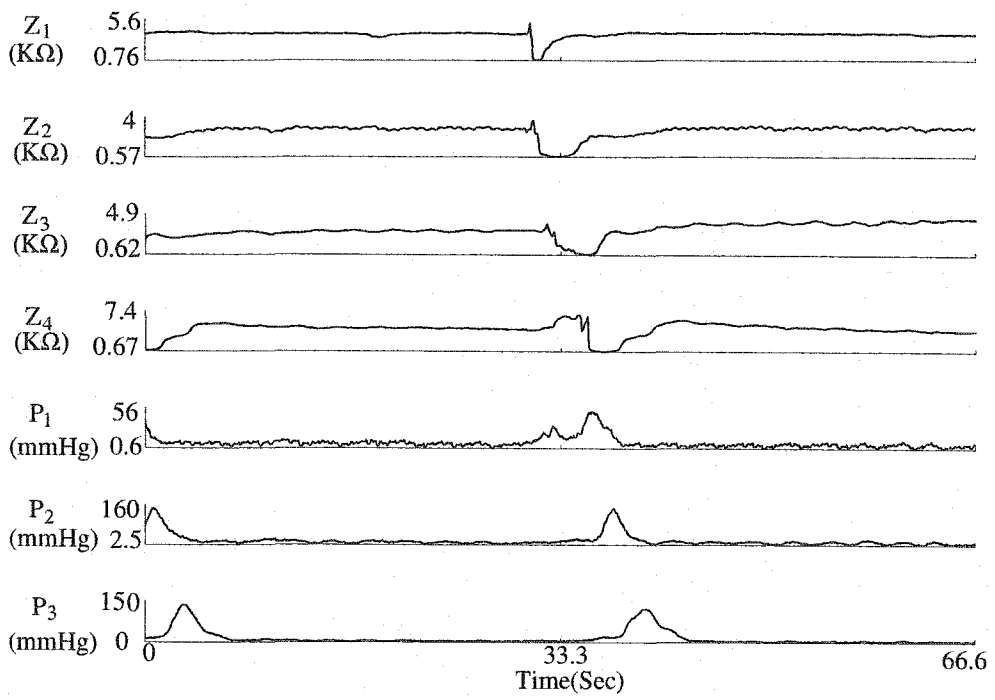

Figure 1.3: Typical impedance signals along with pressure signals along the esophagus. Swallow episode is shown at this time of the study.

This algorithm is currently being considered for computer aided diagnosis of reflux episodes.

1.6 Summary

Multichannel intraluminal impedance measurement is a new and emerging technique that shows great promise in the study of GIT. MII provides valuable information about the esophagus and its function. MII has shown great promise in accurate estimation of the bolus speed and size, in addition to the detection of any activity inside the esophagus such as swallow or gastroesophageal reflux (GER). The

MII system consists of a catheter with current-carrying electrodes. The location of these electrodes and the effect of various parameters on the impedance is an important design factor and will be discussed in more detail in the next few chapters. Many factors contribute to the variability of the MII signals, among them: patient status (esophagus condition, stomach contents, etc.), catheter configuration, and other artifacts such as meal, movement, and respiration. However, reflux episodes can be seen in impedance traces as an inverse pulse shape that propagates from the most distal channel to the upper proximal one. Detection and classification of reflux episodes will be discussed in the following chapters.

Chapter 2

Electromagnetic of MII

2.1 Introduction

Gastroesophageal reflux episodes occurring in normal subjects can be characterized by the following:

- Impedance decreases to the impedance level of the gastric contents.
- Decrement of impedance starts in the most distal channel (close to the stomach) and propagates upward.
- Large impedance change at the start of the episode.
- If combined with gas, there will be an impedance increment to a high value in at least one of the channels.

Under severe esophageal damage, the above characteristics are not clearly visible. Instead, the impedance in such cases is characterized by low baseline impedance and a small impedance change during an episode. In some cases, these changes cannot be seen in the two most distal channels. A number of hypotheses have been

considered to explain the impedance characteristics under pathological conditions, among them:

- Liquid is always present between the electrodes, which drives the impedance to a low value all the time.
- The catheter position is not in the middle of the esophagus; instead, it touches the esophagus wall at one of its sides.
- Refluxate or bolus materials do not cover completely the space between the electrodes.
- Esophagus inflammation (i.e., esophagus wall is always in touch with the catheter).
- Esophagus size (subject is male, female, infant, etc.).
- Esophagus wall width.

In such situations, the fundamental questions that need answer are:

1. Which hypothesis is correct?
2. How to overcome the problems by changing the catheter configuration.
3. Is there a need for different catheter configurations for different subjects after initial diagnosis?

The objective here is to arrive at reasonable answers and to provide better understanding of the different impedance patterns, such as: low baseline, gas propagation, and mixed behavior. Then complete electromagnetic description of each scenario is

needed. The investigation should take into consideration real catheter and esophagus dimensions, realistic conductivity assumptions, investigating all possible configurations, and factors, such as properties of esophagus wall, bolus or refluxate shape, etc.

2.2 Simple model of the esophagus

One of the early attempts to compute the impedance measured by a catheter inside the esophagus was presented in Silny (1991). This computation was based on a simplified application of the method of images in a cylindrical coordinate system. The following presents the theoretical computation of impedance in cylindrical coordinate system to a higher level of accuracy. As a first-order approximation, the catheter inside the esophagus can be modeled in a cylindrical coordinate system as described below:

Figure (2.1) shows a simple model of the catheter inside the esophagus, where the esophagus is modeled as a dielectric cylinder placed in an infinite dielectric medium. The probe is also cylindrical, located at the center of the cylindrical coordinate system, where the probe length is aligned along the z-axis. The MII probes use low frequency current to monitor the esophagus (Al-zaben and Chandrasekar, 2003). The governing equation for the potential is given by:

$$\nabla \cdot (-\sigma(\mathbf{r})\nabla\psi(\mathbf{r})) = J(\mathbf{r}') \tag{2.1}$$

where $J(\mathbf{r}')$ is the current source at $\mathbf{r}'$ (Kleinermann et al., 1999).

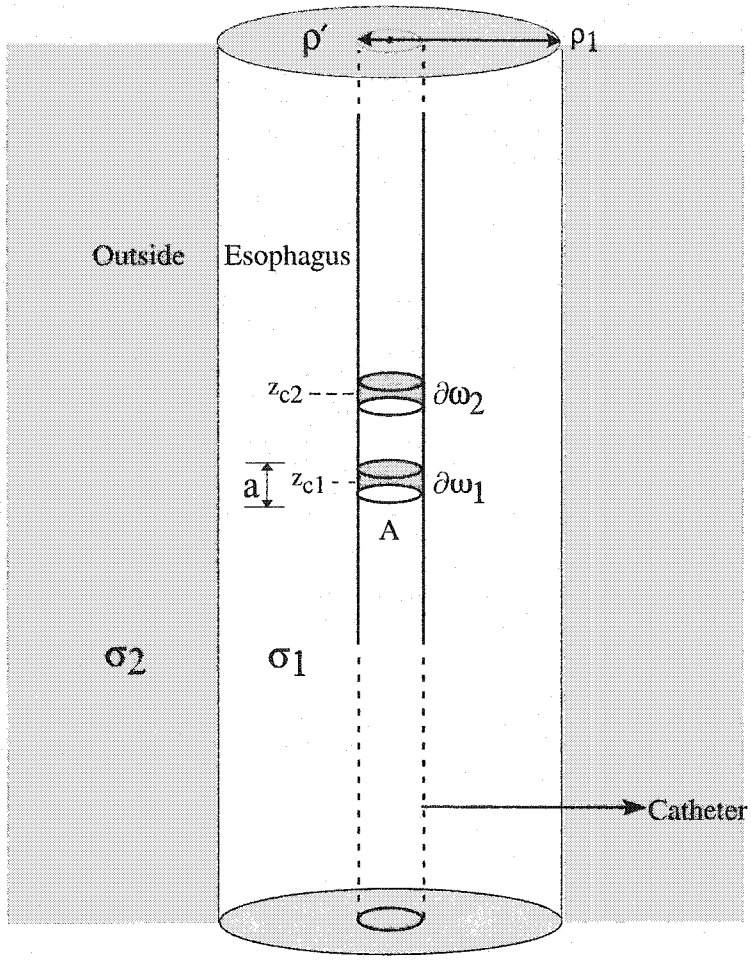

Figure 2.1: Simple cylindrical model of two electrodes inside the esophagus.

The solution for the potential can be written in terms of Green's function in the integral form as (Jackson, 1999; Morse and Feshbach, 1953):

$$\psi(\rho, \theta, z) = \int_A G(\mathbf{r}, \mathbf{r}')\mathbf{J}(\mathbf{r})\, \mathbf{dA} \tag{2.2}$$

where A is the electrode surface area. Equation (2.1) can be solved by finding the Green's function $G(\mathbf{r}, \mathbf{r}')$ that vanishes at ∞ and satisfies:

$$\nabla^2 G(\mathbf{r}, \mathbf{r}') = -\delta(\mathbf{r} - \mathbf{r}') = -\frac{\delta(\rho - \rho')}{\rho}\delta(\theta - \theta')\delta(\mathbf{z} - \mathbf{z}') \tag{2.3}$$

using the relations:

$$\delta(z - z') = \frac{1}{\pi}\int_0^\infty \cos\left(\alpha(z - z')\right)\, d\alpha \quad and \tag{2.4a}$$

$$\delta(\phi - \phi') = \frac{1}{2\pi}\sum_{n=-\infty}^{\infty} e^{in(\phi - \phi')} \tag{2.4b}$$

using the same expansion in Equation (2.4a) for the z and ϕ dependence of G, then

$$\begin{aligned} G(\mathbf{r} - \mathbf{r}') &= \frac{1}{2\pi^2}\sum_{n=-\infty}^{\infty}\int_0^\infty \left(\frac{dg_n}{d\rho} + \frac{1}{\rho}\frac{dg_n}{d\rho} - \left(\alpha^2 + \frac{n^2}{\rho}\right)g_n\right)\cos\left(\alpha(z - z')\right)e^{in(\phi - \phi')} \\ &= -\frac{\delta(\rho - \rho')}{\rho}\sum_{n=-\infty}^{\infty}\int_0^\infty \cos\left(\alpha(z - z')\right)e^{in(\phi - \phi')} \end{aligned} \tag{2.5}$$

Then

$$\left(\frac{dg_n}{d\rho} + \frac{1}{\rho}\frac{dg_n}{d\rho} - \left(\alpha^2 + \frac{n^2}{\rho}\right)g_n\right)\cos\left(\alpha(z - z')\right)e^{in(\phi - \phi')} = -\frac{\delta(\rho - \rho')}{\rho} \tag{2.6}$$

which is the Bessel's equation that has a solution in the form:

$$g_n(\rho, \rho') = I_n(\alpha\rho)I_n(\alpha\rho') + K_n(\alpha\rho)I_n(\alpha\rho') \tag{2.7}$$

Since our assumption is that the current sources are at $\rho' = 0$, then:

$$\sum_{n=0}^{\infty} g_n(\rho, 0) = I_0(\alpha\rho) + K_0(\alpha\rho) \tag{2.8}$$

This will be the general form of the Green's function for the problem at hand. Since there are two layers in the setup, then due to the polarization of the second layer, g_n in layer 1 will be in the form (Smythe, 1967):

$$g_n(\rho, 0) = AI_0(\alpha\rho) + K_0(\alpha\rho) \tag{2.9}$$

and in the second layer will be :

$$g_n(\rho, 0) = BK_0(\alpha\rho) \tag{2.10}$$

Applying the following boundary conditions at the boundary interface (ρ_1)

$$\psi_{layer1} = \psi_{layer2} \quad at \quad \rho = \rho_1. \tag{2.11a}$$

$$\frac{\partial \psi_{layer1}}{\partial \rho}|_{\rho=\rho_1} = \frac{\sigma_2}{\sigma_1}\frac{\partial \psi_{layer2}}{\partial \rho}|_{\rho=\rho_1} \tag{2.11b}$$

and solving for A and B result in:

$$A = \frac{(\sigma_1 - \sigma_2)K_0(\alpha\rho_1)K_1(\alpha\rho_1)}{\sigma_1 K_0(\alpha\rho_1)I_1(\alpha\rho_1) + \sigma_2 I_0(\alpha\rho_1)K_1(\alpha\rho_1)} \tag{2.12a}$$

$$B = \frac{\sigma_2(K_0(\alpha\rho_1)I_1(\alpha\rho_1)}{\sigma_1 K_0(\alpha\rho_1)I_1(\alpha\rho_1) + \sigma_2 I_0(\alpha\rho_1)K_1(\alpha\rho_1)} \tag{2.12b}$$

Therefore, the potential in layer 1 will be:

$$\psi(\rho,\theta,z) = \frac{1}{2\pi^2}\sum_{n=1}^{N}\frac{I_n}{a\sigma_1}\int_{z_c-a/2}^{z_c+a/2}\int_0^{\infty}(K_0(\alpha\rho)+\kappa I_0(\alpha\rho))\times \cos(\alpha(z-z'))\ d\alpha dz' \tag{2.13}$$

where N is the number of electrodes. I_n is the current in the n^{th} electrode, I_0 is the modified Bessel's function of first kind and K_0 is the modified Bessel's function of second kind, σ_1 is Layer 1 (bolus) conductivity, σ_2 is Layer 2 (esophagus and volume conductor) conductivity, and

$$\kappa = \frac{(\sigma_1-\sigma_2)K_0(\alpha\rho_1)K_1(\alpha\rho_1)}{\sigma_1 K_0(\alpha\rho_1)I_1(\alpha\rho_1)+\sigma_2 I_0(\alpha\rho_1)K_1(\alpha\rho_1)}) \tag{2.14}$$

The impedance then can be evaluated from equations (2.13, 2.14) at the observation points located at the center of each electrode ((ρ_0 , Z_{c1}), (ρ_0 , Z_{c2})) and taking the difference it will be:

$$\begin{aligned} Z = {} & \frac{1}{2\pi^2}\frac{I}{a\sigma_1}\int_{z_{c1}-a/2}^{z_{c1}+a/2}\int_0^{\infty}(K_0(\alpha\rho_0)+\kappa I_0(\alpha\rho_0))\times \\ & \{\cos(\alpha(z_{c1}-z'))-\cos(\alpha(z_{c2}-z'))\}\ d\alpha dz' \\ & +\frac{1}{2\pi^2}\frac{I}{a\sigma_1}\int_{z_{c2}-a/2}^{z_{c2}+a/2}\int_0^{\infty}(K_0(\alpha\rho_0)+\kappa I_0(\alpha\rho_0))\times \\ & \{\cos(\alpha(z_{c1}-z'))-\cos(\alpha(z_{c2}-z'))\}]\ d\alpha dz' \end{aligned} \tag{2.15}$$

It can be seen from the previous derivation that the analytical solution is complicated even for such a simple model. Therefore, the solution for more complicated model will be tedious to obtain (refer to Kleinermann et al. (1999), Niknejad et al. (1998), and Lytle et al. (1979) for examples). Therefore, numerical technique is a useful alternative for modeling the realistic geometry of the catheter inside the esophagus. The need for numerical technique will enable modeling MII for the following reasons:

- Esophagus is not a perfect cylinder.
- Bolus shape is not a perfect cylinder.
- Inhomogeneity in the conductivities.
- Finite dimensions of the catheter.
- Finite dimensions of the electrodes and finite conductivity.

2.3 Finite element method of MII

Finite element (FE) is a technique used to obtain solution of a partial differential equation. In general, finite element analysis consists of the following main stages:

- Preprocessing, which includes creating a model of the domain, discretizing the domain into a finite element mesh, and defining the data related to the problem. The finite elements resulting from discretization have dimensions much smaller than the original domain in order to allow the interpolation of the solution within the element using simple functions (called basis functions).

- Processing stage, which includes generation of the element stiffness and mass matrices, assembling the global stiffness matrix, and solving the algebraic system.
- Post-processing stage, which includes the calculations of all required variables.

In order to set up the problem of MII for finite element analysis, the problem is reformulated such that the finite element method can be applied easily. MII uses relatively low frequency, therefore it is a good approximation under quasistatic to ignore the magnetic field effects and use the static formalism of the following equations (Malmivuo and Plonsey, 1995; Melcher, 1989; Shen and Kong, 1995):

$$\nabla \cdot \vec{\mathbf{D}} = \rho_v \tag{2.16}$$

$$\nabla \cdot \vec{\mathbf{B}} = 0 \tag{2.17}$$

$$\nabla \times \vec{\mathbf{E}} = emf \tag{2.18}$$

$$\nabla \times \vec{\mathbf{H}} = \vec{\mathbf{J}} \tag{2.19}$$

where the emf in equation (2.18) has been introduced (Malmivuo and Plonsey, 1995) because there is a current conduction in the GIT (non-conservative $\vec{\mathbf{E}}$). Also under static conditions:

$$\vec{\mathbf{D}} = \epsilon \vec{\mathbf{E}} \tag{2.20}$$

$$\vec{\mathbf{J}} = \sigma \vec{\mathbf{E}} \tag{2.21}$$

where σ is the conductivity as a function of the spatial coordinate of the volume conductor, which is assumed to be inhomogeneous. Neglecting the magnetic induction effect gives:

$$\vec{\mathbf{E}} = -\nabla\psi \tag{2.22}$$

Then taking the divergence of equation (2.19) results in:

$$\nabla \cdot \sigma \vec{\mathbf{E}} = 0 \tag{2.23}$$

$$\nabla \cdot (-\sigma \nabla\psi) = 0 \tag{2.24}$$

which is the Laplace's equation that, when solved for the potential, can be used to determine the electric field and the impedance.

Using the previous model, the strong form of the Laplace's equation can be stated as:

$$\nabla \cdot (-\sigma(x,y,z)\nabla\psi(x,y,z)) = 0 \quad in\,\Omega \tag{2.25}$$

subject to the boundary conditions, which is also known as the continuum model of the electrodes (Cheng et al., 1989; Vauhkonen et al., 1999):

$$\begin{cases} -\sigma(x,y,z)\frac{\partial\psi}{\partial n} &= J_1 \quad at \ \partial\Omega_1, \\ -\sigma(x,y,z)\frac{\partial\psi}{\partial n} &= -J_1 \quad at \ \partial\Omega_2, \\ \psi(x,y,z) &= 0 \quad at \ \partial\Omega_3, \end{cases} \tag{2.26}$$

where $\partial\Omega_1$ is the first electrode, $\partial\Omega_2$ is the second electrode, $\partial\Omega_3$ is the outside boundary (see Figure (2.1)), and J_1 is the current density.

2.3.1 Weak form

Finite element method (Segerlind, 1984; Whiteman, 1963) is a piecewise approximation of the governing equation; therefore, the strong form of the Laplace's equation cannot be used directly because it requires that the second derivative of the solution exist. A weaker demand (first derivative exists) on the solution can be derived by the use of the variational calculus (Morse and Feshbach, 1953). The solution can be obtained by minimizing the following potential function:

$$J = -\int_\Omega \delta\psi \left\{ \frac{\partial}{\partial x}\left[\sigma_x \frac{\partial\psi}{\partial x}\right] + \frac{\partial}{\partial y}\left[\sigma_y \frac{\partial\psi}{\partial y}\right] + \frac{\partial}{\partial z}\left[\sigma_z \frac{\partial\psi}{\partial z}\right] \right\} \partial\Omega \;=\; 0 \quad \forall\delta\psi$$

Integrating by parts, and rearranging:

$$J \;=\; -\int_\Omega \left\{ \frac{\partial}{\partial x}\left[\delta\psi\sigma_x \frac{\partial\psi}{\partial x}\right] + \left[\delta\psi\sigma_y \frac{\partial\psi}{\partial y}\right] + \left[\delta\psi\sigma_z \frac{\partial\psi}{\partial z}\right] \right\} d\Omega$$

$$+\int_{\Omega}\left\{\frac{\partial\delta\psi}{\partial x}\sigma_x\frac{\partial\psi}{\partial x}+\frac{\partial\delta\psi}{\partial y}\sigma_y\frac{\partial\psi}{\partial y}+\frac{\partial\delta\psi}{\partial z}\sigma_z\frac{\partial\psi}{\partial z}\right\}d\Omega$$

Invoking the divergence theorem:

$$\int_{\Omega}\nabla\cdot f d\Omega \;=\; \int_{s} f\cdot\hat{n}ds$$

The first integration in J then reduces to:

$$\int_{\Gamma}\left\{\delta\psi\sigma_x\frac{\partial\psi}{\partial x}+\delta\psi\sigma_y\frac{\partial\psi}{\partial y}+\delta\psi\sigma_z\frac{\partial\psi}{\partial z}\right\}\cdot\hat{n}d\Gamma$$

with $\Gamma=\Gamma_{e_1}\cup\Gamma_{e_2}\cup\Gamma_{e_3}$, then this integral can be written as:

$$\begin{aligned}\int_{\Gamma}\left\{\delta\psi\sigma\frac{\partial\psi}{\partial n}\right\}d\Gamma \;&=\; \int_{\Gamma_{e_1}}\left\{\delta\psi\sigma\frac{\partial\psi}{\partial n}\right\}d\Gamma_{e_1}+\int_{\Gamma_{e_2}}\left\{\delta\psi\sigma\frac{\partial\psi}{\partial n}\right\}d\Gamma_{e_2}\\ &\quad+\int_{\Gamma_{e_3}}\left\{\delta\psi\sigma\frac{\partial\psi}{\partial n}\right\}d\Gamma_{e_2}\end{aligned}$$

but $\delta\psi=0$ on Γ_{e_3}, therefore:

$$\begin{aligned}\int_{\Gamma}\left\{\delta\psi\sigma\frac{\partial\psi}{\partial n}\right\}d\Gamma \;&=\; \int_{\Gamma_{e_1}}\left\{\delta\psi\sigma\frac{\partial\psi}{\partial n}\right\}d\Gamma_{e_1}+\int_{\Gamma_{e_2}}\left\{\delta\psi\sigma\frac{\partial\psi}{\partial n}\right\}d\Gamma_{e_2}\\ &=\; \int_{\Gamma_{e_1}}\{\delta\psi J_1\}\,d\Gamma_{e_1}-\int_{\Gamma_{e_2}}\{\delta\psi J_1\}\,d\Gamma_{e_2}\end{aligned}$$

Then J can be written as:

$$J \;=\; -\int_{\Gamma_{e_1}}\{\delta\psi J_1\}\,d\Gamma_{e_1}+\int_{\Gamma_{e_2}}\{\delta\psi J_1\}\,d\Gamma_{e_2}$$

$$+\int_{\Omega}\left\{\frac{\partial\delta\psi}{\partial x}\sigma_x\frac{\partial\psi}{\partial x}+\frac{\partial\delta\psi}{\partial y}\sigma_y\frac{\partial\psi}{\partial y}+\frac{\partial\delta\psi}{\partial z}\sigma_z\frac{\partial\psi}{\partial z}\right\}d\Omega \qquad (2.27)$$

Equation (2.27) can be written as:

$$\begin{aligned} J &= \int_{\Omega}\left\{\delta\frac{\partial\psi}{\partial x}\sigma_x\frac{\partial\psi}{\partial x}+\delta\frac{\partial\psi}{\partial y}\sigma_y\frac{\partial\psi}{\partial y}+\delta\frac{\partial\psi}{\partial z}\sigma_z\frac{\partial\psi}{\partial z}\right\}d\Omega \\ &\quad -\int_{\Gamma_{e_1}}\{\delta\psi J_1\}\,d\Gamma_{e_1}+\int_{\Gamma_{e_2}}\{\delta\psi J_1\}\,d\Gamma_{e_2} \end{aligned}$$

since $J=0$, then:

$$\int_{\Omega}\left\{\delta\frac{\partial\psi}{\partial x}\sigma_x\frac{\partial\psi}{\partial x}+\delta\frac{\partial\psi}{\partial y}\sigma_y\frac{\partial\psi}{\partial y}+\delta\frac{\partial\psi}{\partial z}\sigma_z\frac{\partial\psi}{\partial z}\right\}d\Omega = \int_{\Gamma_{e_1}}\{\delta\psi J_1\}\,d\Gamma_{e_1}-\int_{\Gamma_{e_2}}\{\delta\psi J_1\}\,d\Gamma_{e_2}$$

the LHS can be written in matrix form as:

$$\begin{aligned} B(\delta\psi,\psi) &= \int_{\Omega}\begin{bmatrix}\delta\frac{\partial\psi}{\partial x} & \delta\frac{\partial\psi}{\partial y} & \delta\frac{\partial\psi}{\partial z}\end{bmatrix}\begin{bmatrix}\sigma_x & 0 & 0\\ 0 & \sigma_y & 0\\ 0 & 0 & \sigma_z\end{bmatrix}\begin{bmatrix}\frac{\partial\psi}{\partial x}\\ \\ \frac{\partial\psi}{\partial y}\\ \\ \frac{\partial\psi}{\partial z}\end{bmatrix}d\Omega \\ &= \int_{\Omega}[\delta\nabla\psi]\,\boldsymbol{\Sigma}\,[\nabla\psi]^T\,d\Omega \end{aligned}$$

Therefore, the required form is:

$$\int_{\Omega}[\delta\nabla\psi]\,\boldsymbol{\Sigma}\,[\nabla\psi]^T\,d\Omega = \int_{\Gamma_{e_1}}\{\delta\psi J_1\}\,d\Gamma_{e_1}-\int_{\Gamma_{e_2}}\{\delta\psi J_1\}\,d\Gamma_{e_2} \qquad (2.28)$$

Using the shape functions for a tetrahedron element:

$$\psi(x,y,z) = \mathbf{N}\boldsymbol{\psi}_\mathbf{e} \quad ; \quad \nabla\psi = \mathbf{N}'\boldsymbol{\psi}_\mathbf{e}$$

$$\delta\psi = \mathbf{N}\delta\boldsymbol{\psi}_\mathbf{e} \quad ; \quad \delta\nabla\psi = \mathbf{N}'\nabla\boldsymbol{\psi}_\mathbf{e}$$

where:

$$\boldsymbol{N} = \begin{bmatrix} N_i & N_j & N_k & N_l \end{bmatrix} \quad and \quad \boldsymbol{\psi}_e = \begin{bmatrix} \psi_i \\ \psi_j \\ \psi_k \\ \psi_l \end{bmatrix}$$

The weak form then can be transformed using finite element notation into a linear equations of the form:

$$\mathbf{K}\boldsymbol{\Psi} = \mathbf{Q} \tag{2.29}$$

corresponding to the sum of all the elements in the finite element mesh.

The solution of equation (2.29) needs the solution of simultaneous linear algebraic equations. This can be done either using direct or iterative methods. Most of the direct solvers are based on the Gauss elimination method. Iterative methods include basic iterative techniques that are based on relaxation of coordinates (examples are Jacobi, Gauss-Seidel and Successive Overrelaxation (SOR)) and projection

techniques such as the generalized minimal residual (GMRES) method (Saad and Schultz, 1986). Robustness is a weakness of the iterative solvers relative to direct solvers. However, preconditioning can improve both efficiency and robustness of iterative techniques. Preconditioning is done to transform the original linear system into one that has the same solution, but is likely to be easier to solve with an iterative solver. Incomplete LU and symmetric successive overrelaxation (SSOR) are examples of preconditioners. For further information on iterative solvers and preconditioners refer to Deuflhard et al. (1990), Freund (1993), Saad and Schultz (1986), Axelsson (1994), and Saad (1996).

2.4 Summary

Multichannel intraluminal impedance uses relatively low frequency, therefore the magnetic field effects can be ignored and the static formalism of Maxwell's equation can be used to solve the problem. The solution is then developed via Green's function approach. The solution developed in this chapter, however, is for a simple unrealistic cylindrical model. The solution for more complicated geometries will be more difficult to obtain and convergence of the solution is not guaranteed. However, numerical technique such as finite element method provides a mechanism to approximate the solution of the problem for more complicated geometries such as the shape of the esophagus, bolus shape, and inhomogeneous conductivities. In the

next chapter, the analytical solution obtained will be compared against the solution obtained from the finite element and the application of the finite element in the problem of MII will be explored in more detail.

Chapter 3

Computation of Impedance in the Esophagus

3.1 Introduction

In order to establish the feasibility of multiple intraluminal impedance for monitoring the esophagus, the various factors that affect the impedance are considered in this chapter. The factors that affect the impedance can be divided into the following:

- Design factors such as electrode length, inter-electrode spacing, channel spacing, and catheter radius.
- Biological factors such as esophagus status, mucosa membrane conductivity, esophagus wall thickness, and reflux characteristics such conductivity, volume, and propagation.

In addition to the evaluation of the analytical solution derived previously, the finite element method is also used to explore the impact of the various factors in the value of the impedance.

3.2 Analytical solution

The equation derived in Section 2.2 is the formula for the potential resulting from a line source for the simplified cylindrical model. The equation is given by:

$$\psi(\rho,\theta,z) = \frac{1}{2\pi^2}\sum_{n=1}^{N}\frac{I_n}{a\sigma_1}\int_{z_c-a/2}^{z_c+a/2}\int_0^{\infty}(K_0(\alpha\rho)+\kappa I_0(\alpha\rho))\times \cos(\alpha(z-z'))\ d\alpha dz' \tag{3.1}$$

Figure (3.1) shows the potential obtained from evaluation of equation (3.1) as a function of the distance from the center (ρ) at two Z values coinciding with those of the electrode locations. The boundary of the esophagus (or the bolus thickness) is assumed at $\rho_1 = 0.5\ cm$. The potential decreases from a high value (for the positive curve) as the observation point increases. Note the change in the potential at the boundary due to the boundary conditions.

The impedance as a function of conductivities inside and outside the esophagus ($\sigma_1 = 5\times10^{-3}S/cm$, and $\sigma_2 = 1\times10^{-3}S/cm$, respectively) is shown in Figure 3.2(a) and for conductivities: $\sigma_1 = 15\times10^{-3}S/cm$, and $\sigma_2 = 3\times10^{-3}S/cm$ see Figure 3.2(b).

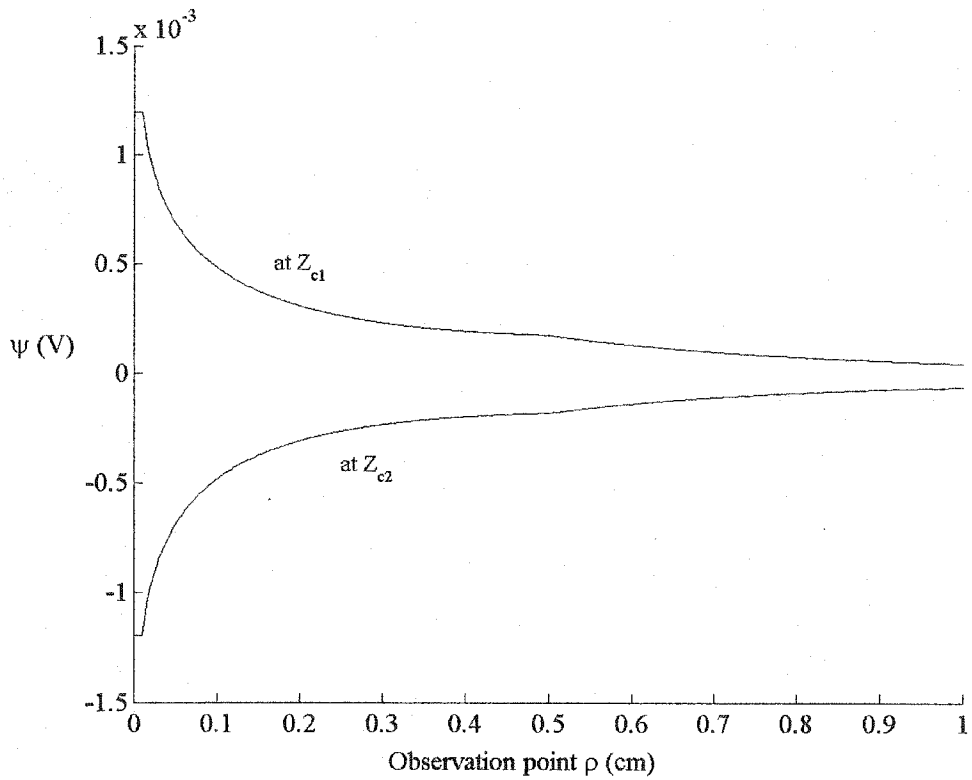

Figure 3.1: Potential obtained from a pair of electrodes as a function of distance from the center. The two curves show the potentials for two Z values coinciding with the electrode locations. Boundary of the esophagus is assumed at $\rho_1 = 0.5\ cm$.

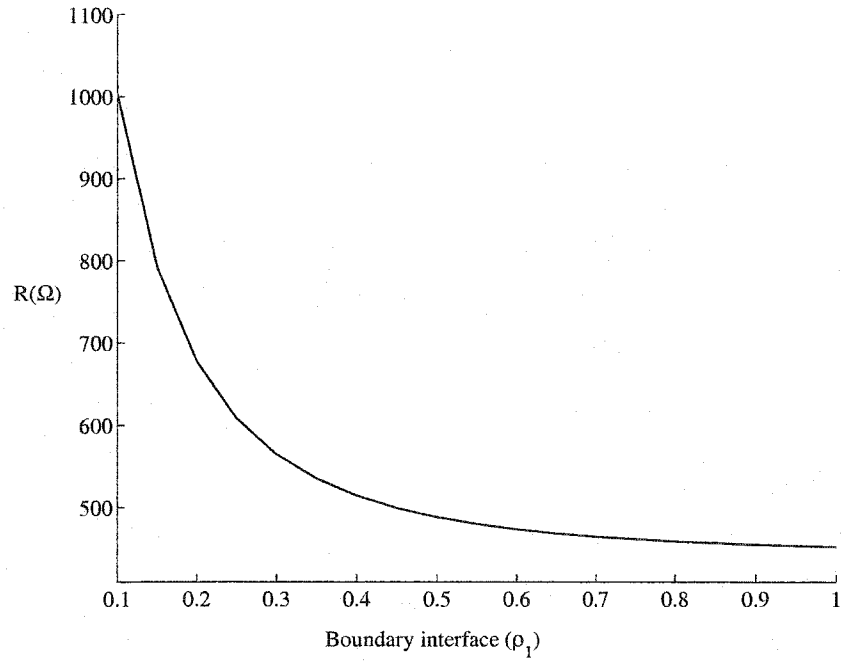

(a) Case 1:$\sigma_1 = 5 \times 10^{-3} S/cm$, and $\sigma_2 = 1 \times 10^{-3} S/cm$.

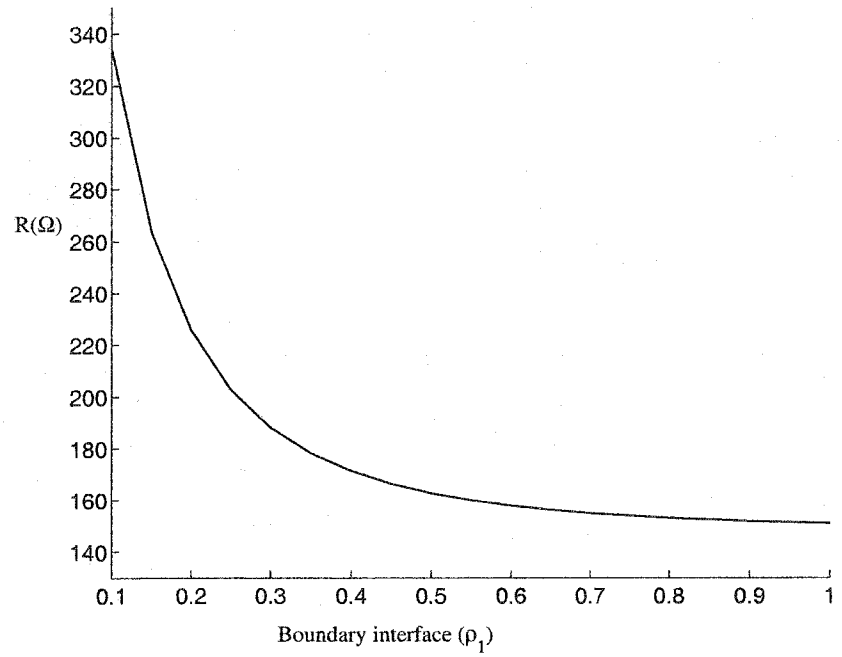

(b) Case 2:$\sigma_1 = 15 \times 10^{-3} S/cm$, and $\sigma_2 = 3 \times 10^{-3} S/cm$.

Figure 3.2: Impedance as a function of the bolus thickness, obtained from equation (2.15).

3.3 Numerical solution

The finite element technique is very useful in modeling the realistic geometry of the catheter inside the esophagus for the following reasons:

- Esophagus is not a perfect cylinder.
- Bolus shape is not a perfect cylinder.
- Inhomogeneity in the conductivities.
- Finite dimensions of the catheter.
- Finite dimensions of the electrodes and finite conductivity.

The ability to model realistic and non-ideal observation conditions is demonstrated in the following: Let the esophagus wall thickness be 0.1 *cm* and a bolus be of spheroidal shape. The axis of the spheroid is aligned along the electrodes. Spheroidal shapes were chosen because they can represent a wide variety of bolus shapes depending on the axis ratio. The minor axis of the bolus varies from 0.1 *cm* to 1 *cm*, while the major axis is kept constant at 1 *cm*. The model configuration is shown in Figure (3.3(a)). Figure (3.3(c)) shows the variability of impedance as a function of the minor axis of the spheroid (or the thickness of the bolus). Figure (3.3(d)) shows the impedance as a function of the bolus's minor axis while keeping the volume of the bolus fixed. Figures (3.3(a),and 3.3(c)) show that as the bolus thickness increases, the impedance decreases.

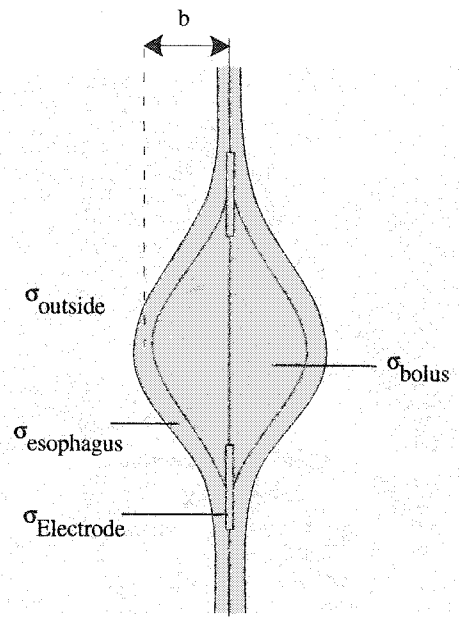

(a) Model of spheroidal bolus, with finite thickness of the esophagus.

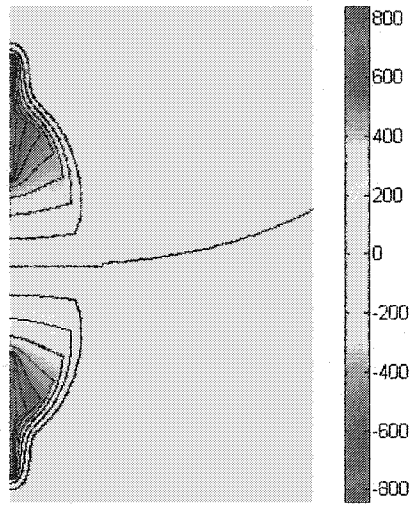

(b) Potential map and contour of the equipotential surfaces (cut through the center in one plane and zoomed around the electrodes) for an excitation current of 1A.

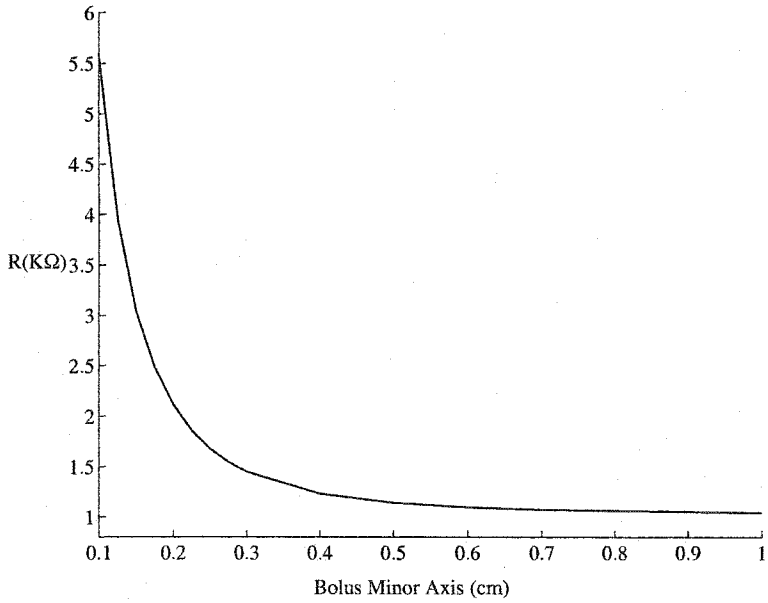

(c) Impedance as a function of bolus minor axis keeping the major axis fixed.

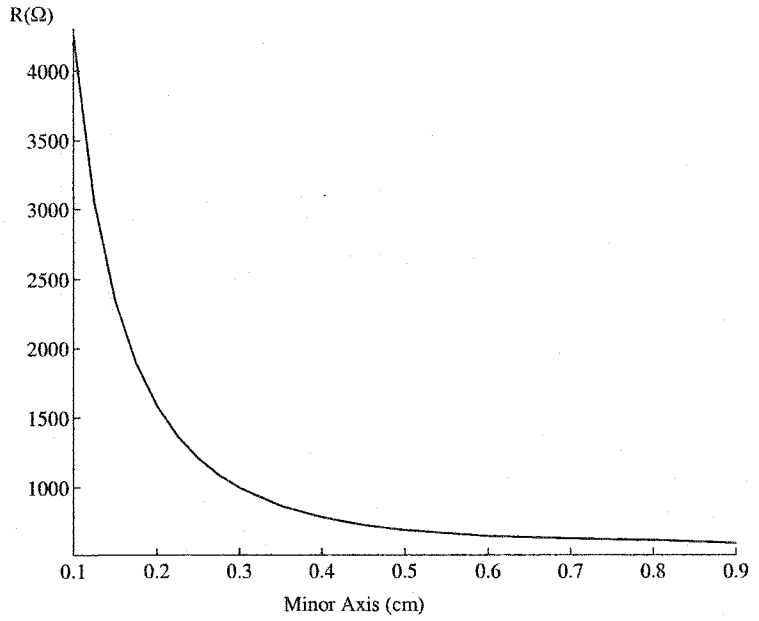

(d) Impedance as a function of bolus minor axis keeping the bolus volume fixed.

Figure 3.3: Examples of the cases of the bolus around the catheter (cylindrical coordinate), electrodes thickness = 0.008cm. Electrodes are of steel material carrying current of 4 μA, esophagus thickness 0.1 cm with conductivity of 5×10^{-6} S/cm, the outside layer conductivity 1×10^{-3} S/cm, and the bolus conductivity 5×10^{-3} S/cm.

3.3.1 Line sources

The difference between the finite element solution and the analytical solution for the two simple cylindrical model considered in the previous section was negligible (less than 0.025%). Figure (3.4(a)) shows a sample of the mesh generated from the finite element program and Figure (3.4(b)) shows a cut through the cylinder. On the other hand, Figure (3.5) shows the conductivity map obtained from applying the point form of Ohm's low. In the following section the finite element method is used to investigate the various factors that affect the impedance using a realistic model for the bolus volume and a catheter with electrodes that are of steel material and have finite thickness.

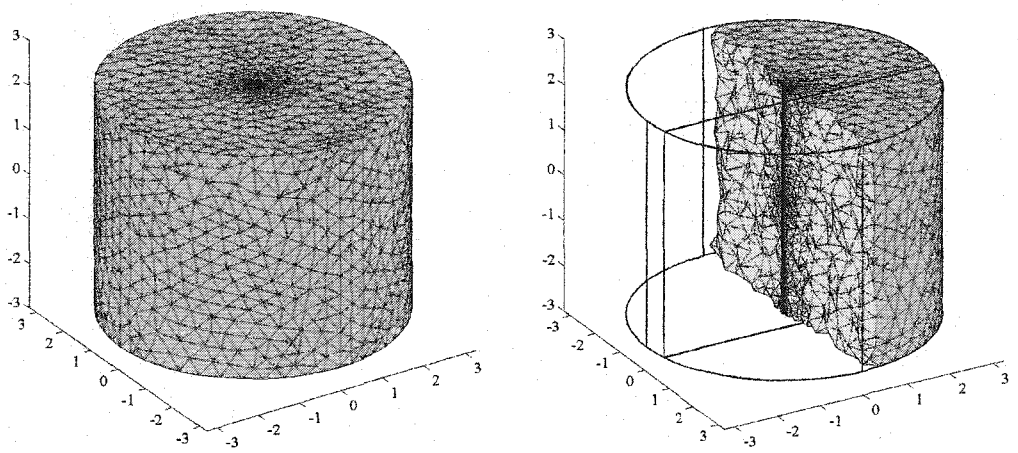

(a) Top view of the mesh generated (b) Cut through the mesh generated

Figure 3.4: Mesh generated for finite element computation (FEM, 2003).

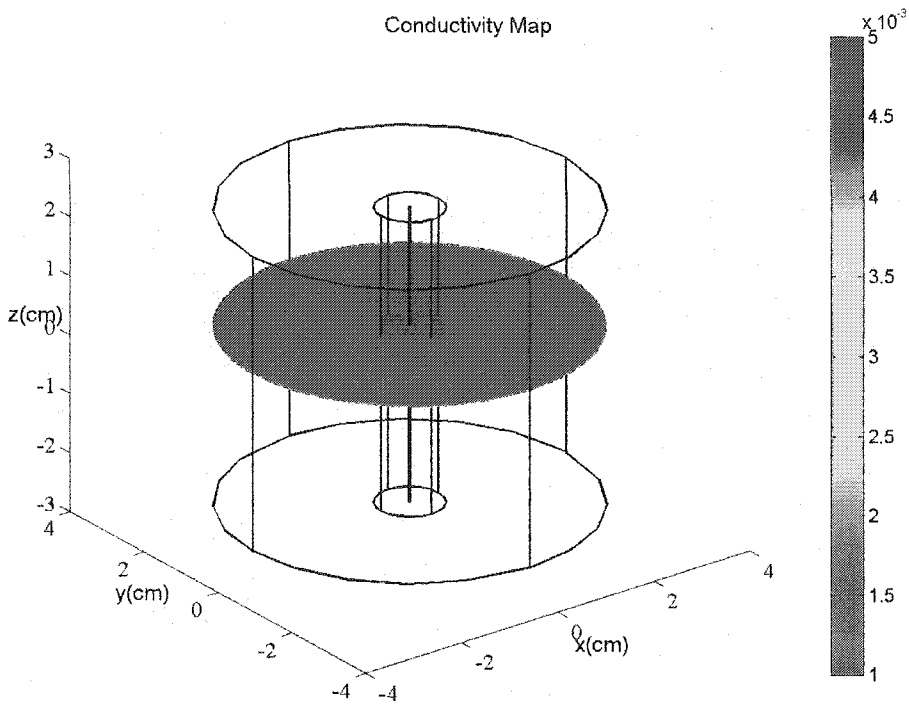

Figure 3.5: Conductivity map obtained from the application of the point form of Ohm's law ($\sigma = \frac{J}{E}$) for the case of bolus conductivity 5×10^{-3} and outside layer conductivity 1×10^{-3}.

3.4 Electrodes location

Inter-electrode spacing is defined as the space between the electrodes. This is an important parameter that determines the number of channels used in the catheter and the minimum bolus length that can be detected. The catheter is assumed to have a radius of 0.05 cm and a 4 mm electrode length. The esophagus is assumed to be of 0.3 cm thickness and to have a conductivity of $1.27 \times 10^{-3} S/cm$, the bolus material is assumed to have a conductivity of $15.5 \times 10^{-3} S/cm$. The outer layer has a conductivity of $9 \times 10^{-4} S/cm$. Figure (3.6) shows the impedance obtained from the FE solution for two cases: case (1) without any bolus material between

the two electrodes is shown in Figure (3.6(a)) and case (2) with bolus material of radius 0.5 cm is shown in Figure (3.6(b)). Figures (3.6(a),and 3.6(b)) show that the impedance increases with increasing electrodes spacing and it can be seen that the change in impedance is large between the conditions of no bolus material and the presence of bolus. The exact numerical values depend on the esophagus and the various conductivities in the model. The ratio of the impedance between the absence and presence of bolus is plotted as a function of the electrode spacing for various esophagus conductivities is shown in Figure (3.6(c)). This family of curves can be used as rudimentary design curves where the electrodes spacing can be chosen to provide a certain level of impedance variation with bolus.

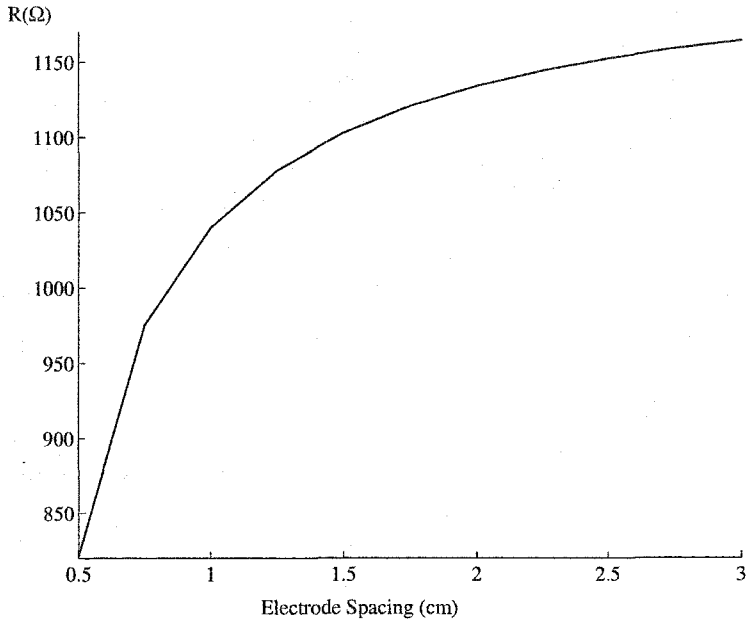

(a) Case of no bolus material, esophagus thickness is 0.3 cm and electrodes thickness = 0.008 cm.

Figure 3.6: Impedance as a function of inter electrode spacing

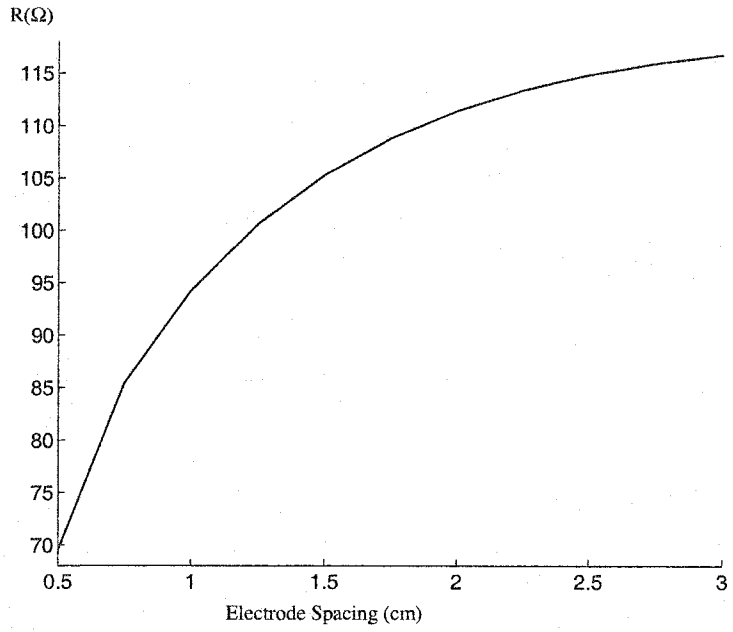

(b) Case with bolus material of conductivity $\sigma = 15.5 \times 10^{-3}$ and radius of 0.5 cm, esophagus thickness is 0.3 cm and electrodes thickness = 0.008cm.

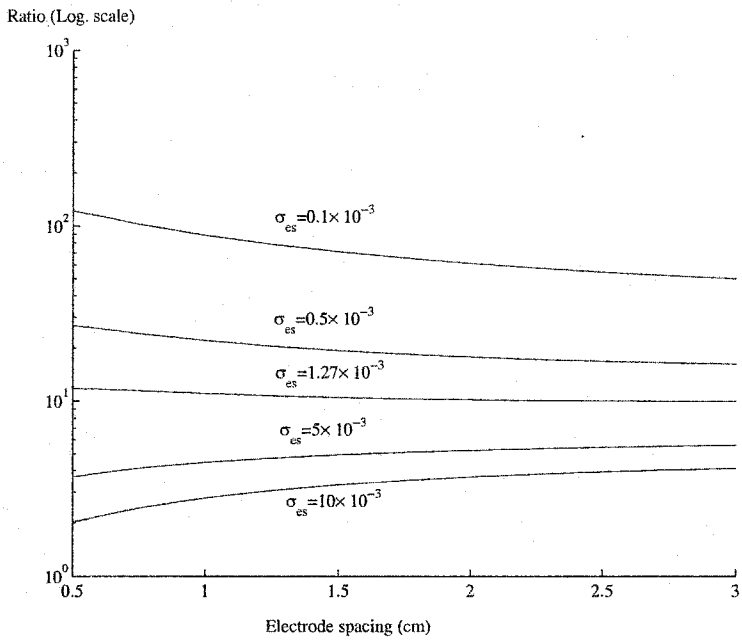

(c) Ratio of the impedance between the absence and presence of bolus as a function of the electrode spacing for various esophagus conductivities.

Figure 3.6: (Cont.) Impedance as a function of inter electrode spacing.

3.4.1 Catheter diameter

Catheter diameter is determined by the the following:

- Mechanical constraints.
- The catheter must not impair the GIT function.

The following analysis evaluates the effect of accounting for finite catheter size. The catheter radius is studied for an example where the electrode length is 4 *mm* and electrodes spacing 2 *cm*. The cases of absence and presence of bolus were studied. Figure (3.7(a)) shows the impedance obtained in the absence of bolus, whereas Figure (3.7(b)) shows impedance when there is bolus present. In both Figures (3.7(a), and 3.7(b)), the esophagus radius is 0.5 *cm*. It can be seen from Figure (3.7) that the impedance changes with the catheter radius. An important design factor of the catheter is that it must not impair the esophagus function (Silny, 1991); therefore, the selection of the catheter radius must be made as small as possible while ensuring that sufficient impedance variation can be observed. The ratio of the impedance between the absence and presence of bolus is plotted as a function of the catheter radius for various esophagus conductivities, is shown in Figure (3.7(c)). It can be clearly seen from Figure (3.7(c)) that the sensitivity to catheter size is not very high, and therefore one can design the smallest possible catheter.

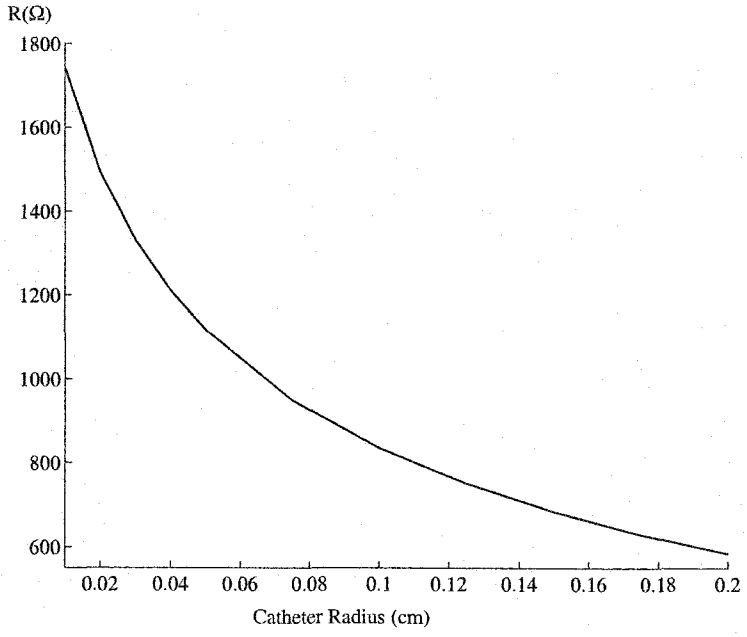

(a) Case of no bolus material, esophagus thickness is 0.3 cm and electrodes thickness= 0.008cm.

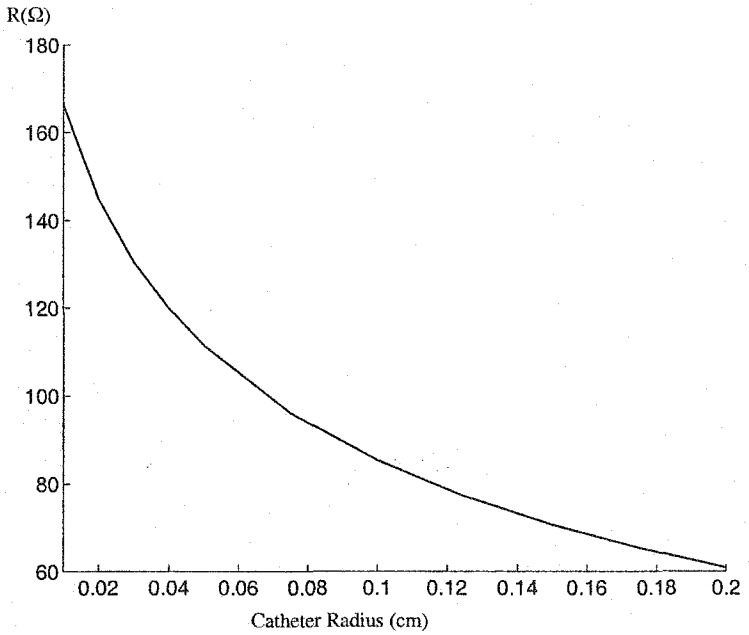

(b) Case with bolus material of conductivity $\sigma = 15.5 \times 10^{-3}$ and radius of 0.5 cm, esophagus thickness is 0.3 cm and electrodes thickness = 0.008cm.

Figure 3.7: Impedance as a function of catheter radius.

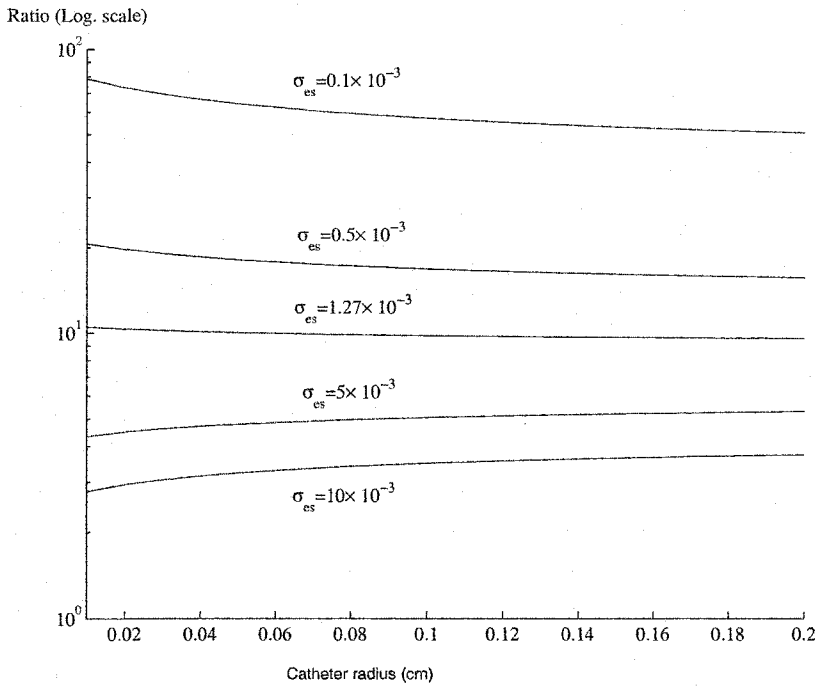

(c) Ratio of the impedance between the absence and presence of bolus as a function of the catheter radius for various esophagus conductivities.

Figure 3.7: (Cont.) Impedance as a function of catheter radius.

3.5 Modeling of electrical properties of the esophagus

The following assumptions are made in the model so that it resembles the actual environment of the catheter inside the esophagus based on the characteristics of the MII signals that have been obtained from normal subjects and individuals who are undergoing an abnormal number of reflux episodes:

- Normal esophagus thickness is 0.3 cm and consists of two layers:
  1. Mucous membrane layer that has thickness of 0.008 cm and has a conductivity of $\sigma_{mm} = 6.2 \times 10^{-6}\ S/cm$.
  2. Second layer that has a conductivity of $\sigma_{mm} = 5.2427 \times 10^{-3}\ S/cm$.
- Patient esophagus has the same setup but the mucous membrane conductivity has changed to $\sigma_{mm} = 6.2 \times 10^{-5}\ S/cm$.
- Conductivities of the tissues surrounding the esophagus are given by $\sigma_o = 9 \times 10^{-4} + \frac{10^{-3}}{z+2.1}$ so that the lower part of the esophagus, which is at $z = 0$, has the a higher conductivity and decreases as the observation point is moved up.
- The bolus or refluxate material has a conductivity $\sigma_r = 15.5 \times 10^{-3}\ S/cm$.

The above assumption of conductivities is based on the values obtained from (Gabriel et al., 996a,b; IFAC-CNR, 2002; Geddes and Baker, 1967). The patient mucosa membrane conductivity has been changed because reflux episodes lead to erosion and ulceration of esophageal mucosa.

Figure (3.8) shows the model of the catheter that is used in the simulation and Figure (3.9) shows the resulting finite element mesh. Figure (3.10) shows the potential map resulting from the activation of all the channels.

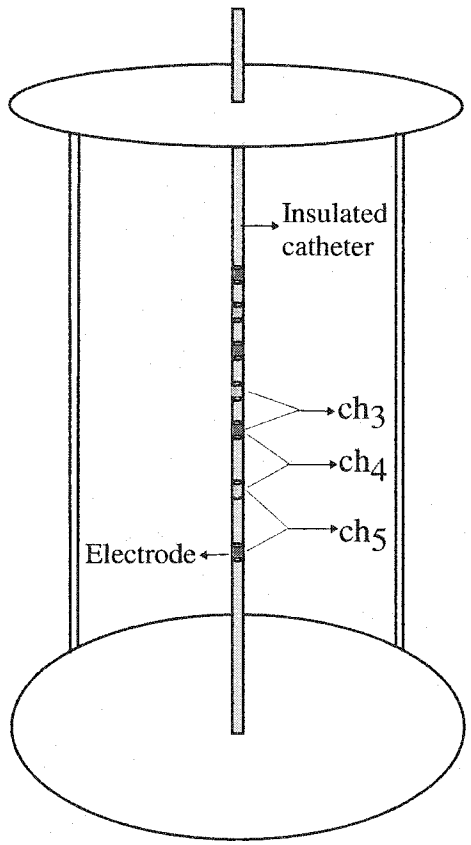

Figure 3.8: The basic model used in the study of the impact of the various parameters on the impedance.

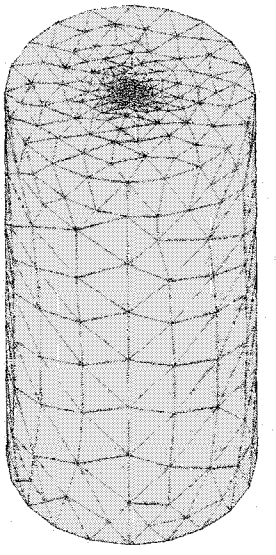

(a) Top view of the mesh.

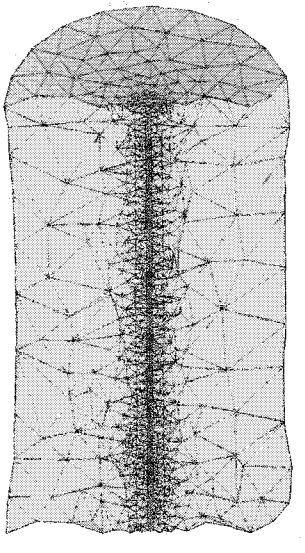

(b) Cut through the mesh.

Figure 3.9: Mesh used in the FE.

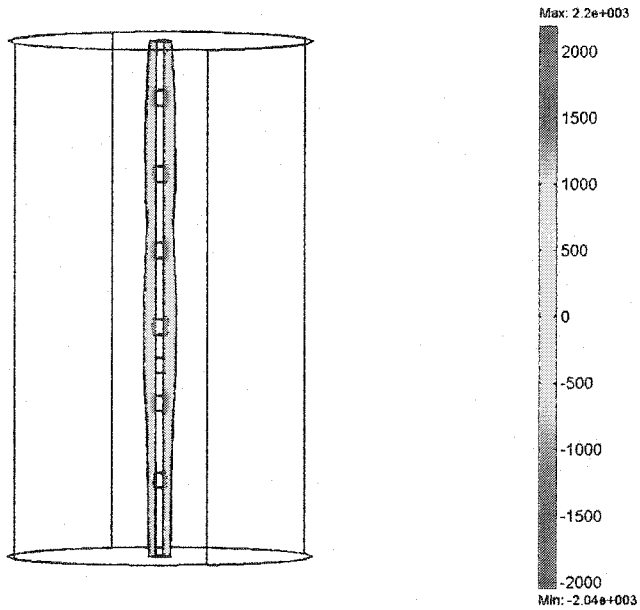

Figure 3.10: Example of the potential map obtained from activation of all the channels. Note that the figure is a cut at the center.

When a reflux episode occurs, the impedance decreases to the level of the gastric contents impedance. The decrements of impedance to that level is dependent on the refluxate material location with respect to the electrodes of the channel. Initially, the impedance drops to half the patient impedance (impedance in the absence of any material between the two electrodes) when the refluxate material reaches the first electrode. The impedance reaches to the gastric contents impedance level when the refluxate reaches the second electrode. This pattern is repeated in all the channels to which the reflux reaches. When the refluxate returns back to the stomach, the impedance increases to about half its baseline value once the refluxate leaves the second electrode of the channel. The impedance reaches to its baseline value when the refluxate leaves the first electrode of the channel. This is can be seen clearly in Figure (3.11(a)), which shows the impedance of the four distal channels from a six channel MII system as the refluxate material propagates into the esophagus. The x-axis represents the distance that the refluxate reaches (note that it is a nonuniform sampling of distance). The refluxate is assumed to be continuous and the esophagus is assumed to be normal. Figure (3.11(b)), on the other hand, shows real MII data obtained from a normal subject during a reflux episode. Note that the speed of the reflux can be determined by measuring the time the refluxate takes from point e_{1s} to any other point, say e_{3s}. The differences seen between the simulation results and the real data are due to the differences in the conductivities and to the changes of the esophagus with time.

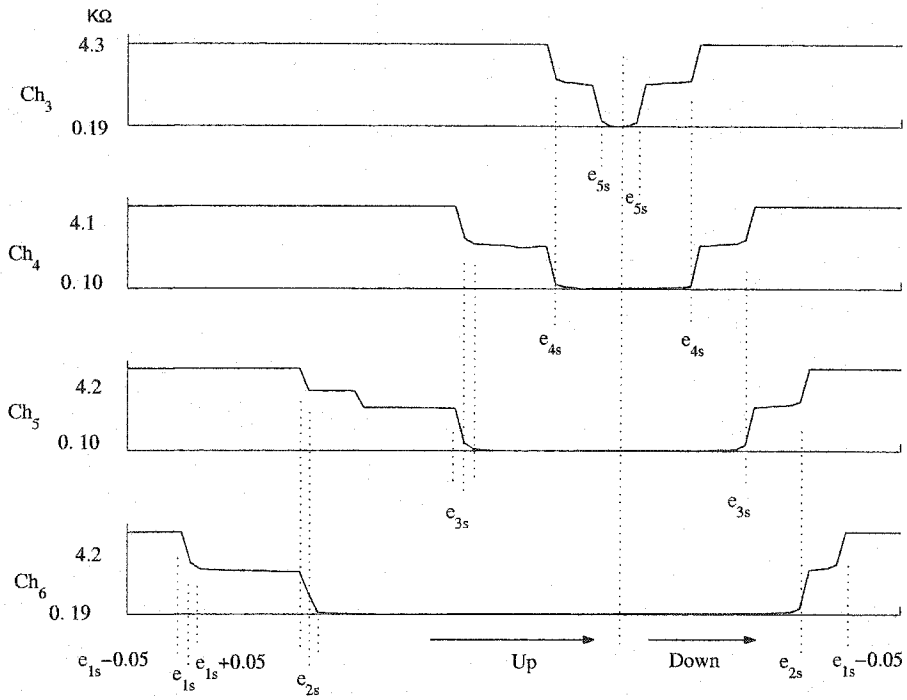

(a) Typical impedance traces during a reflux episode obtained from simulation. e_{1s} is the distance from the lower esophageal sphincter to the start of the electrode number 1, e_{2s} is the same but for electrode number 2 and so on. The region marked (Up) indicates that the refluxate material is propagating upwards while the region marked (Down) indicates the return of the refluxate to the stomach.

Figure 3.11: Reflux patterns: (a) results of finite element analysis; (b) real data obtained from normal esophageal condition.

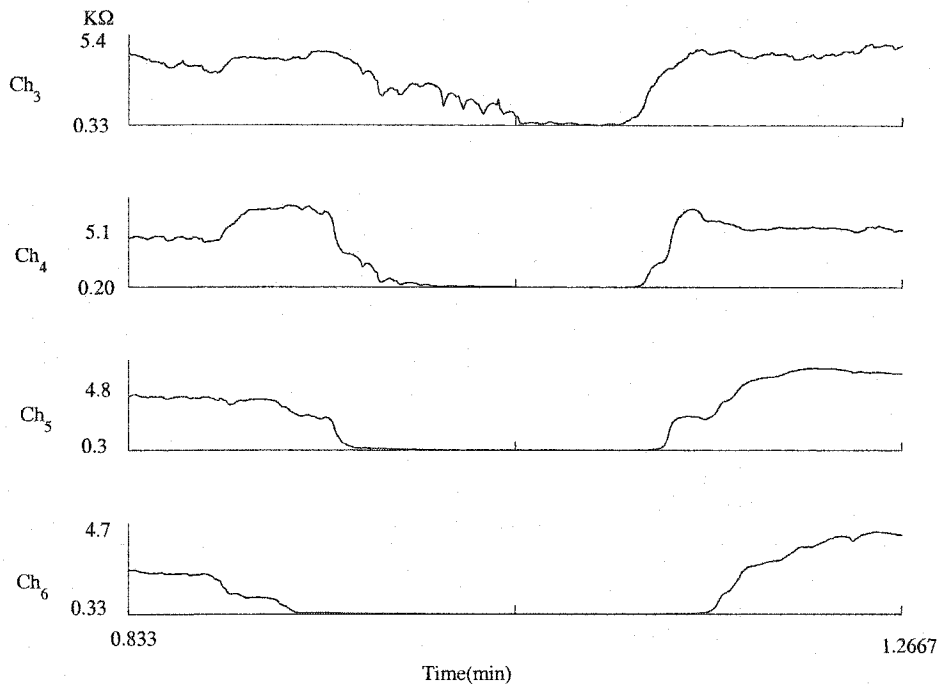

(b) Typical impedance traces during a reflux episode obtained from patient due to a continuous refluxate. Note the similarities between the simulation and the real data. The values of the impedance are patient-dependent (esophagus and bolus conductivities.)

Figure 3.11: (Cont.) Reflux patterns: (a) results of finite element analysis; (b) real data obtained from normal esophageal condition.

3.5.1 Esophagus thickness

The mucosa membrane appears to be the most significant part of the esophagus that determines the impedance in normal subjects and drives the patient impedance to a low value in esophagitis patients (mucosa membrane characteristics have been changed because acid reflux episodes lead to erosion and ulceration of esophageal mucosa and probable inflammation). This is demonstrated in Figure (3.12), where the impedance of each channel of the system is shown as a function of the esophagus thickness with constant mucosa membrane thickness and the outer layers conductivities were assumed as described in Section (3.5). It can be seen that the relative change of impedance with esophagus wall thickness may have more influence on the patient's impedance than on normal subjects.

3.5.2 Catheter position

The catheter may not be centered inside the esophagus, and thus the refluxate material may be in touch with the catheter on one of its sides while the other side touchs the esophagus. When this situation is modeled for both patient and normal subjects, the effect of the catheter position results in an impedance change that is acceptable to indicate bolus entrance into the channel region of effect unless the refluxate thickness is very small. This is shown in Figure (3.13).

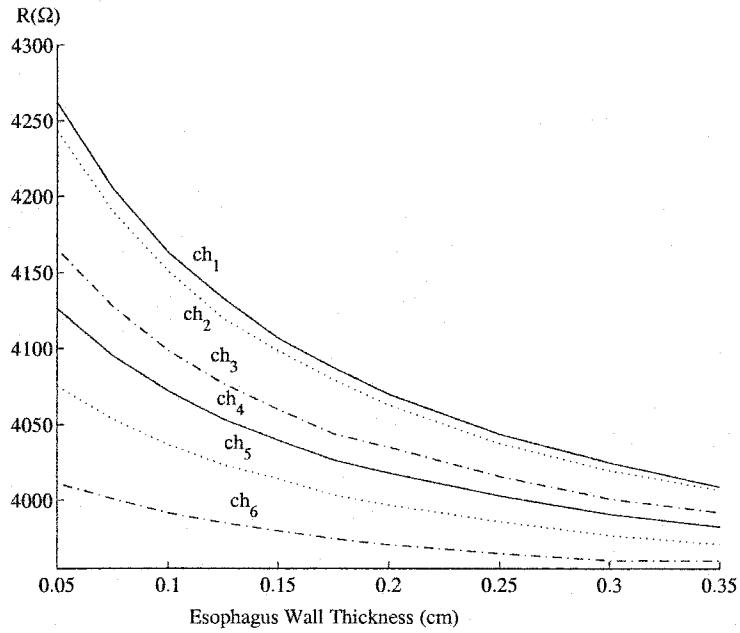

(a) Normal subject : $\sigma_{mm} = 6.2 \times 10^{-6}$ $\sigma_{es} = 5.24 \times 10^{-3}$.

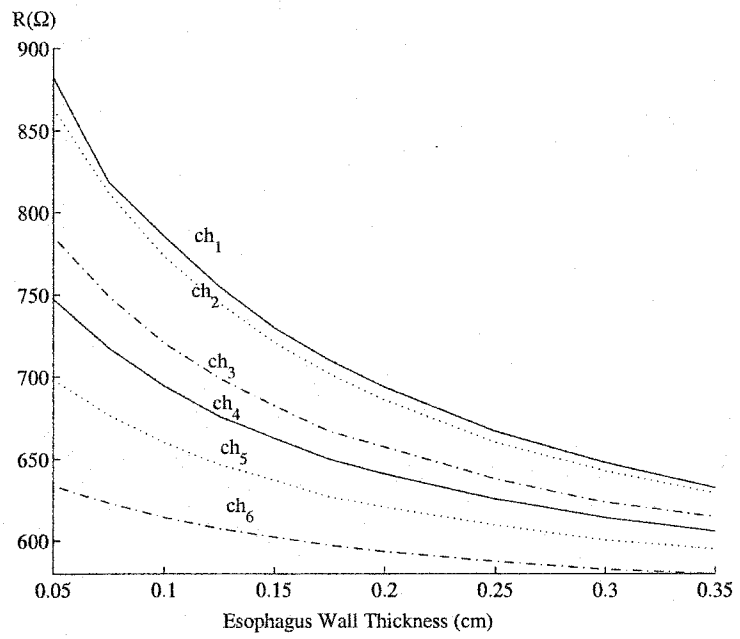

(b) Patient subject : $\sigma_{mm} = 6.2 \times 10^{-5}$ $\sigma_{es} = 5.24 \times 10^{-3}$.

Figure 3.12: Resistance as a function of the esophagus wall thickness: catheter diameter=2.13 mm, electrode length=4 mm, electrode thickness=0.008 mm, and mucosa membrane thickness=0.008 mm.

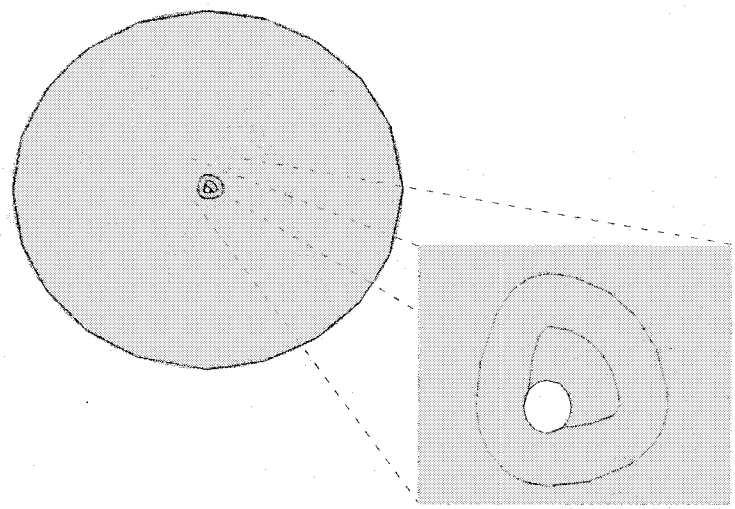

(a) Top view of the model used for the study of the catheter position-centered and non-centered catheter position.

Figure 3.13: Model used in the simulation of the centered and non-centered catheter inside the esophagus.

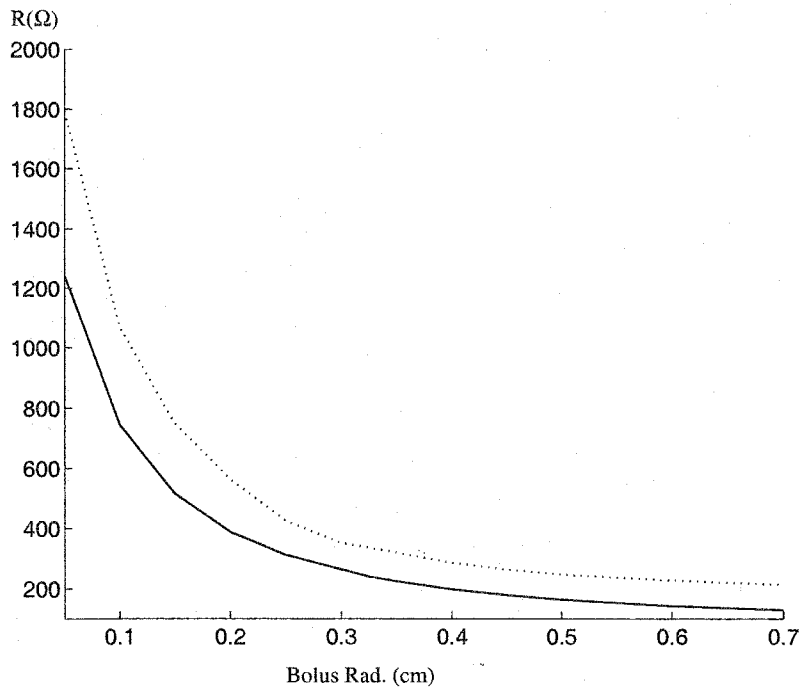

(b) Resistance comparison of centered and non-centered catheter: Normal esophagus case: Electrode length: 0.4cm, inter-electrode spacing=2cm, electrode thickness=0.01cm.

Figure 3.13: (Cont.) Model used in the simulation of the centered and non-centered catheter inside the esophagus.

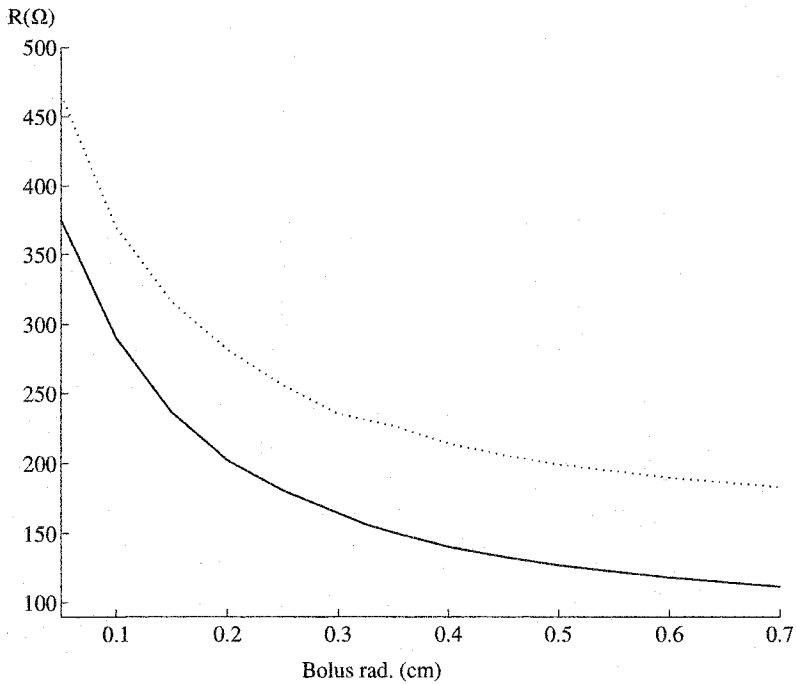

(c) Resistance comparison of centered and non-centered catheter: Patient esophagus case: Electrode length: 0.4cm, inter-electrode spacing=2cm, electrode thickness=0.01cm.

Figure 3.13: (Cont.) Model used in the simulation of the centered and non-centered catheter inside the esophagus.

3.5.3 Catheter diameter

As was described previously, the catheter diameter must be chosen such that the catheter does not effect the GIT function. This certain care in designing the catheter as shown in the following: Figure (3.14(a)) shows the change in impedance in ch_1 as a function of the catheter diameter in normal esophagus conditions and in the absence of any bolus material between the two electrodes of the channel, while Figure (3.14(b)) shows the change when a bolus material of thickness 1 cm enters the space between the two electrodes. It can be seen that there is a large change in impedance at every catheter diameter if a bolus material enters into the channel region of effect. However, under severe esophagus damage (the case with mucous membrane change), the change in impedance decreases as the catheter diameter increases, indicating that the catheter diameter has to be as small as possible in order to see the changes resulting from the presence of reflux material in the channel region of effect. This is demonstrated in Figure (3.14(c)) and Figure (3.14(d)).

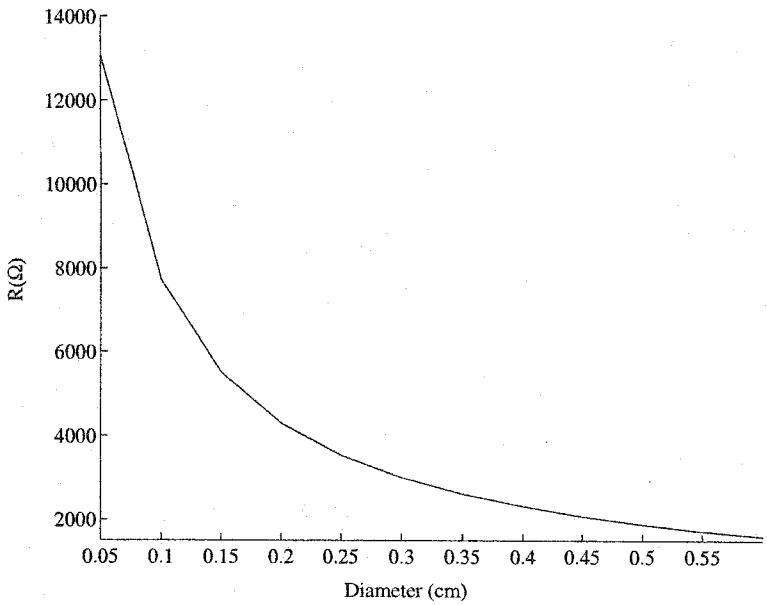

(a) Case of normal subject without any bolus material, and $\sigma_e s = 5.24 \times 10^{-3}$ and $\sigma_{mm} = 6.2 \times 10^{-6}$.

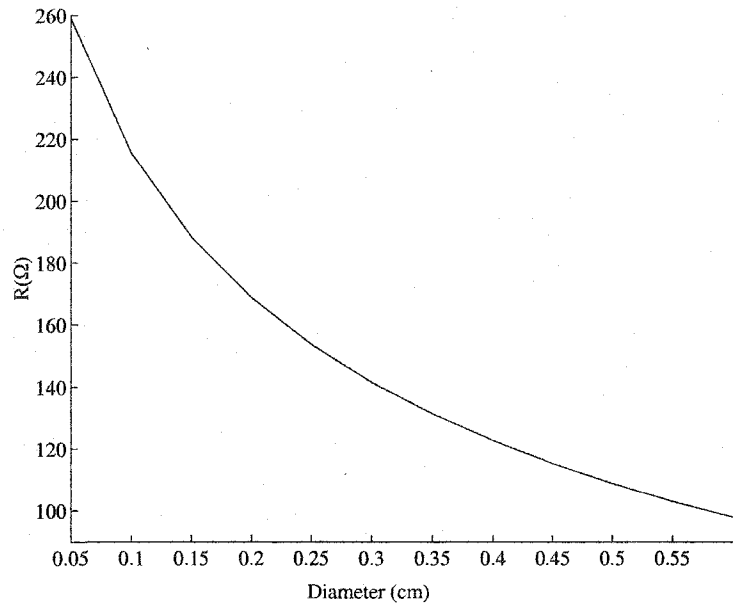

(b) Case of normal subject with bolus material (diameter=1cm), $\sigma_b = 10 \times 10^{-3}$, $\sigma_e s = 5.24 \times 10^{-3}$ and $\sigma_{mm} = 6.2 \times 10^{-6}$.

Figure 3.14: Resistance as a function of catheter diameter.

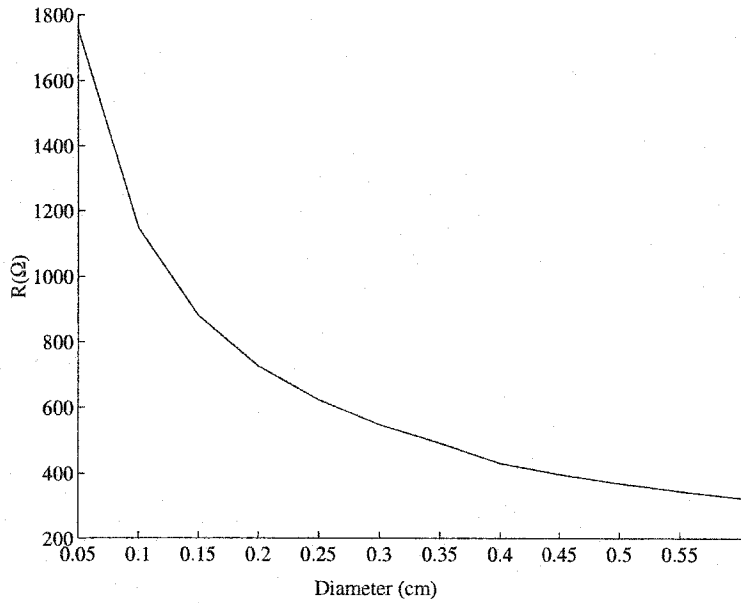

(c) Case of patient subject without any bolus material, and $\sigma_e s = 5.24 \times 10^{-3}$ and $\sigma_{mm} = 6.2 \times 10^{-5}$.

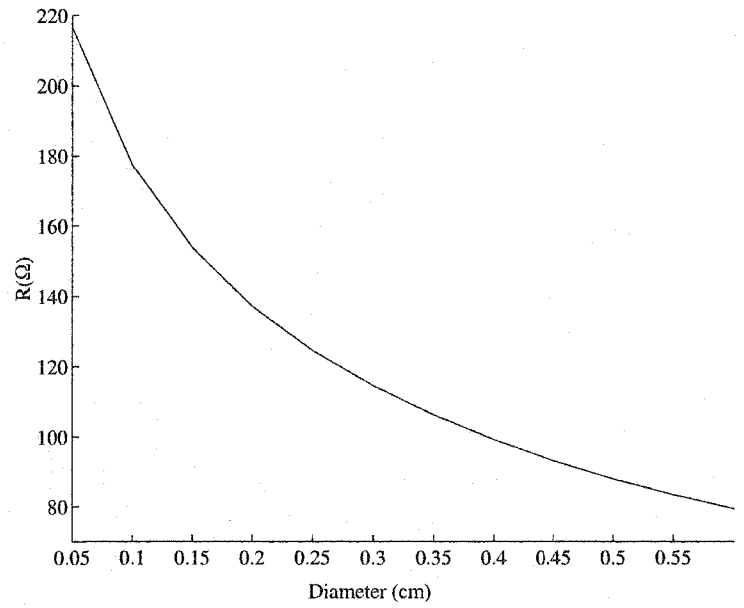

(d) Case of normal subject with bolus material (diameter=1cm), $\sigma_b = 10 \times 10^{-3}$, $\sigma_e s = 5.24 \times 10^{-3}$ and $\sigma_{mm} = 6.2 \times 10^{-6}$.

Figure 3.14: (Cont.) Resistance as a function of catheter diameter.

3.5.4 Length of electrode

It is not only the catheter diameter that has an effect on the impedance value but also the electrode length. There are also some constraints on the electrode length which include: mechanical constraints, electrode spacing, and the number of channels in the system. The impact of electrode length on impedance value is demonstrated in the following: Figure (3.15(a)) shows the change in impedance of ch_1 as a function of the electrode length for a normal esophagus condition and in the absence of any bolus material between the two electrodes of the channel, while Figure (3.15(b)) shows the change when a bolus material of thickness 1 cm enters the space between the two electrodes. Under severe esophagus damage (the case with mucous membrane change), then the change in impedance decreases as the electrode length increases, indicating that the electrode length has to be as small as possible in order to see the change when a reflux episode occurs. This is demonstrated in Figure (3.15(c)) and Figure (3.15(d)).

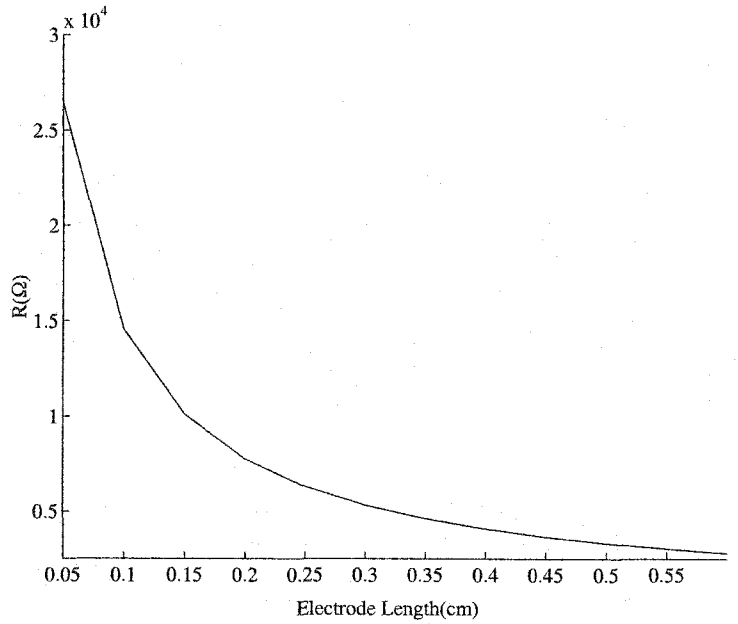

(a) Case of normal subject without any bolus material, and $\sigma_e s = 5.24 \times 10^{-3}$ and $\sigma_{mm} = 6.2 \times 10^{-6}$.

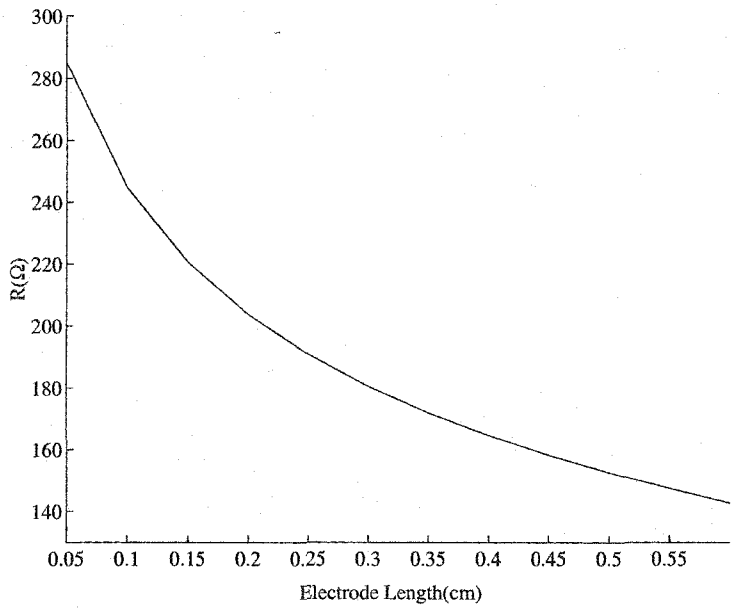

(b) Case of normal subject with bolus material (diameter=1cm), $\sigma_b = 10 \times 10^{-3}$, $\sigma_e s = 5.24 \times 10^{-3}$ and $\sigma_{mm} = 6.2 \times 10^{-6}$.

Figure 3.15: Resistance as a function of electrode length.

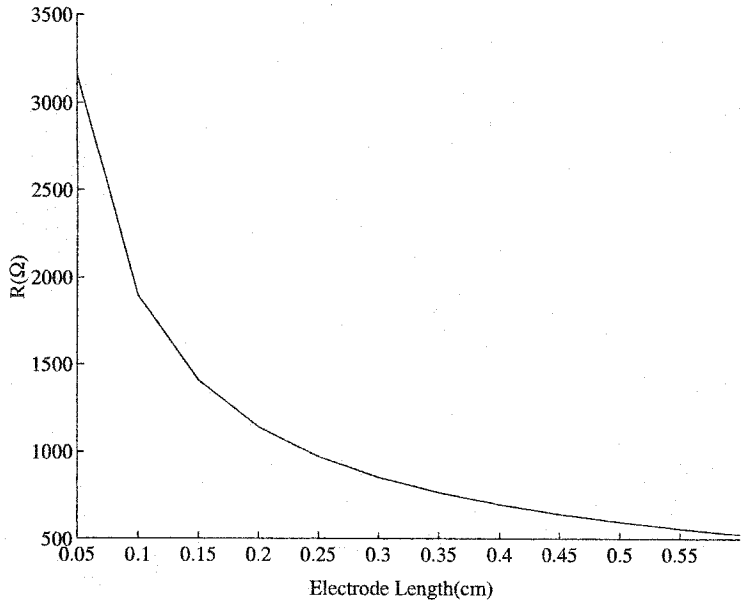

(c) Case of patient subject without any bolus material, and $\sigma_e s = 5.24 \times 10^{-3}$ and $\sigma_{mm} = 6.2 \times 10^{-5}$.

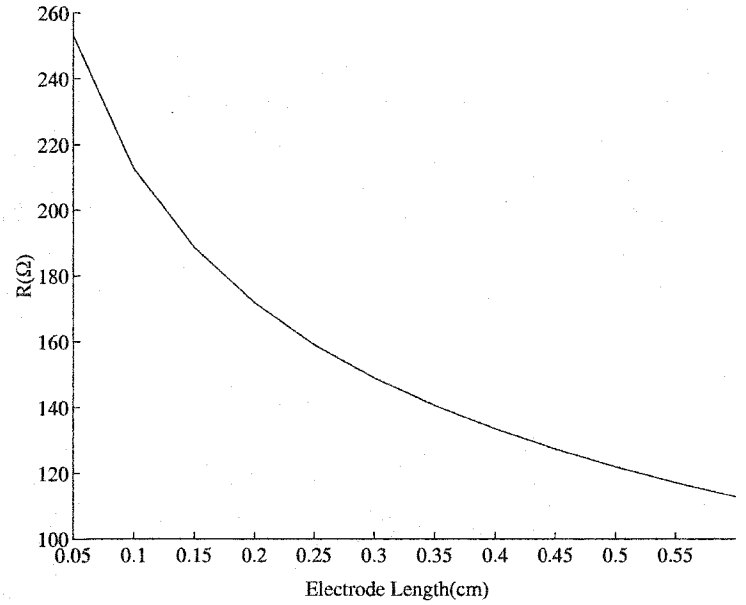

(d) Case of normal subject with bolus material (diameter=1cm), $\sigma_b = 10 \times 10^{-3}$, $\sigma_e s = 5.24 \times 10^{-3}$ and $\sigma_{mm} = 6.2 \times 10^{-6}$.

Figure 3.15: (Cont.) Resistance as a function of electrode length.

3.6 Summary

In this chapter, the impact of various biological properties as well as the probe characteristics on the impedance was presented. The important findings can be summarized as follows:

- Design Considerations:
  - Catheter radius as small as possible.
  - Channels spacing chosen based on the minimum bolus length to be detected and the number of channels in the system.
  - Electrode length chosen to be as small as possible.
  - Electrodes spacing for each channel chosen to be as small as possible (minimum electrode spacing for each channel possible 0.6 cm).

  These design considerations are affected by the esophagus condition. It was shown that for a severely damaged esophagus they have to be satisfied for at least the two most distal channels, and that is always limited by mechanical construction and of course the cost of building disposable catheters.

Chapter 4

MII Signals and Analysis of Esophageal Episodes

4.1 Introduction

It was shown earlier in this thesis that when a reflux episode occurs, the impedance decreases to the level of the gastric contents impedance. The decrements of impedance to that level is dependent on the refluxate material location with respect to the electrodes of the channel. Figure (4.1) shows a reflux episode as seen in ch_6 and ch_5. The important parameters that are used to distinguish reflux from any other activity are shown also in the Figure. These parameters are the impedance in the absence of any activity such as swallow or reflux (refereed to as patient impedance (Z_p) or baseline impedance), The minimum impedance reached during the episodes and is refereed to as the gastric contents impedance Z_c, the value of the impedance drop, and the propagation direction. These characteristics are not always clear and visible due many factors including noise level, movement artifact, esophagus impedance, type of gastric contents, and refluxate speed.

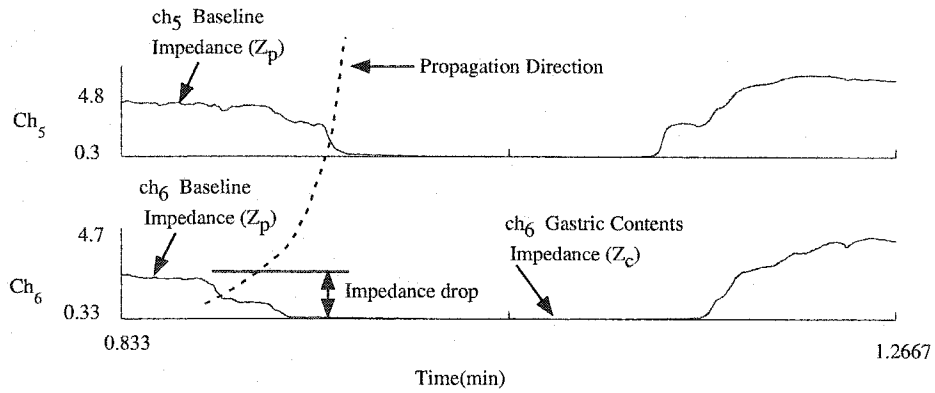

Figure 4.1: Typical impedance traces during a reflux episode obtained from patient due.

4.2 Characteristics of reflux episodes

Gastroesophageal reflux episodes are seen in MII as an impedance change from a baseline impedance to the level of gastric contents impedance. Figure (4.2) shows sample impedance traces observed over various observation points along the esophagus. Note the leading edge of the decreased impedance (i.e., the "inverse pulse" shape) can be seen to have a movement from ch_6 (distal) to ch_1 (proximal), indicative of bolus movement in that direction. The combination of drop in impedance values and the direction of movement of the "inverse pulse" indicates that it is a reflux. However, the direction of movement may not be easily determined. This

can be seen in the example shown in Figure (4.3) where the reflux propagation direction, and the possible swallow direction are marked as shown. In such cases, it is very difficult to classify this episode as a reflux from the value of the impedance drop and propagation direction. Since possible swallow is involved in the interpretation of the episode, further characteristics such as the delay between successive channels, the speed of reflux clearance, the distance to which the reflux reaches, and the minimum impedance reached compared to other reflux episodes minimum must be considered.

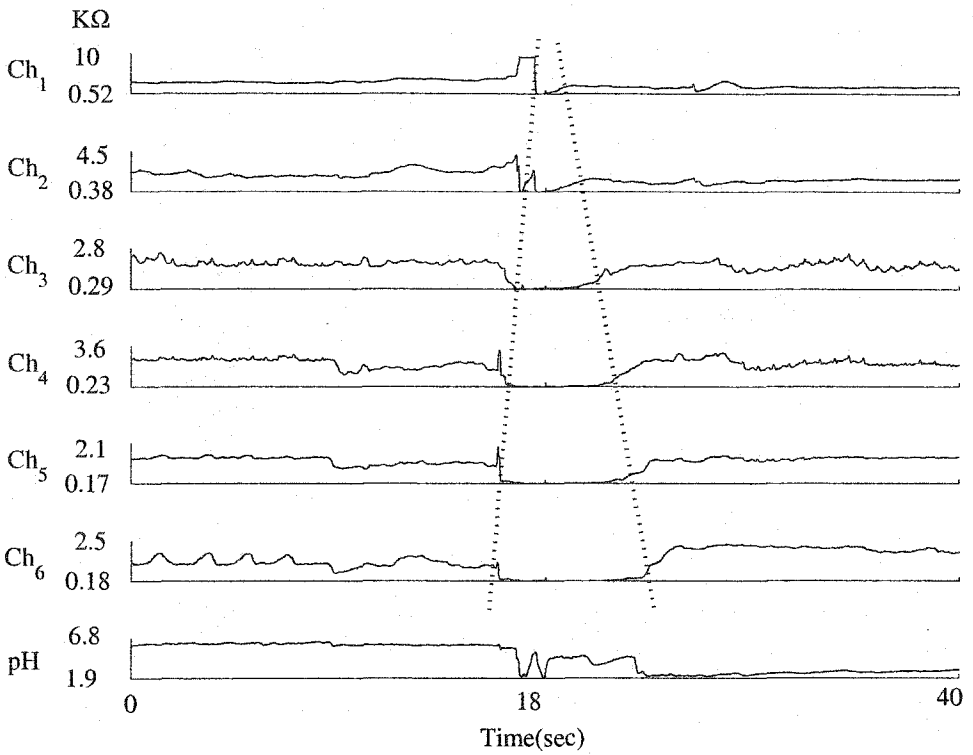

Figure 4.2: Typical impedance signals along with one pH channel: dotted line shows a region where a reflux episode occurs. The common abscissa of the graphs is time and the various ordinates are the various impedance values. Note the propagation direction of the inverse pulse shape starting from ch_6.

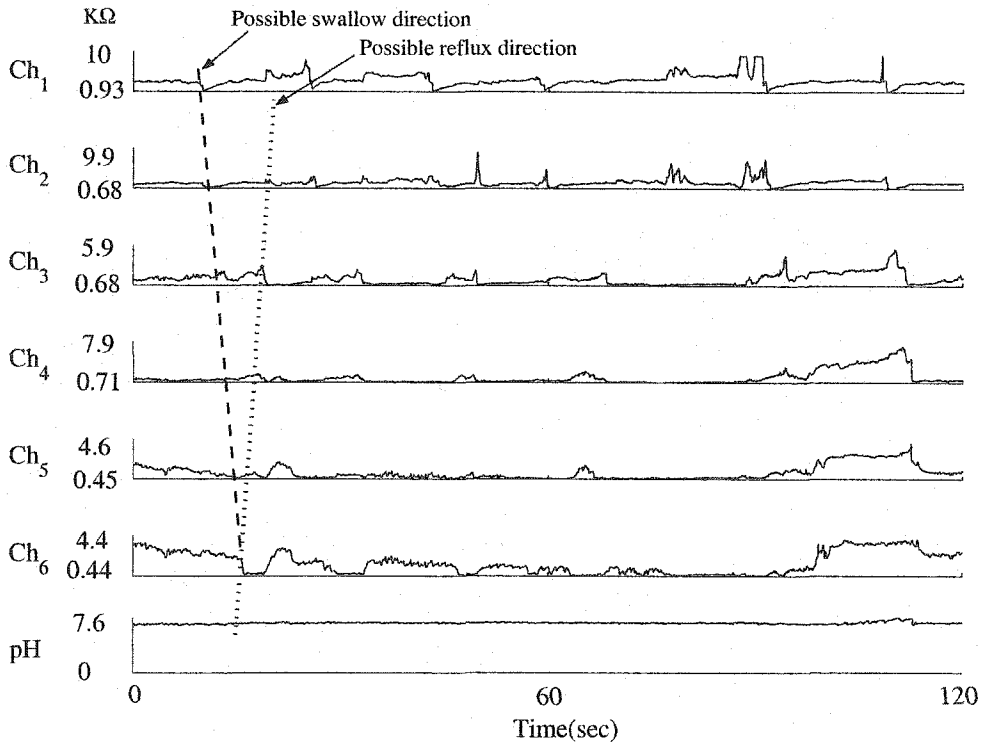

Figure 4.3: Reflux episode. Note the propagation direction of the impedance drop is not clearly visible, possible swallow interpretation of this episode.

On the other hand, the drop in impedance is determined from the ratio of the minimum impedance reached after the start of the episode (gastric content impedance z_c) to the baseline impedance (z_p). The baseline impedance (z_p) is not constant, and can vary during the study period for the same patient as shown in Figure (4.4). Furthermore, it also varies from patient to patient. Figure (4.5) shows a histogram of the pre-episode baseline impedance for 5 patients for cross-patient comparison. comparison.

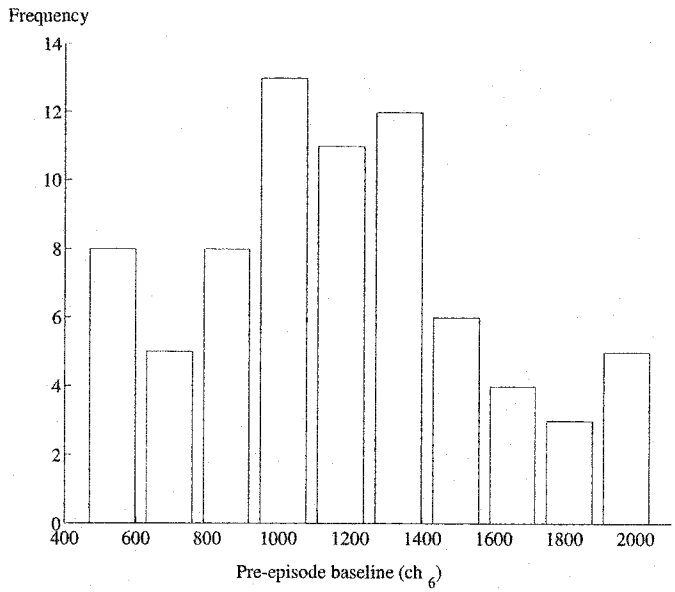

(a) Pre-episode baseline impedance of ch_6 histogram.

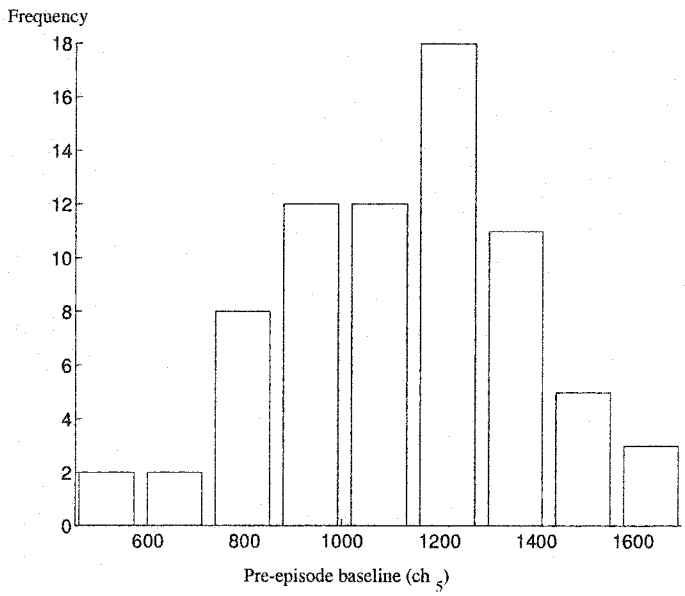

(b) Pre-episode baseline impedance of ch_5 histogram.

Figure 4.4: Histogram of baseline impedance of a typical (randomly selected) patient.

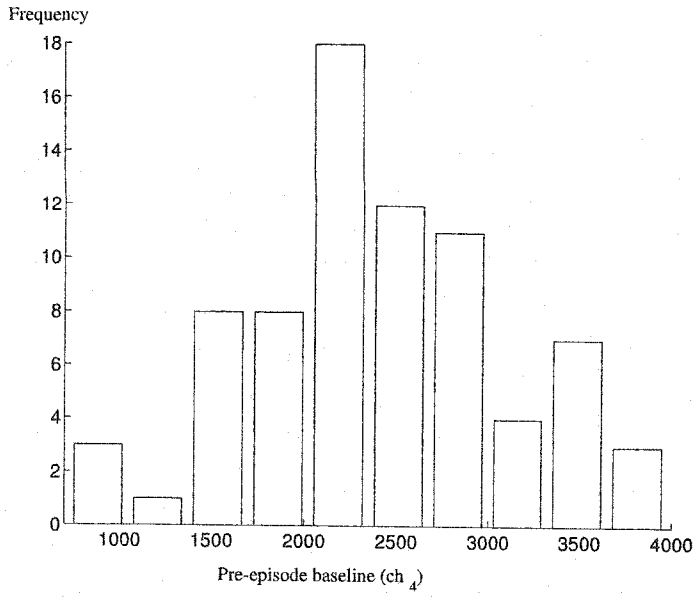

(c) Pre-episode baseline impedance of ch_4 histogram.

Figure 4.4: (Cont.) Histogram of baseline impedance of a typical (randomly selected) patient.

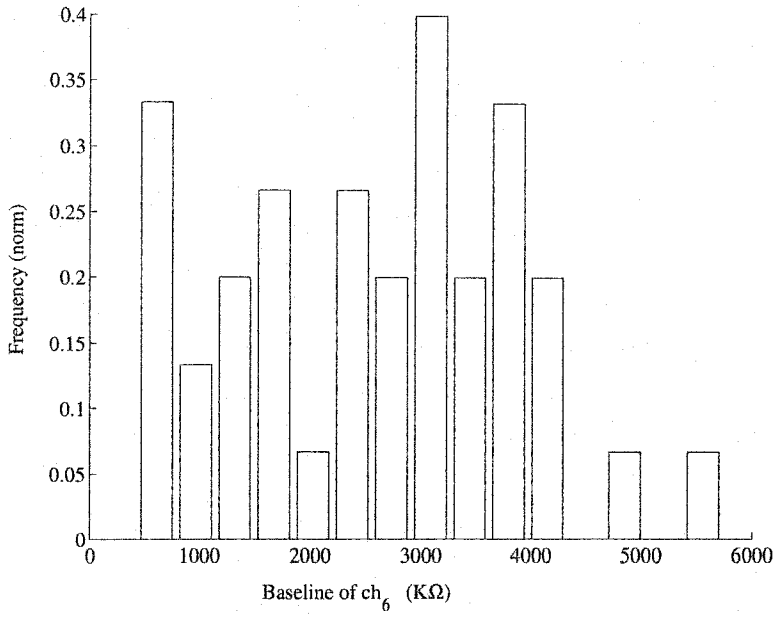

Figure 4.5: Histogram of the baseline impedance of different patients.

The gastric content impedance z_c is affected by the gastric contents, and the gastric content change during the study period, and those changes are also patient dependent. Figure (4.6(a)) shows a histogram of normalized gastric content impedance to the baseline impedance taken from six normal subjects. It can be seen from Figure (4.6(a)) that the drop in impedance is more than 50%, describing the statistical behavior of impedance drop in reflux episodes. Figure (4.6(b)), on the other hand, shows the same histogram taken from esophagitis patients. It can be seen from Figure (4.6(b)) that the distribution of the drop in impedance is nearly uniform and not as narrow as that for Figure (4.6(a)), thereby indicating that special analysis is needed for such data. The reflux episodes considered in Figure (4.6(a)) and Figure (4.6(b)) are of liquid and mixed (gas and liquid) episodes. Note that there are a few occurrences of large impedance values in both Figure (4.6(a)), and Figure (4.6(b)). These are attributed to reflux contents that are a mixture of gas and liquid. Figure (4.7) shows the corresponding minimum impedance reached in ch_6 for the above two cases.

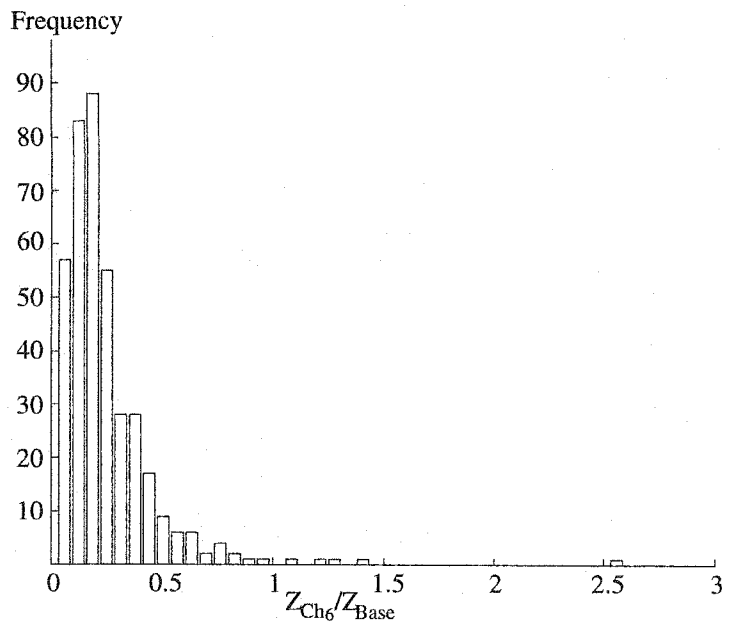

(a) Normal subjects.

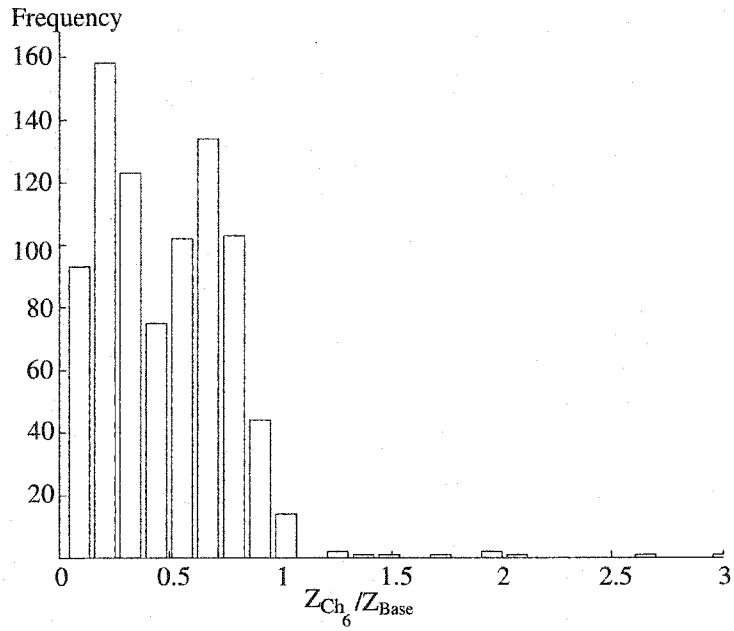

(b) Patients with different esophageal diseases.

Figure 4.6: Histogram of normalized gastric content impedance to the baseline impedance.

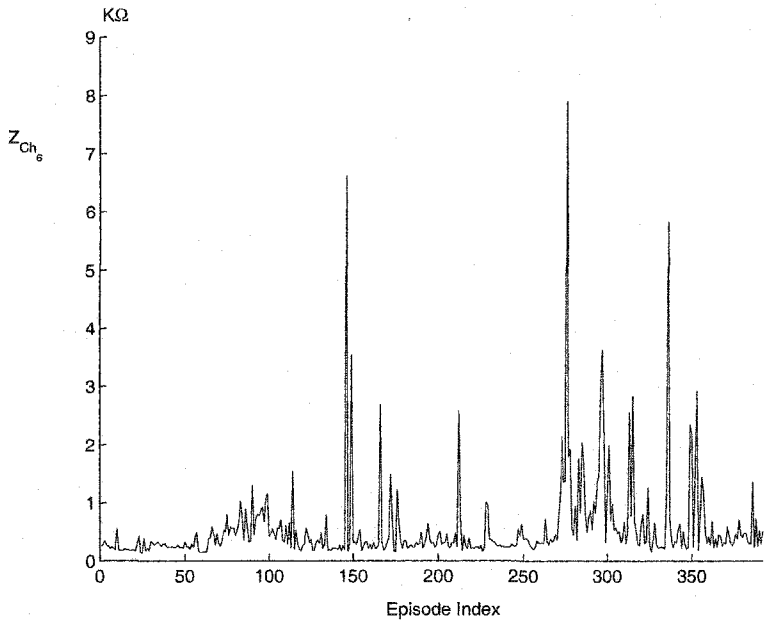

(a) Gastric content impedance in ch_6, x-axis is the episode number, Normal subjects.

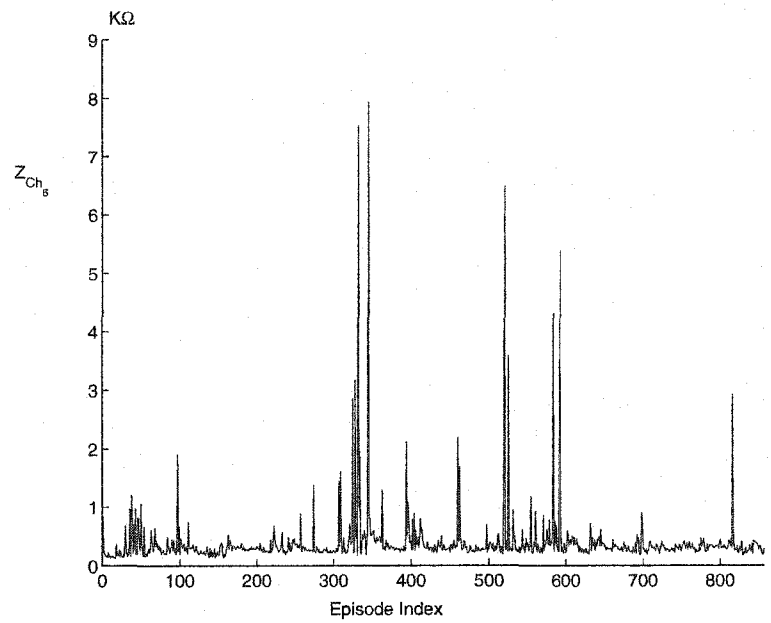

(b) Gastric content impedance in ch_6, x-axis is the episode number, patients with different esophageal diseases.

Figure 4.7: Minimum impedance reached during reflux episodes. Note the large values corresponds to minimum impedance reached during some mixed episodes.

4.3 Reflux patterns

4.3.1 Liquid reflux

When the contents of reflux are liquid, the reflux is referred to as a liquid reflux episode. Such episodes are seen in MII traces as impedance drop to the gastric contents impedance and propagates upward. The level of the impedance during the episode is the global minimum that can be reached in that part of the study and it depends on the acidity of the reflux. The acidity of the refluxate is determined by the pH channel values from the start of the episode to few seconds (< 10) after the episode is initiated. Figure (4.8) shows some examples of liquid reflux episodes patterns. Figure (4.8(a)) shows an acid liquid reflux that reaches up to ch_3 and lasts about 20 seconds, and pH drops to below 4 few seconds after the start of the episode. Figure (4.8(b)) shows a non-acid liquid reflux episode that reaches up to ch_1 and lasts about 50 seconds. Figure (4.8(c)) shows a non-acid liquid reflux episode that reaches up to ch_4 and lasts about 15 seconds. Figure (4.8(d)) shows a low baseline patient non-acid liquid reflux episode that reaches up to ch_1 and lasts about 20 seconds. Note the change in impedance in the distal channel is close to 150 Ω compared to > 1 $K\Omega$ in normal baseline patient.

4.3.2 Mixed reflux

Mixed reflux episodes occurs when the contents of the refluxate material are mixed of liquid and gas. A mixed reflux episode is seen in MII as an impedance drop to

the gastric contents impedance (due to the liquid contents) with an instantaneous change to a high impedance value (due to the gas contents). This does not have to happen in all the channels; it is sufficient if this pattern occurs in at least two channels. Figure (4.9) shows some examples of mixed-type refluxes.

4.3.3 Gas reflux

Gas reflux episodes occur when the contents of the refluxate material is gas. They are seen in MII as an instantaneous change to a high impedance value (due to the gas contents). Figure (4.10) shows some examples of gas-type refluxes.

4.4 Other patterns

Some other patterns that can be seen in the MII signals include cough; swallow-initiated LES relaxation; undetermined propagation; bolus clearance which occurs in most of the channels but one or two; and baseline impedance variability during the study period, specially after meals. Figure (4.11) shows some examples of these patterns.

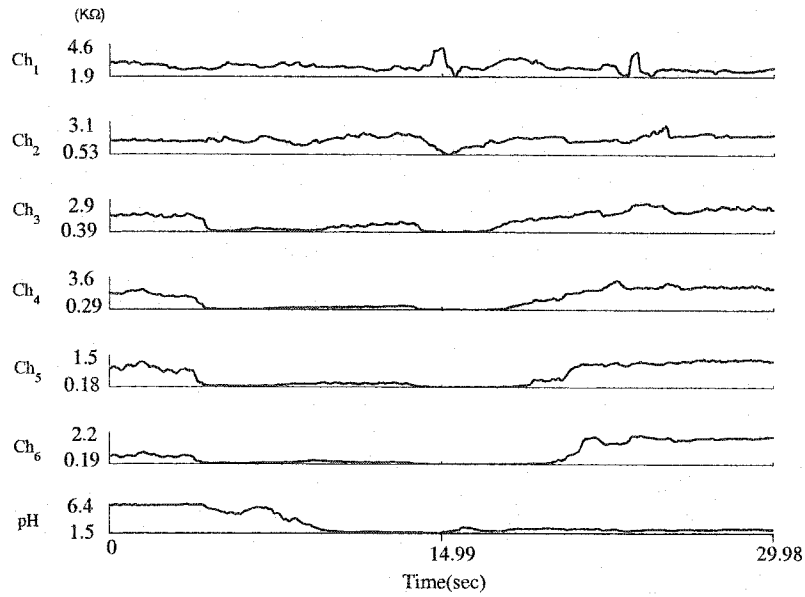

(a) Acid reflux of liquid type. The pH drops below 4 a few seconds after the episode due to delay in the pH sensor.

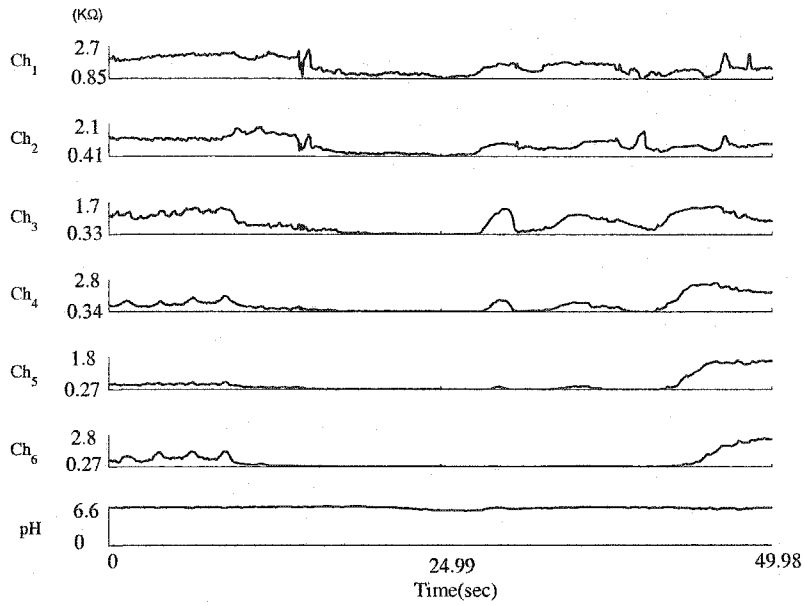

(b) Non-acid liquid-type episode.

Figure 4.8: Different forms of liquid type reflux episode.

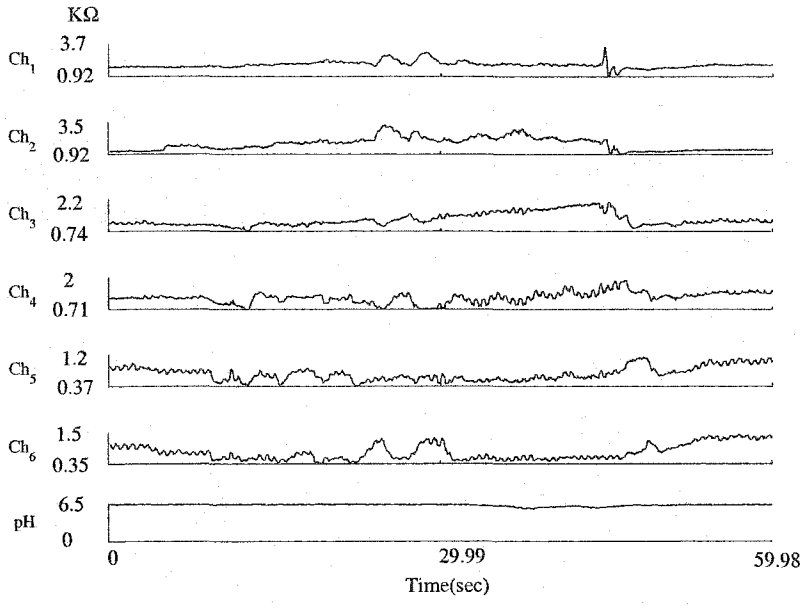

(c) Non-acid liquid-type episode. Very small impedance change and no pH drop.

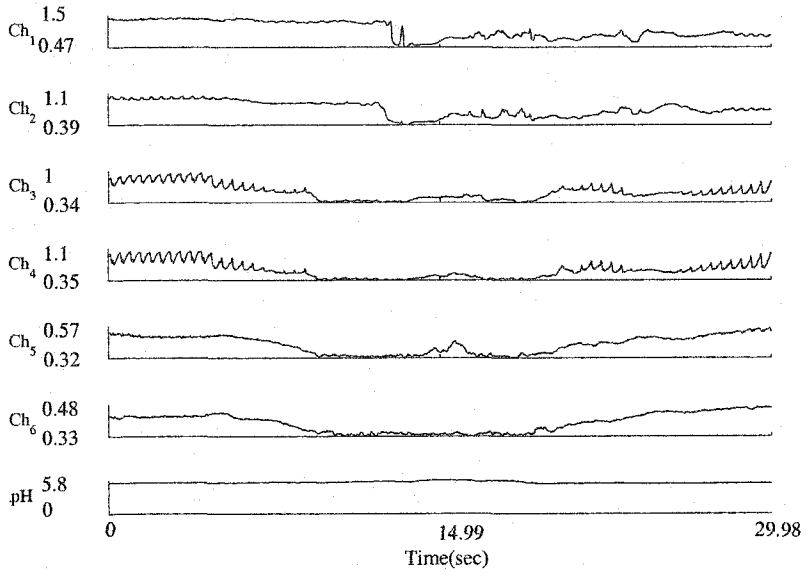

(d) Non-acid liquid type episode. Note that the change in impedance in the distal channels is very small (compared to normal impedance changes).

Figure 4.8: (Cont.) Different forms of liquid type reflux episode

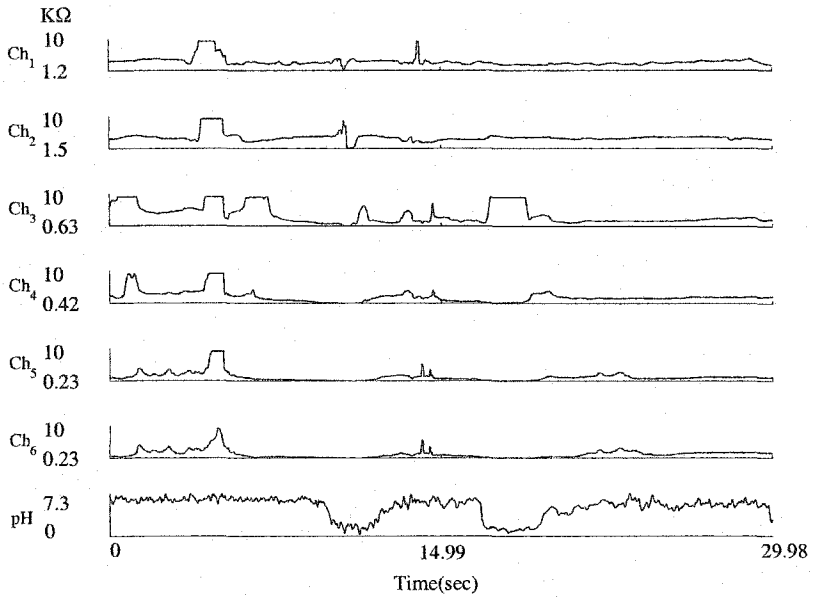

(a) Acid reflux of mixed type. Note the maximum impedance reached in all the channels is $> 9\ K\Omega$, indicating the presence of gas content in all the channels.

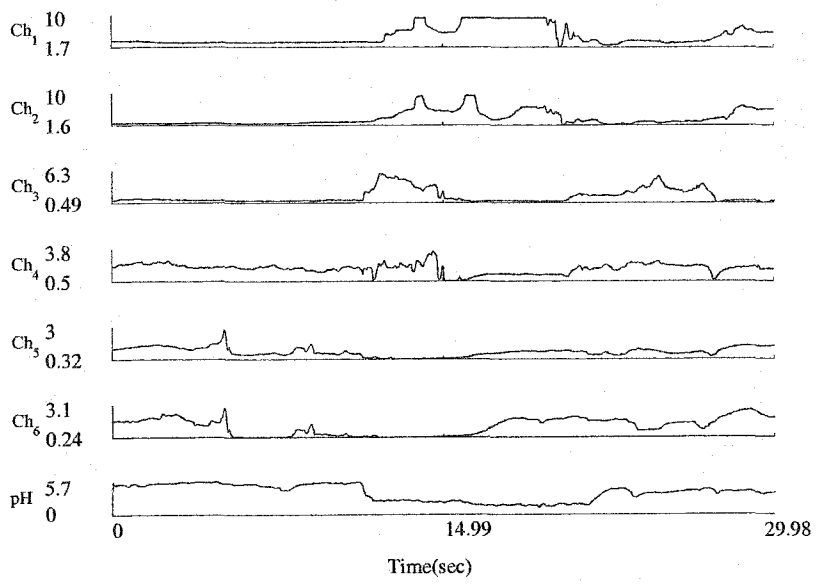

(b) Acid reflux of mixed-type episode. Note that the gas is present in the proximal channels only and the distal channels have the range of impedance that corresponds to liquid episodes.

Figure 4.9: Different forms of mixed-type reflux episode.

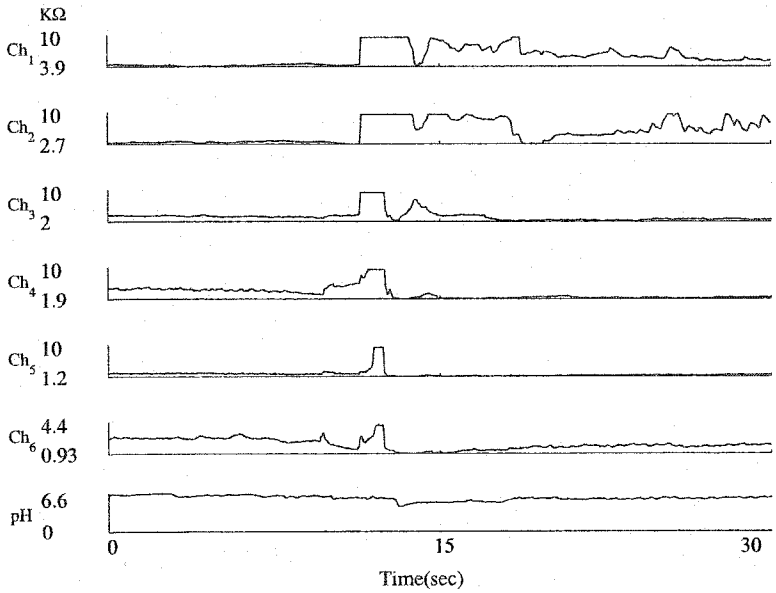

(c) Acid reflux of mixed-type. Note the maximum impedance reached in all channels except the distal one is $> 9\ K\Omega$, indicating the presence of gas contents in all the channels.

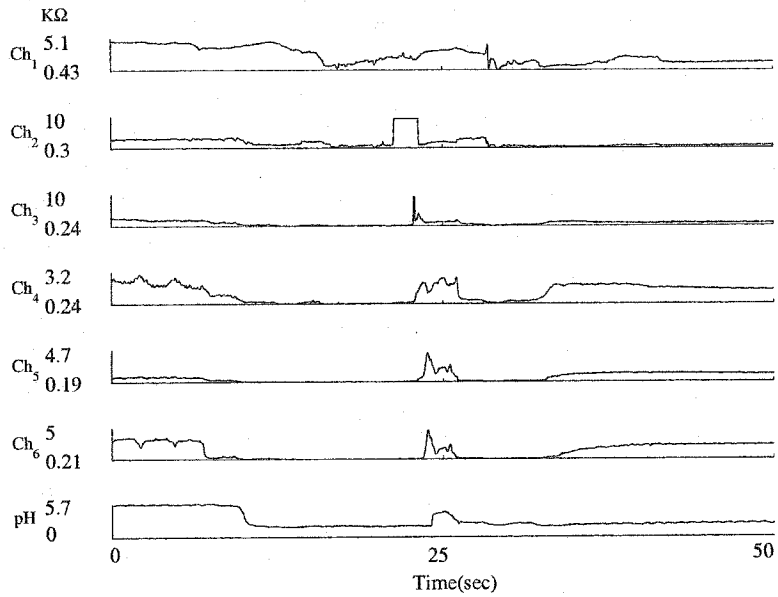

(d) Acid reflux of mixed-type episode. Note that the gas occurs during the episode.

Figure 4.9: (Cont.) Different forms of mixed-type reflux episode.

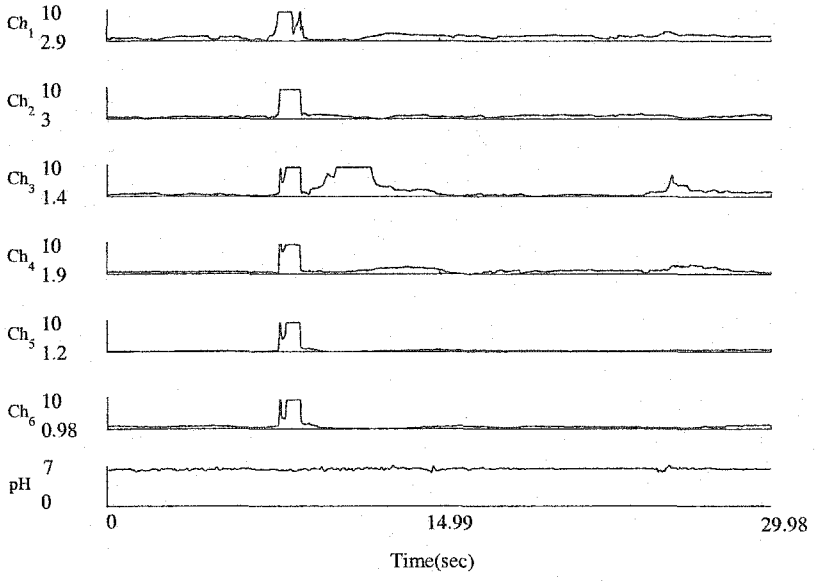

(a) Gas type reflux episode where the gas is seen in all the channels.

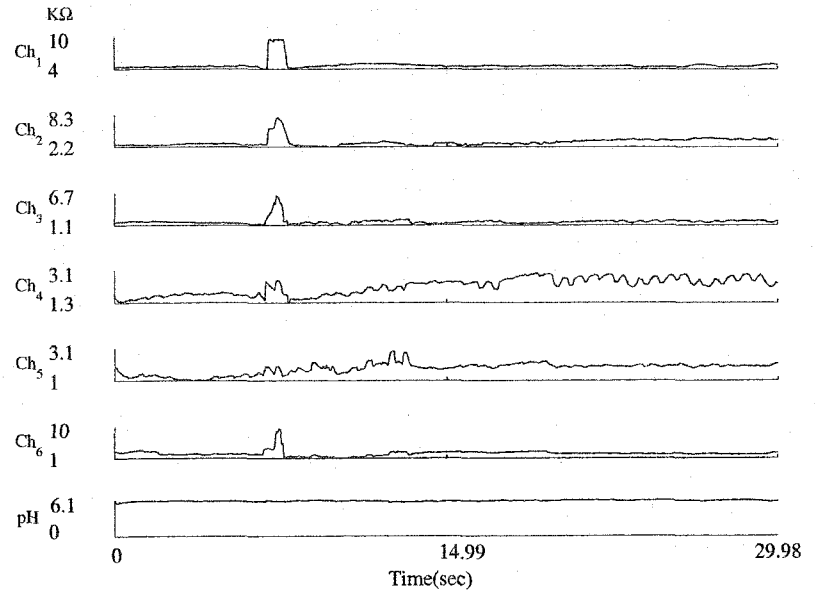

(b) Gas type episode where the gas is seen in the proximal channels and the most distal channel only.

Figure 4.10: Different forms of gas type reflux episode.

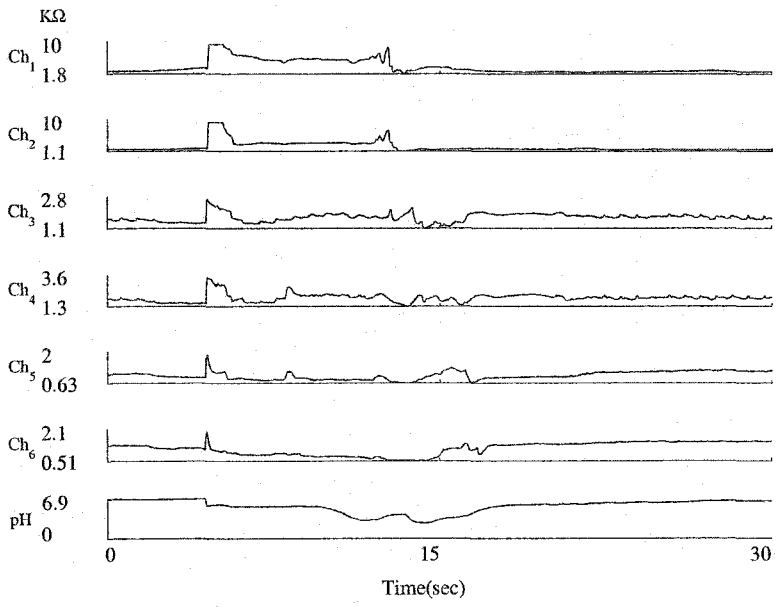

(c) Gas type episode where the gas is seen in the two proximal channels (ch_1 and ch_2) followed by a pH drop.

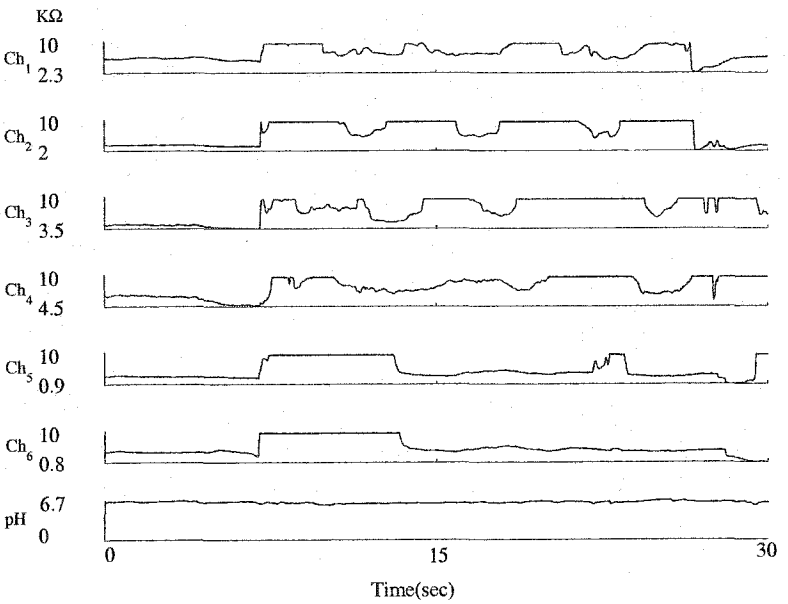

(d) Gas type episode where the gas is seen in all the channels, long episode.

Figure 4.10: (Cont.) Different forms of gas type reflux episode.

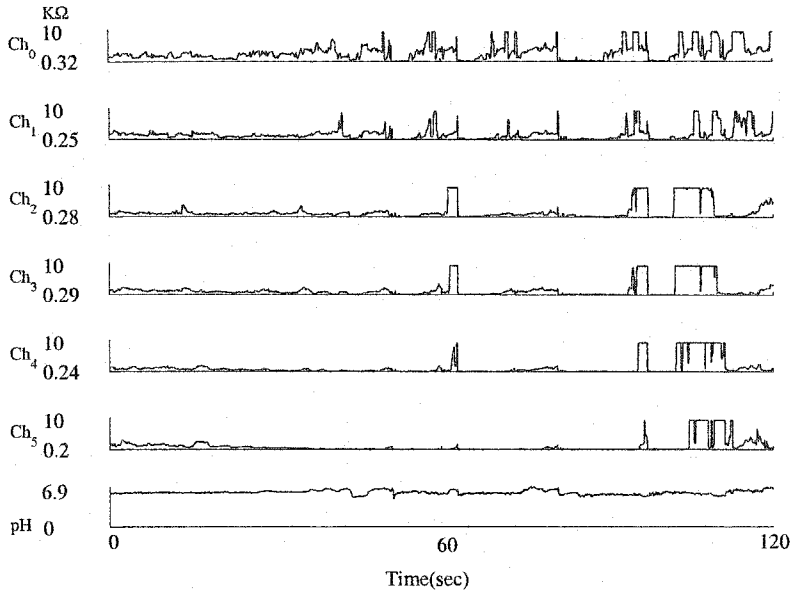

(a) Cough event.

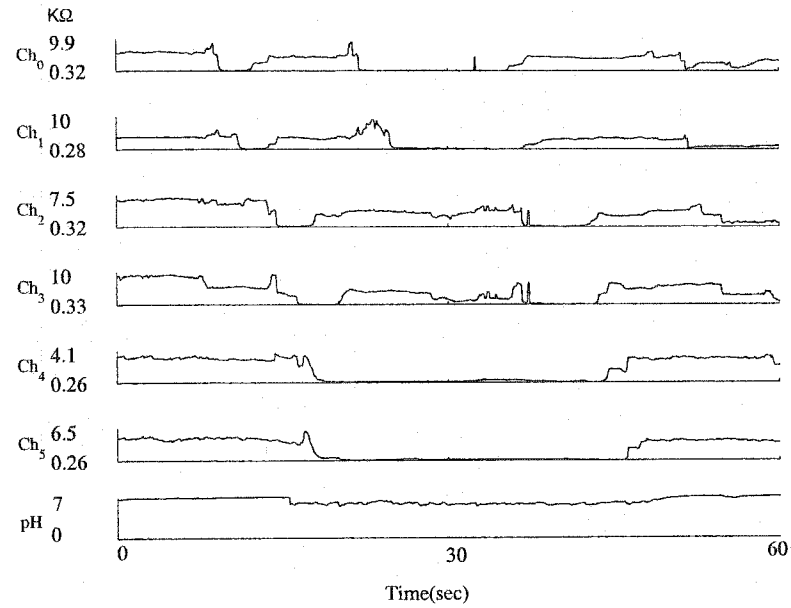

(b) Undetermined propagation direction

Figure 4.11: Other patterns.

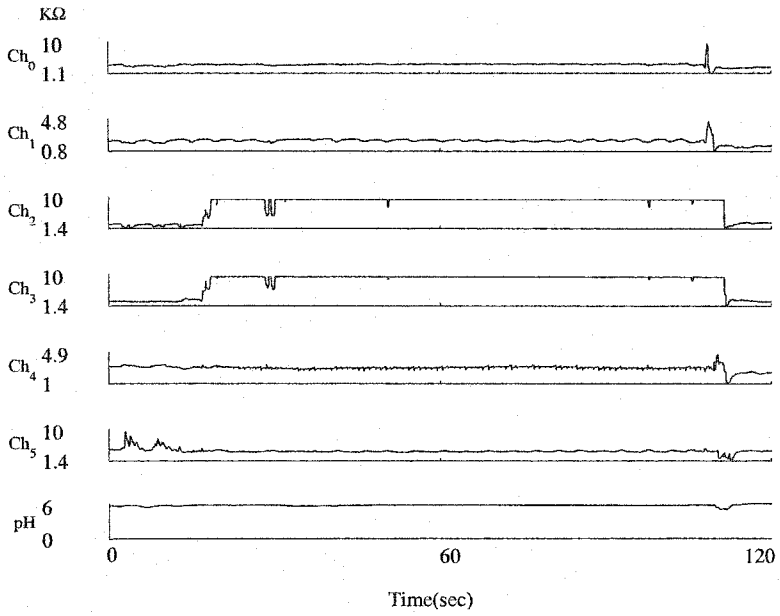

(c) Presence of gas in the center of the esophagus. Gas seen only in two channels and all others show no sign of presence of gas (gas is trapped or problem with channels).

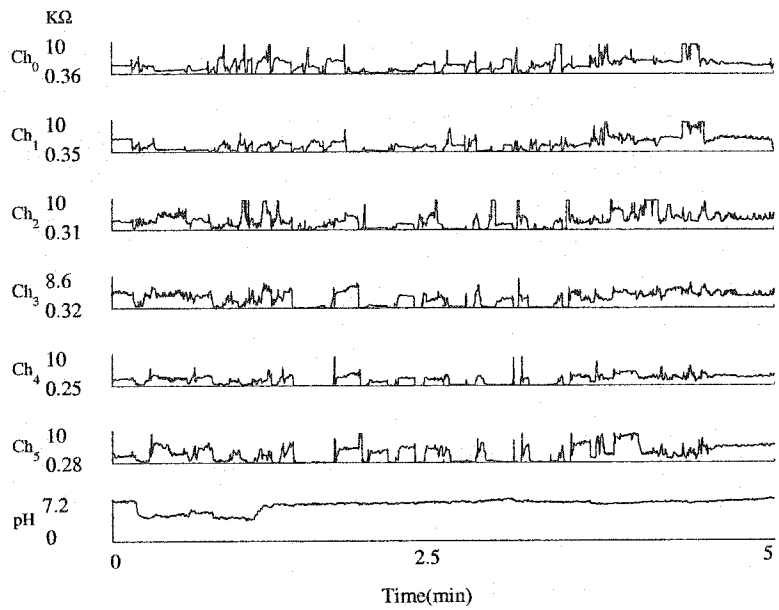

(d) Meal patterns.

Figure 4.11: (Cont.) Other patterns.

4.5 Summary

From the study of the different episode types and patterns, the following are general patterns of the reflux episodes:

- Liquid reflux:
  - Impedance change from patient impedance (baseline) to a low value in at least two channels and the inverse pulse shape propagates upward. The important factor is the impedance change and not the minimum impedance reached during the episode. The minimum impedance reached depends on many factors including: stomach contents, and refluxate position with respect to the channel as was shown in the simulation.
  - Inverse pulse shape propagates from the distal channel to the higher channel, and so on.
  - Most of the time, clearance of reflux occurs in the higher channel before the lower and the last one to be cleared is the distal channel. This pattern corresponds to a continuous reflux.
  - pH alone is not enough to determine reflux. Reflux could occur with or without pH change, and pH drop may or may not be as a result of reflux.
- Mixed reflux:
  - Impedance change from patient impedance (baseline) to a low value in at least two channels and the inverse pulse shape propagates upward. An

impedance change to a very high value in at least two channels occurs any time during the episode duration. Most of the time, the change occurs either in the two distal channels or in the two proximal channels and at the start of the episode.

  - Inverse pulse shape propagates from the distal channel to the higher channel, and so on.
  - pH alone is not enough to determine reflux. Reflux could occur with or without pH change, and pH drop may or may not be as a result of reflux.

- Gas reflux:

  can be identified by sharp narrow instantaneous change in impedance to a high value in at least two channels. Most of the time, this occurs either in the most distal or the most proximal channels. It also could be sharp narrow instantaneous change in impedance to high value in the distal channel accompanied by pH drop.

CHAPTER 5

Algorithm for Reflux Episode Detection

5.1 Introduction

Reflux episodes are the most important events of MII signals that need to be detected and identified. MII study is performed usually for 24 hours, and yields a large amount of data. It is very time consuming to read and mark episodes manually. Therefore, it is important to have an algorithm that detects and marks episodes automatically in a relatively short time. This chapter presents the technique developed to detect and classify reflux episodes from intraluminal impedance reflux episodes and classify them according to their contents such as liquid, mixed or gas. The main stages of the system are shown in Figure (5.1) and will be described in detail in the following sections.

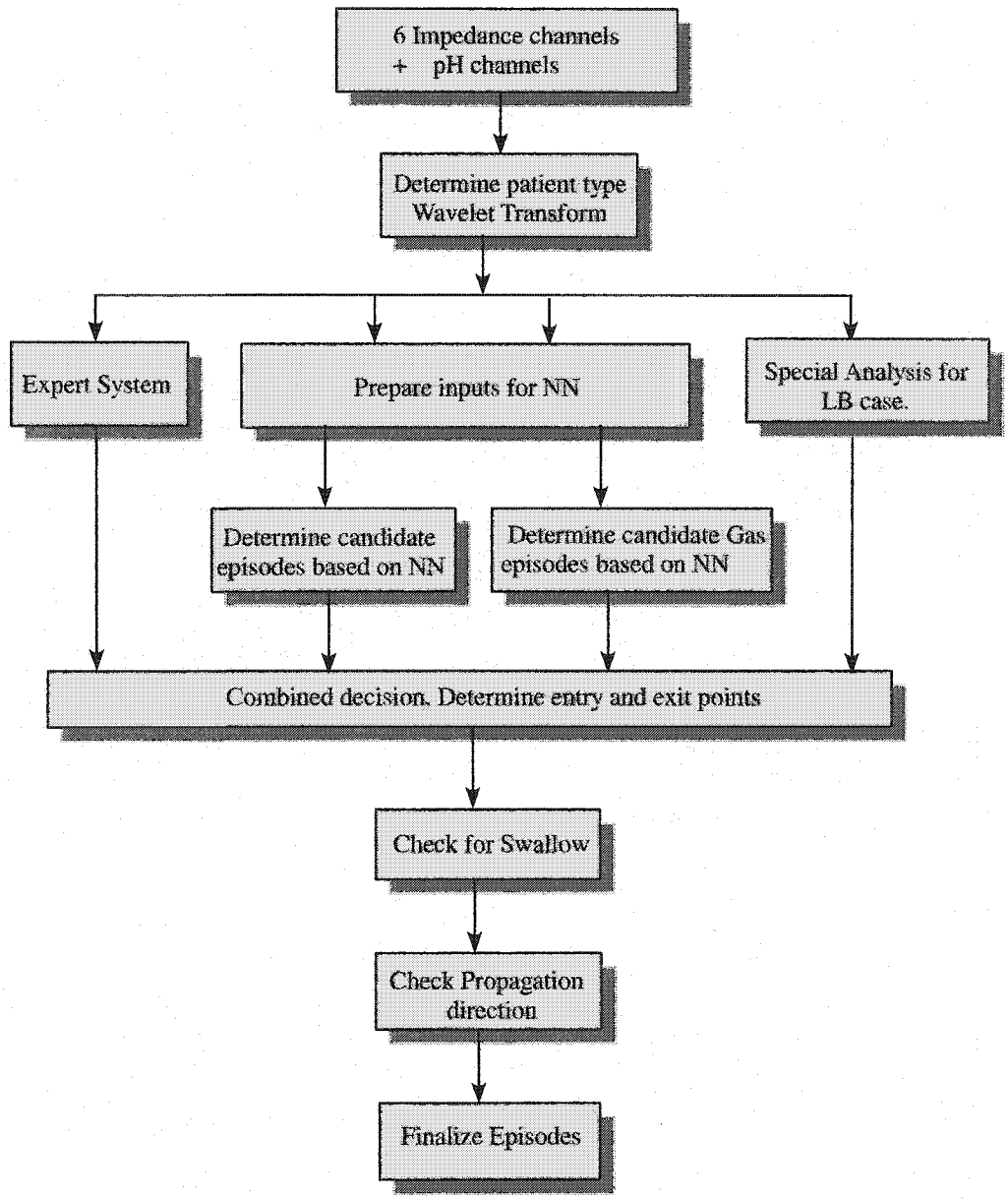

Figure 5.1: Expert system used to detect reflux episodes. NN stands for neural network, LB stands for low baseline, and FP stands for false positive.

5.2 Expert system

The expert system consists of the following operations:

- Wavelet transform (WT) of the signal from all the channels.
- Analysis of the WT to determine the propagation of the impedance change by tracking the shape of the impedance waveform.
- Decision-making, which will be one or more of the following rules:
  - Rules for normal signals.
  - Rules for low baseline signals.
  - Rules for acid reflux episodes.

These stages are described in the following subsections.

5.2.1 Wavelet analysis of MII

Impedance traces in practice are far from any idealized waveforms due to various factors such as measurement noise, changes due to patient movement, respiration, etc. Sharp variations occur due to events in the GIT. These variations are caused by air that is in front of the bolus and the reflux material, or by the bolus or refluxate material entering or leaving the measurement segment (denoted as channel). These variations can be mathematically modeled as singularities. Multiresolution analysis using wavelets is used to address this problem. If a wavelet is chosen as the first derivative of a smoothing function (any function whose integral is equal to 1 and asymptotically reaches 0), and the first and the second derivative of the function

exists, then the local maxima of the absolute value of the wavelet transform can be used to detect the occurrence of singularities (Mallat and Zhong, 1989, 1992; Mallat and Hwang, 1992). To obtain a wavelet with symmetry and compact support, wavelet $\psi(t)$ and its dual $\tilde{\psi}(t)$ are chosen to be linearly independent and satisfy the bi-orthogonality condition as:

$$< \psi_{m,n}(t), \tilde{\psi}_{k,l}(t) > \quad = \quad \delta(m-k)\delta(n-l) \tag{5.1}$$

Such wavelet functions can be constructed by using a cascade of perfect reconstruction filters. For detection, a wavelet $\psi(t)$ is chosen to be equal to the first derivative of a smoothing function (Mallat and Zhong, 1989, 1992), implying that $\psi(t)$ must have a zero of order 1 at $\omega = 0$, in the frequency domain. The Fourier transform of a wavelet, which satisfies the above properties is

$$\Psi(\omega) = -\frac{i\omega}{4}\left(\frac{sin(\omega/4)}{w/4}\right)^4 e^{-i\omega/2} \tag{5.2}$$

A cursory inspection of equation (5.2) shows that $\Psi(\omega)$ corresponds in time domain to a derivative of a function whose Fourier transform is $\Theta(\omega) = (\frac{sin(\omega/4)}{w/4})^4 e^{-i\omega/2}$ which is the delayed 4^{th} order convolution of a rectangular function (Morse and Feshbach, 1953). Figure (5.2) shows the wavelet used in this research both in frequency and time domains. These wavelets and scaling functions can be constructed

using a cascade of perfect reconstruction filters $(h,\tilde{h})$ and $(g,\tilde{g})$ that satisfy

$$H^*(\omega)\tilde{H}(\omega) + H^*(\omega+\pi)\tilde{H}(\omega+\pi) = 2$$

and

$$G(\omega) = e^{-i\omega}\tilde{H}^*(\omega+\pi) \;\; ; \;\; \tilde{G}(\omega) = e^{-i\omega}H^*(\omega+\pi)$$

Figure (5.3) shows the impulse response of these filters.

Wavelet analysis can be used to develop the smooth version $A_{j+1}(k)$ and details $D_{j+1}(k)$ of the waveform.

$$\begin{aligned} A_{j+1}(k) &= \sum_{n=-\infty}^{\infty} h(n-2k)A_j(n) \quad ; \\ D_{j+1}(k) &= \sum_{n=-\infty}^{\infty} g(n-2k)A_j(n) \end{aligned}$$

In addition, such a decomposition can be accomplished for many resolution levels successively.

Wavelet transform is applied to the waveform from all the channels, 1 through 6, resulting in a detail signal and a smooth signal for each channel. Figure (5.4) shows a sample impedance waveform and the sum of energy in the details from levels $(2-5)$ of the multiresolution analysis. The details are further classified into positive and negative values. The positive details correspond to the positive slope

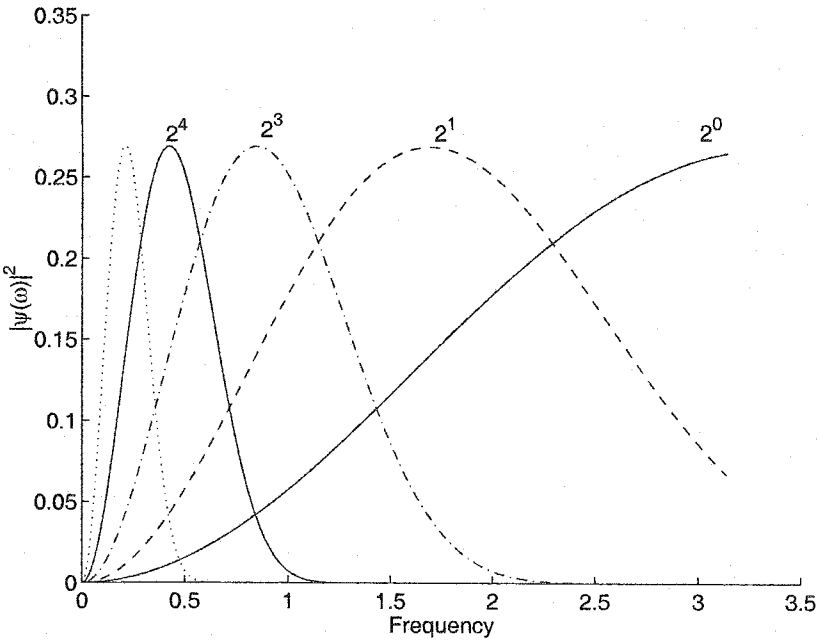

(a) $|\Psi(\omega)|^2$

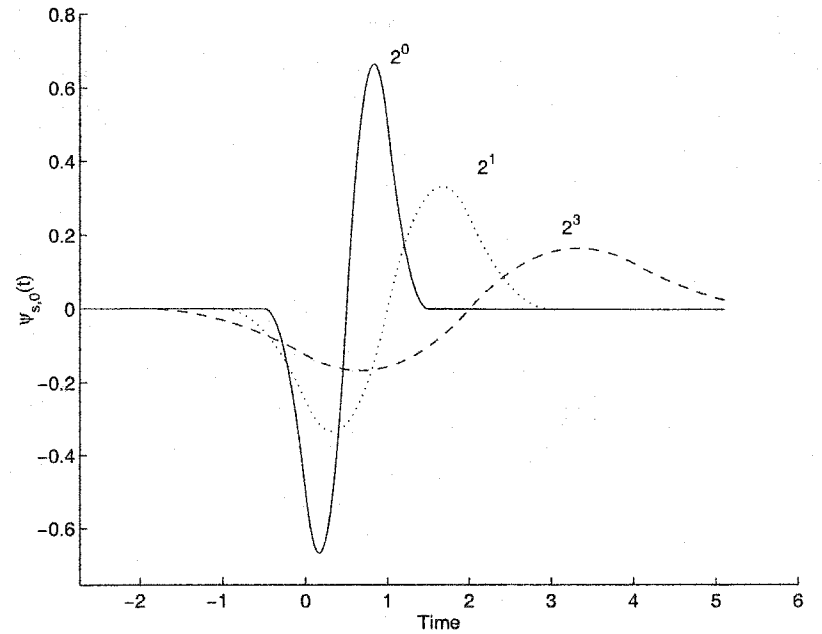

(b) $\psi_{s,0}(t)$

Figure 5.2: Spline wavelet.

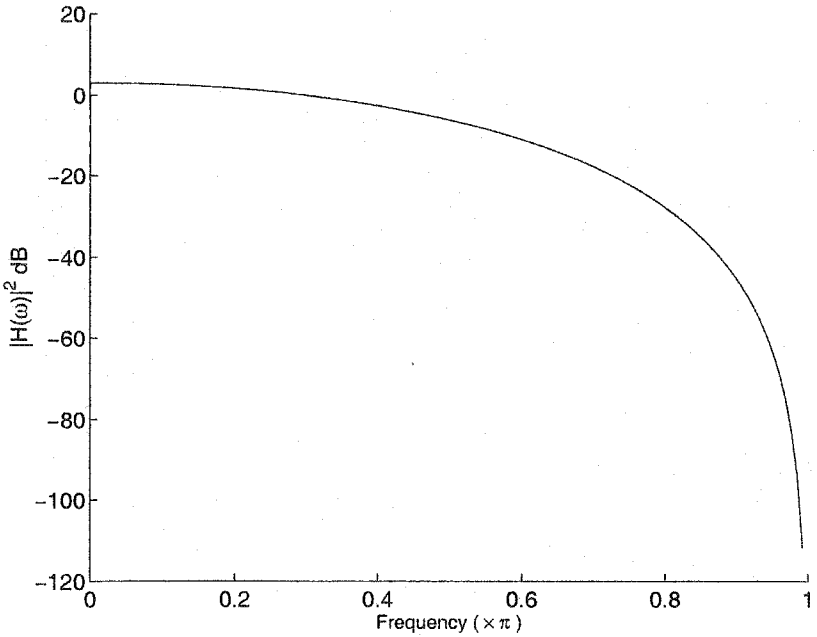

(a) Low-pass filter frequency response

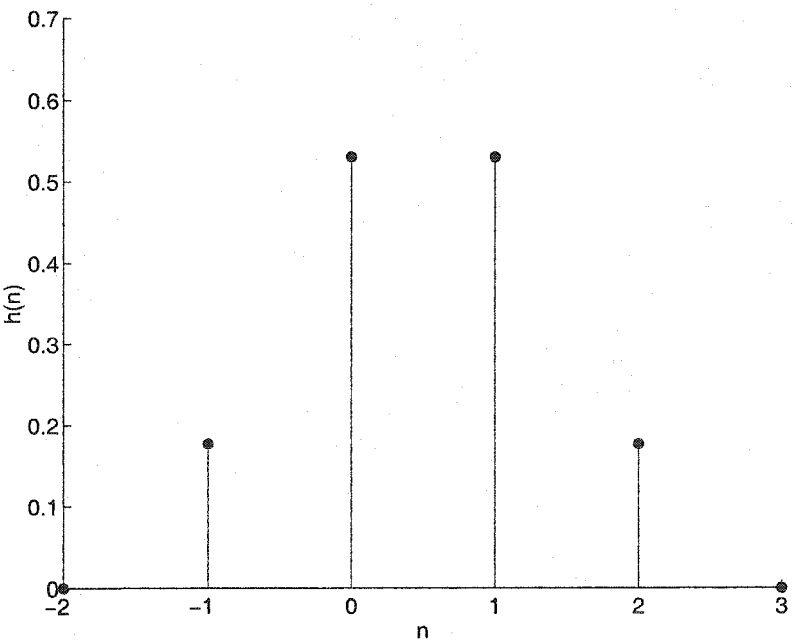

(b) Low-pass impulse response.

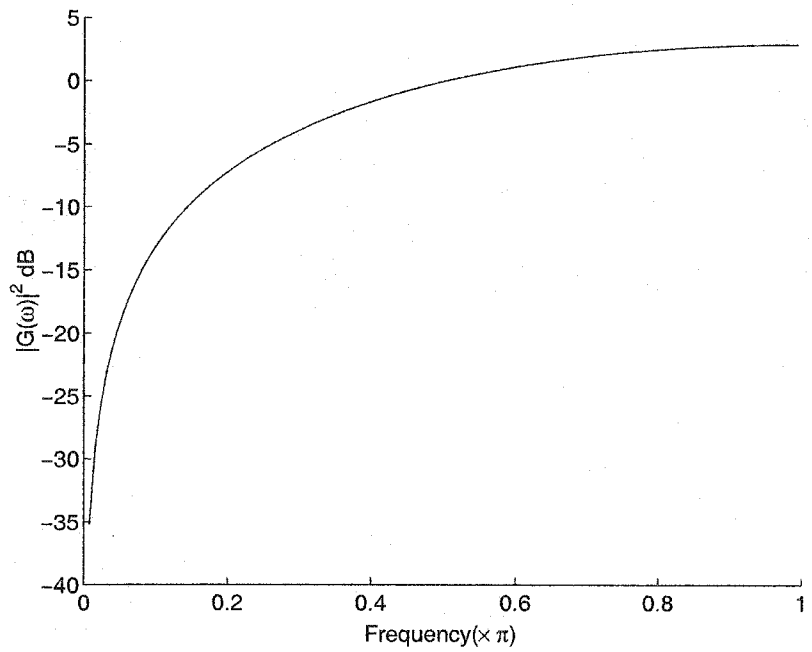

(c) High-pass filter frequency response.

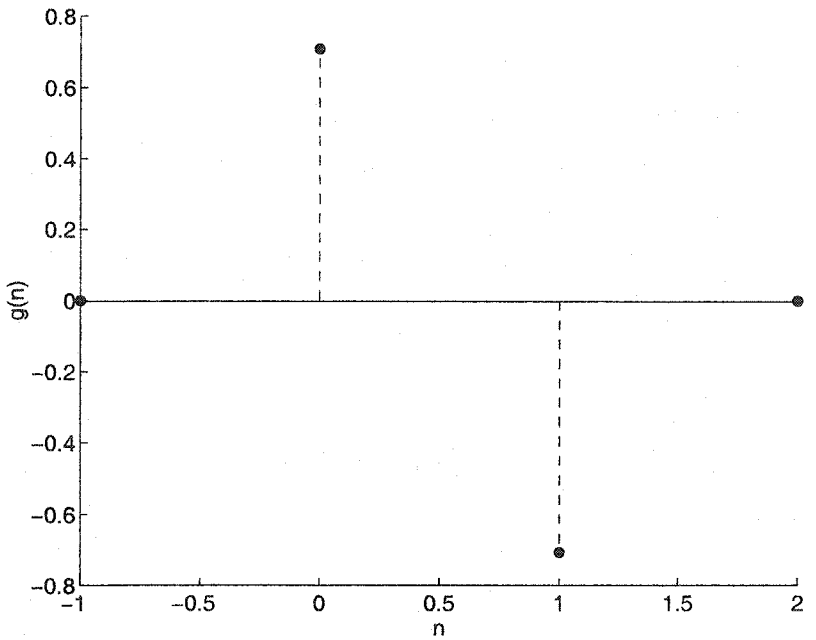

(d) Low-pass impulse response.

Figure 5.3: Low-pass and high-pass filter responses.

in the impedance and the negative details correspond to negative slope. The sum of the energy in the negative details and that of the positive details are also shown in the figure. The location of the maxima of the negative details corresponds to the occurrence of a candidate episode if it simultaneously appears propagating across channels. Similarly, the maxima of the positive details corresponds to the end of the episode. Respiration artifacts are rejected by monitoring the location between successive maxima of the sum of the energy in the negative details (i.e frequency range $0.2 - 0.33$ Hz).

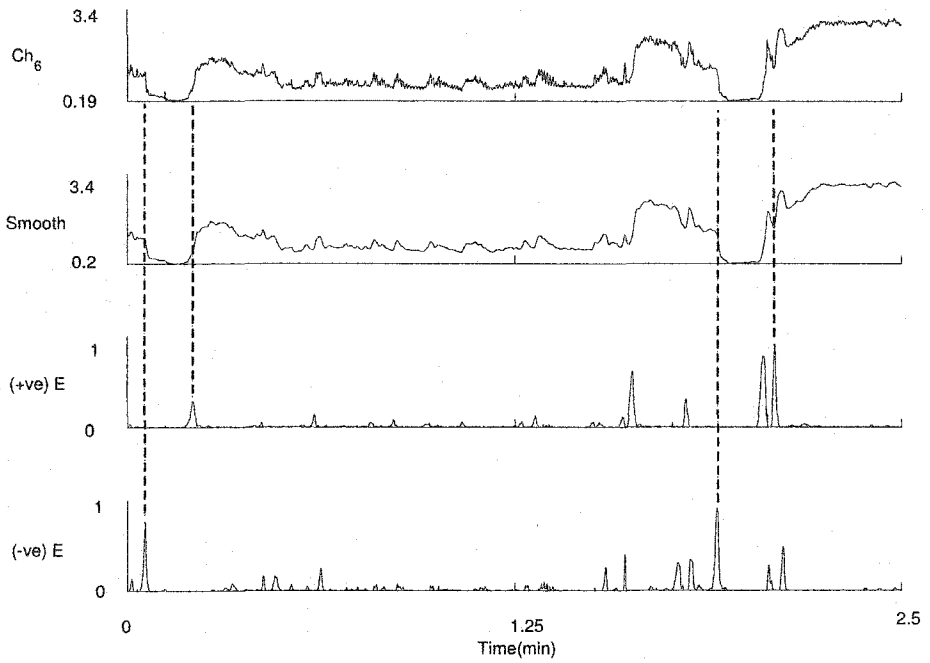

Figure 5.4: Signal of one channel (ch_6), the resulting smooth version, and the corresponding sum of the energy in the negative details and that of the positive details (normalized). Dotted lines shows the location of the maxima and the corresponding location on the signal.

5.2.2 Normal (and semi-normal) impedance signals

From a signal description perspective, if the change in impedance in the two distal channels is large (i.e., the mean of the distribution of minimum to baseline impedance ≤ 0.5 as shown in Figure (4.6(b)), then these signals are termed normal. When the mean of the distribution of minimum to baseline impedance > 0.5 and ≤ 0.8, then these signals are termed semi-normal. The series of the times at which the impedance exhibit transition to the gastric content at each channel starting from the most distal channel is refereed to as the propagation direction. Initial propagation direction is determined from the energy of the wavelets coefficients of the three distal channels, and then the proximal channels are added. The impedance of gastric contents (Z_c) along with the propagation direction are sufficient information to determine a well defined episode. But in reality, all episodes may not be "well defined". Some examples are:

a) Refluxes after swallow will result in propagation impedance waveform shapes that will meet at channel 3.

b) Patient impedance (Z_p) is close to Z_c, and

c) Undetermined propagation direction due to closely spaced episodes.

Additional analysis is performed to enhance the sensitivity of episode detection. The following additional parameters are evaluated to assist in the analysis:

i. Minimum impedance reached after the episode in ch_6, and ch_5 compared to gastric content impedance threshold.

ii. Impedance change in ch_6, and ch_5.

iii. Variances in the impedance of the distal three channels.

iv. Strength of the change in impedance in the swallow direction compared to the impedance change in the reflux direction.

All of the above parameters are used in a combined decision-making process, with emphasis on the gastric contents threshold and the propagation direction.

Reflux could be acidic or non-acidic depending on pH value a few seconds after the episode. Therefore, two gastric contents impedance thresholds are used. To determine these thresholds, one pass over about 2.27 hours of data is used to determine an initial gastric content impedance by performing clustering analysis of the impedance value during the episodes (Chiu, 1994; Al-Zaben and Chandrasekar, 2002). The initial value from the first pass is used in both acid and non-acid reflux types, and it is then changed adaptively as a new episode is observed.

The gastric contents impedance is not constant over the study period and it increases especially after meals, and the adaptive algorithm is used to keep up with rate of change of Z_c according to:

$$Z_{cT_{new}} = Z_{cT_{old}} \pm \epsilon \| Z_{cT_{old}} - Z_{min} \|^2 \tag{5.3}$$

Figure 5.5 shows the minimum impedance Z_{min} reached in ch_6 (distal) during each episode along with the adaptively changing threshold $Z_{cT_{new}}$ on the gastric content impedance. Two thresholds were used, one corresponds to acid reflux episodes and the other corresponds to non-acid reflux episodes. The pre-episode baseline impedance is also shown in the figure.

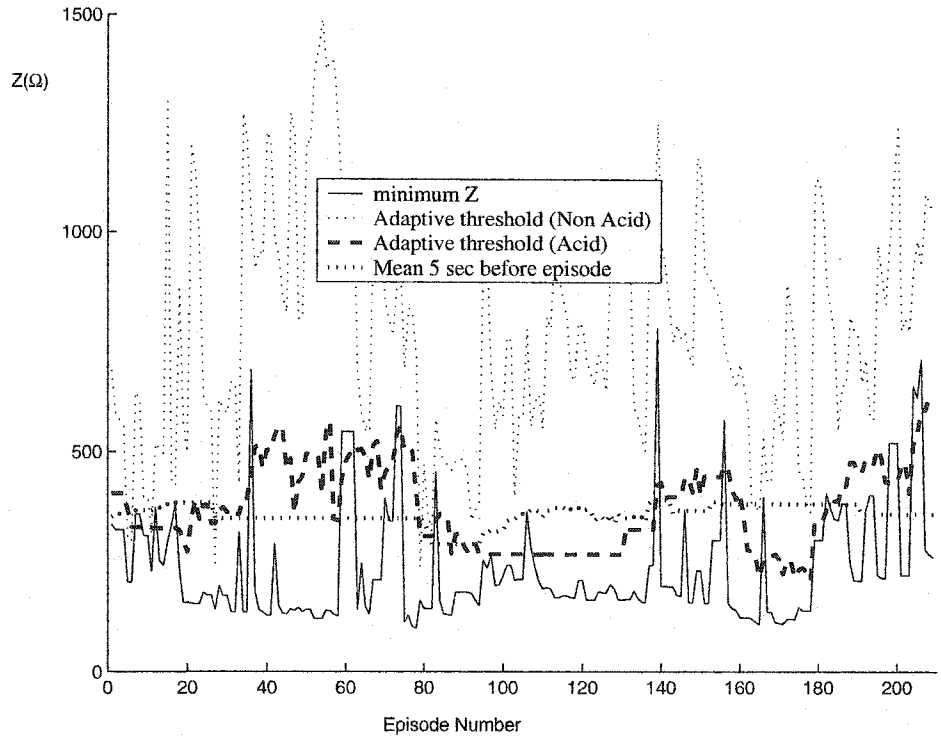

Figure 5.5: Adaptively changing gastric content thresholds. Two thresholds are shown in the Figure, one corresponds to acid reflux episodes and one corresponds to non-acid reflux episodes.

5.2.3 Low baseline

Whenever the value of the patient impedance as well as the change in impedance during GIT events are also low, these are termed as "low baseline" waveforms.

The analysis is more challenging since we have a smaller dynamic range for signal variations. However, the analysis developed still works fairly well, but it is not of the same quality. The analysis in this case starts by applying an adaptive filter to the smooth version of ch_4. The primary input d_k for the filter is a delayed sequence of the smooth signal X_k. The weight vector of the filter is obtained from Widrow-Hoff least mean square (LMS) algorithm

$$W_{k+1} = W_k - 2\mu(d_k - y_k)X_k \tag{5.4}$$

where y_k is the output and μ is a factor that controls stability and convergence. If the filtered signal at any local maxima of the details exhibits impedance transition to the gastric contents impedance level, then there will be a candidate episode and the previously mentioned conditions are evaluated to make a firm decision regarding the episode.

5.2.4 pH based observations

In low baseline waveforms all the analysis were initiated from ch_4 observations. Similarly, the pH observations can also be used to initiate the analysis by observing the propagation starting with the pH channel. If pH drops below a threshold, then the propagation direction and the conditions in section (5.2.2) are used to determine the presence of GIT events.

5.3 Neural networks

In addition to the expert system described previously, there are three neural networks developed for episode detection purposes. Each neural network has a specific task. These tasks are:

- Gas episodes detection.
- Episodes of large impedance changes detection.
- Assimilate the statistics obtained from all stages to further refine the classification of episodes.

Since the idea of the three neural networks are similar, the third neural network will be described in detail as an example in the following section.

5.3.1 False positive neural network

The positive predictive value of the detection process was found to be low when the data contain episodes of a liquid type. Most of the time these false positive episodes are due to closely located swallows. In order to enhance the positive predictive value and maintain the sensitivity, a neural network (NN) is introduced as an extra step that is used when the reflux episode is of a liquid type. After studying the characteristics of the false positive episode, a NN (shown in Figure (5.6)) with the following parameters extracted from the impedance measurements ch_1 , ch_2 , $\cdots ch_6$ was applied to reject false positive episodes:

- x_1 : Ratio of a one-second impedance mean after the minimum value is reached to a 2-second mean starting 3 seconds before the start of the episode in ch_1.
- x_2 : Ratio of a one-second impedance mean after the minimum value is reached to a 2-second mean starting 3 seconds before the start of the episode in ch_2.
- x_3 : Minimum value reached in ch_6 a few seconds after the episode (max 4 sec).
- x_4 : Minimum value reached in ch_5 few seconds after the episode (max 4 sec).
- x_5 : Ratio of a one-second impedance mean after the minimum value is reached to a 2-second mean starting 3 seconds before the start of the episode ch_3.
- x_6 : Ratio of a one-second impedance mean after the minimum value is reached to a 2-second mean starting 3 seconds before the start of the episode in ch_4.
- x_7 : Ratio of the minimum pH reached after the episode to a one-second pre-episode mean.

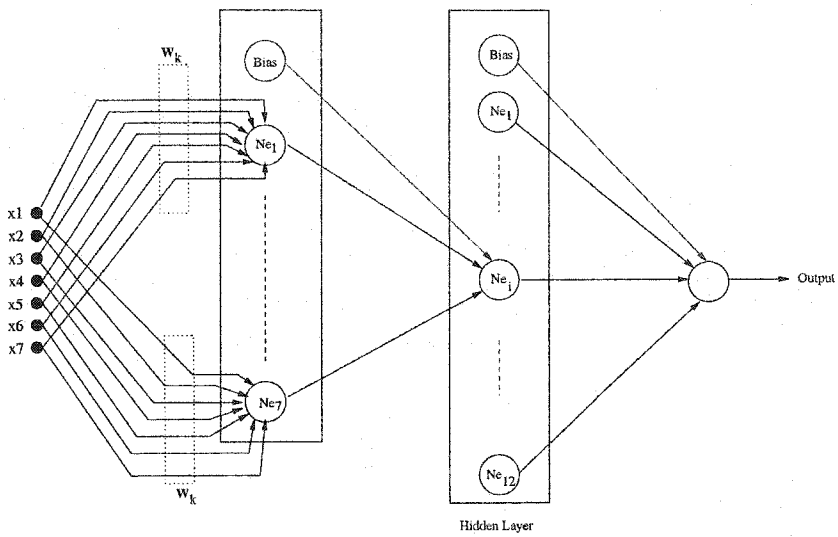

Figure 5.6: Neural network structure.

Figure (5.7) shows the ROC curve of the input features.

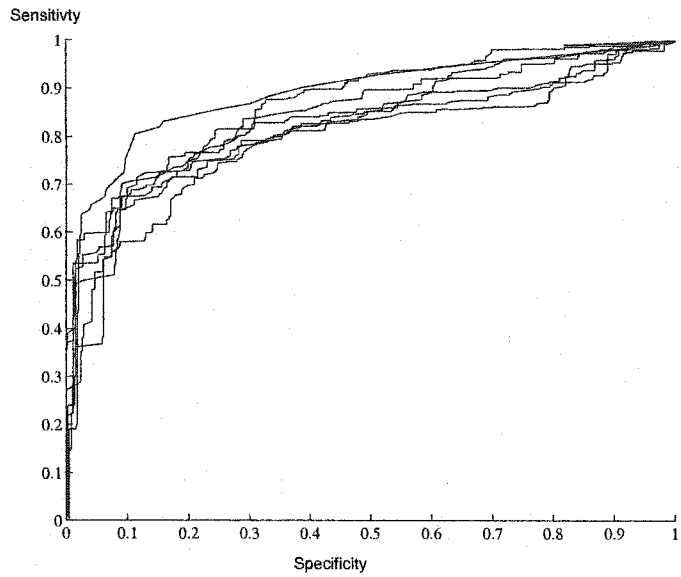

Figure 5.7: ROC curve of the features used as network inputs.

The activation function used in the neurons is the tan-sigmoid given by:

$$f(x) = \frac{2.0}{1+e^{-2x}} - 1 \tag{5.5}$$

Delta rule is employed in the training process of the neural network. The algorithm can be described as follows:

- Start with epoch i, propagate the input $\mathbf{x_k}$ through the network and compute the output $\mathbf{y_k}$.
- Compute weights and biases correction terms as follows:

– Output layer weights:

$$\delta \mathbf{W_o} = \alpha(\mathbf{T} - \mathbf{y}) \times \mathbf{f'}(\mathbf{Y_h}) \tag{5.6}$$

where $f'(x) = \frac{4e^{-2x}}{(1+e^{-2x})^2}$, $\mathbf{T}$ is the target given by

$$T = \begin{cases} 1 & if\ episode\ is\ true; \\ -1 & if\ episode\ is\ not \end{cases} \tag{5.7}$$

and $\mathbf{Y_i}$ is the output of the hidden layer.

– Hidden layer weights:

$$\delta \mathbf{W_h} = \alpha(\mathbf{T} - \mathbf{y}) \times \mathbf{f'}(\mathbf{Y_i}) \tag{5.8}$$

where $\mathbf{Y_h}$ is the output of the hidden layer.

– Input layer weights:

$$\delta \mathbf{W_i} = \alpha(\mathbf{T} - \mathbf{y}) \times \mathbf{f'}(\mathbf{X_k}) \tag{5.9}$$

- Update the weights and the biases.
- Repeat the above steps until the error term reach a specific value or until a specified number of epochs is reached.

5.4 Other analysis

This includes all the supporting functions used in removing false positive episodes, including making sure that the propagation direction of the inverse pulse shape is from the distal to the proximal, and checking if the propagation is not a result of a pre-episode swallow. These functions are shown in the block diagrams of Figure (5.8(a)) and Figure (5.8(b)), respectively.

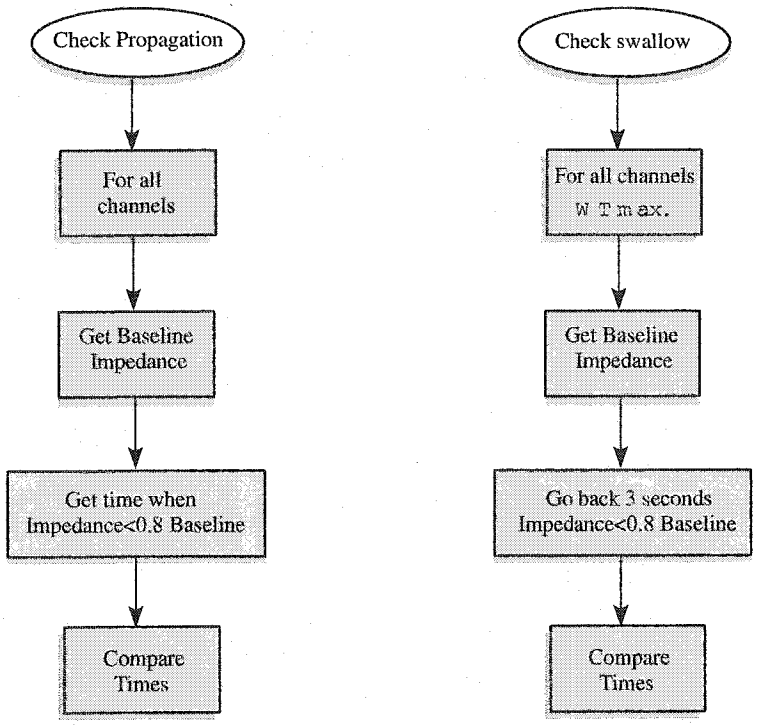

(a) Propagation direction routine.

(b) Swallow patterns routine.

Figure 5.8: Supporting routines used to enhance the FP removal.

5.5 Data analysis and discussion

The techniques developed in this study were implemented into an algorithm such that the following decisions/classifications were made:

1. The impedance waveforms were analyzed and events of interest were detected and marked.
2. Once an event was detected, it was classified into one of the following categories:
    a) Liquid /acid reflux.
    b) Liquid /non-acid reflux.
    c) Gas and liquid contents (mixed) /acid reflux.
    d) Mixed /non-acid reflux.

The decision algorithm was evaluated against the manual decision from experts. Using the experts' decision as the truth, the figure of merits such as sensitivity and positive predictive value are computed. The data used to evaluate the methodology were collected by Sandhill Scientific, Inc., for evaluation of this newly developed impedance device (Sandhill, 2003). The data were collected with a written consent of the patients and with permission of each hospital's internal review board. The data set consists of two groups: normal volunteers and patients with different diseases (ranging from simple GER patients to esophageal disease patients). Each data file is read and episodes are marked by experts in MII signals interpretations

from USA and Europe. Table 5.1 shows the performance of the algorithm developed. Each data file is classified according to the impedance values as normal, low baseline, or contains large number of mixed episodes. In the Table, the number of true positive episodes is refereed to as Tp, the number of false negative episodes is refereed to as Fn, and the number of false positive episodes is refereed to as Fp. The sensitivity and positive predictive value (PPV) are calculated according to:

$$sensitivity = \frac{Tp}{Tp + Fn} \tag{5.10a}$$

$$PPV = \frac{Tp}{Tp + Fp} \tag{5.10b}$$

The total number of files is 30, which corresponds to 660 hours of data. It can be seen from the table that very reasonable sensitivities are obtained with wide range for the positive predictive value (PPV). That is due to the fact that the PPV is dependent on both the degree of the manual reading accuracy as well as the accuracy of the algorithm. The total number of episodes detected is 2209, among which 267 episode are false negatives and 231 episode are false positives.

File Number	File status	Tp	Fn	Fp	Sensitivity	PPV
1	N	70	3	2	95.9	97.2
2	N+L	98	13	4	88.2	96.1
3	L	101	33	23	75.4	81.5
4	L	337	22	13	93.9	96.3
5	N	45	7	6	86.5	88.2
6	N	55	2	2	96.5	96.5
7	N	79	28	13	73.8	85.9
8	L	63	9	13	87.5	82.9
9	N	46	3	4	93.9	92
10	N	83	6	17	93.3	83
11	N	18	5	4	78.3	81.8
12	N	66	13	12	83.5	84.6
13	L	48	1	2	98	96
14	N	69	5	4	93.2	94.5
15	N	61	2	6	96.8	91
16	M	50	3	5	94.3	90.9
17	N	19	4	3	82.6	86.4
18	N	32	2	3	94.1	91.4
19	N	74	7	3	91.4	96.1
20	L	35	9	7	79.5	83.3
21	L	26	1	0	96.3	100
22	N	20	3	4	87	83.3
23	M	51	11	10	82.3	83.6
24	N	46	12	5	79.3	90.2
25	L	16	2	4	88.9	80
26	N	43	4	4	91.5	91.5
27	N	66	12	12	84.6	84.6
28	L	132	18	26	88	83.5
29	N	27	1	4	96.4	87.1
30	L	333	26	16	92.8	95.4

Table 5.1: Sensitivities and positive predictive values; Tp stands for the number of true positive episodes, Fn is the number of false negative episodes, Fp is the number of false positive episodes, N stands for normal impedance values, L stands for Low baseline impedance values, M means contains large number of mixed (gas and liquid) episodes

5.6 Summary

This chapter summarized techniques for detecting gastroesophageal reflux episodes from multichannel intraluminal impedance measurements. The impedance variations due to the esophageal contents are used in monitoring the esophagus status. The problem of interpreting the MII is complicated due to the variability of the impedance signals from patient to patient as well as within the same patient during the study period, further complicated with variability due to esophageal contents. The underlying framework to establish analysis techniques of MII signals is presented in this chapter. This framework is developed using a combination of wavelet transforms and neural networks in order to detect and classify reflux episodes from MII signals. The properties of MII signals are evaluated using wavelet analysis. The most important task in MII analysis is the ability to detect an event of interest such as reflux buried within a large amount of data. Extensive study of the MII signals was used to develop such a procedure. While the wavelet analysis was used to detect the events with very high sensitivity, the neural network stage was used to enhance the positive predictivity of the detection process.

The algorithms developed were evaluated using data collected by Sandhill Scientific in collaboration with various hospitals across the United States. Data from a total of 30 patients were studied, with data from each patient lasting typically 24 hours. The impedance measurements were sampled at the rate of 50 samples/second, yielding large data sets of the order of 50 Mbytes per patient. The

algorithm developed detected the events to a sensitivity of 89.2% and positive predictive value of 90.5%. In addition, on a simple desktop PC or notebook with a 1GHz Pentium processor, it takes negligible time (a few minutes) to analyze 24 hours of patient data using the algorithm, thereby showing promise for clinical applications.

Chapter 6

Discussion and Summary

Multichannel intraluminal impedance measurement is a new and emerging technique that shows great promise in the study of GIT. Multichannel intraluminal impedance provides valuable information about the esophagus and its functioning as was shown by Silny et al. (1993); Srinivasan et al. (2001); Shay et al. (2002). Multichannel intraluminal impedance has shown great promise in accurate estimation of the bolus speed and size, in addition to the detection of any activity inside the esophagus such as swallow or gastroesophageal reflux (GER). The multichannel intraluminal impedance system consists of a catheter with current-carrying electrodes.

The measured impedance depends on many factors including, the electrode configuration (i.e., electrode length, inter-electrodes spacing), esophagus conductivity, and the conductivities of the materials inside the esophagus. By choosing a suitable configuration of the catheter, the events occurring inside the esophagus such as swallow or gastroesophageal reflux can be clearly observed by monitoring the impedance values. The impedance traces can vary from patient to patient as well

as within the same patient during the study period, in addition to variability due to esophageal contents. In order to study the impedance characteristics due to various esophageal conditions as well as interpret rare impedance observations, it is important to develop theoretical solution of the impedance measurement. A solution of the multichannel impedance problem by the use of Green's function is presented in this work. The solution derived here, however, is for a simple unrealistic cylindrical model and cannot be used to solve the inverse problem. The solution for more complicated geometries will be more difficult to obtain and convergence of the solution is not guaranteed. However, finite element method provides a technique to approximate the solution of the problem for more complicated geometries such as the realistic shape of the esophagus, bolus shape, and inhomogeneous conductivities. The analytical solution derived is compared against the solution obtained from the finite element. The application of the finite element in the problem of MII is explored in more detail to determine the effect of various parameters on the measured impedance. The important findings in this regard can be summarized as follows:

- Design Considerations:
  - Catheter radius as small as possible.
  - Channel spacing chosen based on the minimum length to be detected and the number of channels in the system.
  - Electrode length chosen to be as small as possible.

- Electrodes spacing for each channel chosen to be as small as possible (minimum electrode spacing for each channel possible 0.6 cm).

These design considerations are affected by the esophagus condition. It was shown that for a severely damaged esophagus it have to be satisfied for at least the two most distal channels, and that is always limited by mechanical construction and the cost of building disposable catheters.

Low baseline signals seen in some patients are attributed to erosion and ulceration of esophageal mucosa due to repeated reflux episodes, which makes mucosa membrane conductivity change, resulting in low baseline impedance. This means that low baseline signal is an indication of the mucosa membrane status.

From the study of the different esophageal reflux episodes patterns, the following are general patterns of the reflux episodes:

- Liquid reflux:
  - Impedance change from patient impedance (baseline) to a low value in at least two channels and the inverse pulse shape propagates upward. The important factor is the impedance change and not the minimum impedance reached during the episode. The minimum impedance reached depends on many factors, including, stomach contents, and refluxate position with respect to the channel, as was shown in the simulation.

- Inverse pulse shape propagates from the distal channel to the higher channel, and so on.
- Most of the time, clearance of reflux occurs in the higher channel before the lower and the last one to be cleared is the distal channel. This pattern corresponds to a continuous reflux.
- pH alone is not enough to determine reflux. Reflux could occur with or without pH change, and pH drop may or may not be a result of reflux.

- Mixed reflux:
  - Impedance change from patient impedance (baseline) to a low value in at least two channels and the inverse pulse shape propagates upward. An impedance change to a very high value in at least two channels occurs any time during the episode duration. Most of the time, the change occurs either in the two distal channels or in the two proximal channels and at the start of the episode.
  - Inverse pulse shape propagates from the distal channel to the higher channel, and so on.
  - pH alone is not enough to determine reflux. Reflux could occur with or without pH change, and pH drop may or may not be as a result of reflux.

- Gas reflux:

  can be identified by sharp narrow instantaneous change in impedance to a high value in at least two channels. Most of the time, this occurs either in the most distal or the most proximal channels. It also could be sharp

narrow instantaneous change in impedance to high value in the distal channel accompanied by pH drop.

The problem of interpreting the MII is complicated due to the variability of the impedance signals from patient to patient as well as within the same patient during the study period, in conjunction with variability due to esophageal contents. The underlying framework to establish analysis techniques of MII signals is presented in this thesis. This framework is developed using a combination of wavelet transforms and neural networks in order to detect and classify reflux episodes from MII signals. The most important task in MII analysis is the ability to detect an event of interest such as reflux buried within large amount of data. Extensive study of the MII signals were used to develop such a procedure. While the wavelet analysis was used to detect the events with very high sensitivity, the neural network stage was used to enhance the positive predictivity of the detection process.

The algorithms developed were evaluated using data collected by Sandhill Scientific, Inc., in collaboration with various hospitals across the United States. Data from a total of 30 patients were studied, with data from each patient lasting typically 24 hours. The impedance measurements were sampled at the rate of 50 samples/sec yielding large data sets of the order of 50 Mbytes per patient. The algorithm developed detected the events to a sensitivity of 89.2% and positive predictive value of 90.5%. In addition, on a simple desktop PC or notebook with a 1GHz Pentium processor, it takes negligible time (a few minutes) to analyze 24 hours of patient

data using the algorithm. In summary, the signal analysis techniques developed in this thesis can be used successfully in esophagus monitoring.

Future research areas

There are a number of multiple intraluminal impedance topics that can be further studied and explored, among them:

- Study of GER episodes characteristics, including:
  - Time between episodes.
  - Episodes duration.
- Correlation between impedance and other types of measurements such as EGG, and Manometry.
- Signal compression.
- Site interpolation, or prediction (e.i., adding more virtual channels).
- Deeper analysis of the inverse problem and study of the effect of the applied current frequency on the impedance.

References

Al-Zaben, A. and V. Chandrasekar (2002). Thresholding reflux episodes in impedance measurements using neuro fuzzy system. *Biomedical Sciences Instrumentation 38.*

Al-zaben, A. and V. Chandrasekar (2003). Simulation of intraluminal impedance. *Biomedical Sciences Instrumentation 39.*

Al-zaben, A., V. Chandrasekar, and T. Stuebe (2001). Detection and classification of gastrointestinal tract event from multiple intraluminal impedance measurements. *Biomedical Sciences Instrumentation 37.*

Axelsson, O. (1994). *Iterative solution methods.* Cambridge University Press.

Baker, L. E. (1989). Principle of impedance technique. *IEEE Engineering in Medicine and Biology.*

Breckon, W. and M. Pidcock (1987). Ill-posedness and non-linearity in electrical impedance tomography. 10^{th} *International Conference on Information Processing in Medical Imaging.*

Cheng, K., D. Isaacson, J. Newell, and D. G. Gisser (1989). Electrode models for electric current computed tomography. *IEEE Transactions on Biomedical Engineering 36, NO. 9.*

Chiu, S. (1994). Fuzzy model identification based on cluster estimation. *J. Intell. Fuzzy Syst. 2.*

Deuflhard, P., R. Freund, and A. Walker (1990). Fast secant methods for the iterative solution of large nonsymmetric linear systems. *IMPACT Computing in Sc. and Eng. 2, 244-276.*

FEM (2003). Multiphysics in MATLAB, Comsol, Inc.

Freund, R. W. (1993). A transpose-free quasi-minimal residual algorithm for non-hermitian linear systems. *SIAM J. of Sci. Comp. 14, 470-482.*

Gabriel, C., S. Gabriel, and E. Corthout (1996a). The dielectric properties of biological tissues: I. literature survey. *Physics in Medicine and Biology 41.*

Gabriel, S., R. Lau, and C. Gabriel (1996b). The dielectric properties of biological tissues: Iii. parametric models for the dielectric spectrum of tissues. *Physics in Medicine and Biology 41.*

Geddes, L. and L. Baker (1967). The specific resistance of biological material- a compendium of data for the biomedical engineer and physiologist. *Med. & Bio. Eng. 5*, 271–293.

Gutman, S. (1989). Alternating directions methods for impedance computed tomography. *Inverse problems 5.*

IFAC-CNR (2002), Florence (Italy). An internet resource for the calculation of the dielectric properties of body tissue. *http://niremf.iroe.fi.cnr.it/tissprop/.*

Jackson, J. D. (1999). *Classical Electrodynamics.* John Wiley & Sons.

Katz, Philip O. (2001). Gastroesophageal Reflux Disease-State of the Art, *Reviews in Gastroenterological Disorders, Vol.1 NO. 3* .

Kleinermann, F., N. J. Avis, and F. A. Alhargan (1999). Analytical solution to the three dimensional electrical forward problem for a circular cylinder. *1st World Congress on Industrial Process Tomography, Buxton, Greater Manchester April 14-17.*

Lytle, R. J., A. G. Duba, and J. L. Willows (1979). Alternative methods for determining the electrical conductivity of core samples. *Rev. Sci. Instrum., 50(5), 611-615.*

Mallat, S. G. and W. L. Hwang (1992). Singularity detection and processing with wavelets. *IEEE Transactions on Information Theory 38*, 617–643.

Mallat, S. G. and S. Zhong (1989). Complete signal representation with multiscale edges. *Technical report, Courant Institute of Mathematical Sciences.*

Mallat, S. G. and S. Zhong (1992). Characterization of signals from multiscale edges. *IEEE Transactions on Pattern Analysis and Machine Intelligence 14*, 710–732.

Malmivuo, J. and R. Plonsey (1995). *BIOELECTROMAGNETISM.* New York: Oxford University Press.

Melcher, H. (1989). *Electromagnetic fields and energy.* New York: Prentice-Hall,Inc.

Morse, P. M. and H. Feshbach (1953). *Methods of theoretical physics.* McGraw-Hill Book Company.

Niknejad, A. M., R. Gharpurey, and R. G. Meyer (1998). Numerically stable green function for modeling and analysis of substrate coupling in integrated circuits. *IEEE transactions on computer-aided design of integrated circuits and systems, VOL. 17, NO. 4.*

Pope, C. E. (1994). Acid-reflux disorders. *The New England Journal of Medicine Vol.331. No. 10.*

Rahbek, H. (Ed.) (1973). *The Function of the esophagus.* Proceedings of an European Symposium, Odense University, October 16 - 18, 1972.

Sandhill Scientific,Inc., Highlands Ranch,USA, CO 80129,.

Saad, Y. (1996). *Iterative methods for sparse linear system.* PWS.

Saad, Y. and M. H. Schultz (1986). Gmres: A generalized minimal residual algorithm for solving nonsymmetric linear systems. *SIAM J. of Sci. Statist. Comp. 7, 856-869.*

Segerlind, L. J. (1984). *Applied finite element analysis.* John Wiley & Sons.

Shay, S. S., S. Bomeli, and J. Richter (2002). Multichannel intraluminal impedance accurately detects fasting, recumbent reflux events and their clearing. *Am J Physiol Gastrointest Liver Physiol 283, Issue 2.*

Shen, L. C. and J. A. Kong (1995). *Applied electromagnetism* (third ed.). PWS publishing company.

Silny, J. (1991). Intraluminal multiple electric impedance procedure for measurements of gastrointestinal motility. *Journal of Gastrointestinal Motility 3.*

Silny, J., K. Kingge, J. Fass, G. Rau, S. Matern, and V. Schumpelick (1993). Verification of the intraluminal multiple electrical impedance measurement for the recording of gastrointestinal motility. *Journal of Gastrointestinal Motility 5*(2), 107–122.

Skopnik, H., J. Silny, O. Heiber, J. Schulz, G. Rau, and G. Heimann (1996). Gastroesophageal reflux in infants: Evaluation of a new intraluminal impedance technique. *Journal of pediatric Gastroenterology and Nutrition 23*, 591–598.

Smythe, W. R. (1967). *Static and dynamic electricity.* McGraw-Hill.

Srinivasan, J., M. Vela, P. O. Katz, R. Tutuian, J. Castell, and D. O. Castell (2001). Esophageal function testing using multichannel intraluminal impedance. *Am. J. Physiol Gastrointest Liver Physiol 280*, G457–G462.

Trachterna, M., T. Wenzl, J. Silny, G. Rau, and G. Heimann (1999). Procedure for the semi-automatic detection of gastro-oesophageal reflux patterns in intraluminal impedance measurements in infants. *Medical Engineering & Physics 21*, 195–201.

Vauhkonen, P. J., M. Vauhkonen, T. Savolainen, and J. Kaipio (1999). Three-dimensional electrical impedance tomography based on the complete electrode model. *IEEE Transactions on Biomedical Engineering 46, No 9.*

Whiteman, J. R. (Ed.) (1963). *The mathematics of finite elements and applications.* Academic press.